043
PAN
13937

ISOTOPIC AND CHEMICAL STUDIES OF ULTRAMAFIC NODULES IN ALKALI BASALTS FROM KUTCH, WESTERN INDIA

BY

KANCHAN PANDE

A THESIS

SUBMITTED FOR THE DEGREE OF

DOCTOR OF PHILOSOPHY

OF THE

GUJARAT UNIVERSITY

JULY 1988

043
B13937

PHYSICAL RESEARCH LABORATORY

AHMEDABAD

INDIA

Dedicated to

My Guru

Prof. K.S. Valdiya

C E R T I F I C A T E

I hereby declare that the work presented in this thesis is original and has not formed the basis for the award of any degree or diploma by any University or Institution.



KANCHAN PANDE
(AUTHOR)

Certified by:



K. GOPALAN
Professor-in-Charge

CONTENTS

		Page No
BRIEF OUTLINE OF THE THESIS		i
ACKNOWLEDGEMENTS		vi
LIST OF FIGURES		viii
LIST OF TABLES		xi
CHAPTER I	INTRODUCTION	1
1.1	Perspective	1
1.2	Regional Distribution of Xenoliths	7
1.3	Petrographic and Chemical Overview	9
1.4	Background to the Present Study	11
CHAPTER II	EXPERIMENTAL TECHNIQUES	13
2.1	Rock Crushing and Mineral Separation	14
2.1.1.A.	Whole Rock Basalt Samples	14
2.1.1.B.	Ultfamafic Nodules	14
2.1.2	X-Ray Fluorescence and Electron Microprobe Studies	15
2.1.3	Mass Spectrometry	18
2.2.1	^{40}Ar-^{39}Ar Technique	20
2.2.2	Principle	20
2.2.3	Experimental Details	25
2.2.3.A.	Irradiation of Samples in Nuclear Reactors	25

2.2.3.B.	Sample Preparation for Irradiation	26
2.2.3.C.	Argon Extraction and Purification	27
2.2.4	Results	32
CHAPTER III	FIELD, PETROGRAPHIC, CHEMICAL AND GEOCHRONOLOGICAL STUDIES	44
3.1	Introduction	44
3.2	Field Relations	46
3.3	Mode of Occurrence of Nodules	48
3.4	Petrography and Texture of Nodules	49
3.5	Mineral Compositions	50
3.5.A.	Olivine Compositions	54
3.5.B.	Orthopyroxene Compositions	59
3.5.C.	Clinopyroxene Compositions	59
3.5.D.	Spinel Compositions	59
3.6	Basalts from Kutch	64
3.6.A.	Mineralogy	64
3.6.B.	Chemistry	69
3.7	$^{40}Ar-^{39}Ar$ Geochronology	70
3.8	Summary	87
CHAPTER IV	RARE EARTH ELEMENT AND ISOTOPIC STUDIES	88
4.1	Introduction	88
4.2	Kutch Alkali Basalts and Spinel Peridotites	90
4.3	Rare Earth Elemental Data	92

4.3.1.A. Bulk Xenoliths 92

4.3.1.B. Clinopyroxenes and Orthopyroxenes 94

4.3.2 Nd and Sr Isotopes 95

4.3.2.A. Spinel Peridotites 95

4.3.2.B. Basalts from Kutch 99

4.3.3 Discussion 105

4.4 Summary 109

CHAPTER V SUMMARY AND RECOMMENDATION 112

REFERENCES 120

BRIEF OUTLINE OF THE THESIS

This thesis describes detailed field, chemical, isotopic and geochronological studies of alkali basalts and spinel peridotites of upper mantle origin entrained in them, from the Kutch region in the western part of the Deccan volcanic province. Chemical and isotopic analyses of the samples were made at the Scripps Institution of Oceanography, La Jolla, USA and geochronoligical studies were carried out in a ^{40}Ar-^{39}Ar system developed at the Physical Research Laboratory, India during this study, using the Indian nuclear reactors for the first time in India. The findings give an insight into the evolution of the sub-Deccan lithosphere and the relationship between the alkali basalts in Kutch and the tholeiites of the Deccan province. The thesis comprises of five chapters, a brief summary of each is given below.

The first chapter describes the significance of xenoliths as mantle samples which lead to a better understanding of the mantle composition and process, their regional and tectonic distribution, petrographic and chemical characteristics and background information for present study. Much of our knowledge regarding mantle composition is based on indirect approaches. However, ultramafic nodules/xenoliths transported rapidly by kimberlitic and alkali-basaltic melts provide more direct samples of the upper mantle. Chemistry of these nodules has

been used to constrain the upper mantle chemical composition. The ultramafic xenoliths also record a variety of upper mantle processes like mantle metasomatism,which play an important role in mantle evolution.These processes are studied by geochemical and isotopic methods. The regional distribution and tectonic setting of spinel peridotite nodules and their host alkali basalts provide insights into the upper mantle in a variety of tectonic settings although most of the major known nodule localities in continental settings are associated with zone of crustal weakness ranging from faults to major rift zones.Based on their petrographic and chemical characters, these deep seated inclusions can be classified as either accidental or cognate and broadly grouped as type I and type II.Spinel peridotite bearing alkali basalts from Kutch,in the Deccan province, were first reported by De (1964). However, no detailed information was available.In view of the potential importance of such rare samples for understanding the sub-Deccan lithosphere and to complement the results of extensive trace element and isotopic studies of the Deccan tholeiites (Mahoney,1984) the present work was undertaken.

Chapter II describes the experimental techniques employed during the course of this work.The first section outlines briefly the procedures for rock crushing,mineral separation, sample preparation and chemical separation adopted for major and trace element determination by X-ray fluorescence spectrometry and electron microprobe and mass-spectrometric measurement of the concentration and

isotopic composition of Sm,Nd,Rb and Sr carried out at the Scripps Institution of Oceanography,La Jolla,USA.The second section describes in detail the development of ^{40}Ar-^{39}Ar dating technique for the first time in India using the Indian nuclear reactors, Apsara and Cirus at Bhabha Atomic Research Centre, Bombay. The low fast neutron flux in positions available for irradiation of samples necessitates longer irradiation times, about two weeks, for adequate production of Ar isotopes.Moreover,large fluence variations in the irradiation can volume, about 25% in the vertical direction and 8-20% in the horizontal direction,require determination of fluence seen by each sample relative to the monitor by irradiating a high purity Ni wire along with each sample. ^{40}Ar system blanks are comparable with blanks in similar extraction systems used in other laboratories. Five tholeiite samples from the thickest exposed Deccan lava sequence at Mahabaleshwar yield ages that are consistent with stratigraphy.

Chapter III presents the field,petrographic,chemical and geochronological studies. Spinel peridotite bearing alkali basalts occur as plugs or sheet-like bodies intruding the flat-lying to gently dipping Jurassic sandstones but are nowhere seen to be in direct contact with the Deccan tholeiites. Chemically host basalts are undersaturated and alkaline in nature.The nodules,in most of the cases, are small averaging only 1-2 cm in diameter although at few localities larger xenoliths upto 4 cm are found. The ultramafic nodules are of two types:dunites and

spinel peridotites.The dunites appear to be cognate whereas spinel peridotites are accidental.The olivine composition of spinel peridotites are quite homogeneous,averaging Fo_{90}, orthopyroxenes are enstatites of $En_{89.6}, Fs_{9.7}, Wo_{0.7}$ with relatively low Al_2O_3. The clinopyroxenes are chrome-diopsides with a very limited range of composition, En_{48-49} Wo_{46-49} Fs_{4-5}. The $^{40}Ar-^{39}Ar$ ages of alkali basalts from Kutch cluster around 66 Ma,not significantly different from that of tholeiite from this region.These ages are within the range observed for the tholeiites from the main Deccan province. There appears to be no major break between the emplacement of alkali basalts and the tholeiites suggesting a close temporal relationship.

Chapter IV presents the rare earth element and isotopic data for the spinel peridotites and basalts from Kutch. Selected fresh spinel peridotites were used for REE and isotopic studies. REE determinations were made on acid-leached and unleached separated clinopyroxenes, orthopyroxenes and host rocks. Leach separates show a net loss of REE though chondrite normalized REE patterns for the leached and unleached fractions are not significantly different. The clinopyroxenes are LREE enriched whereas orthopyroxenes show a U-shaped pattern.The isotopic (Sr and Nd) compositions of the alkali basalts define a narrow field in a Nd-Sr diagram and are strikingly similar to those of the least crustally contaminated tholeiites from the Mahabaleshwar section studied by earlier workers.This suggests a genetic relationship between the alkali and

tholeiitic basalts or their coincidentally similar source regions. The tholeiitic basalts from the Kutch region, on the other hand, show a much wider range and fall along the Mahabaleshwar mixing trend again supporting a genetic link. In contrast to the host basalts, the isotopic compositions of the separated xenolith minerals (mainly Cpx and Opx) exhibit a wide range, with $^{87}Sr/^{86}Sr$ varying from 0.7039 to 0.7075 and $^{143}Nd/^{144}Nd$ from 0.511420 to 0.513105. The peridotite nodules of Kutch probably represent fragments of lithosphere unrelated to the source of either their host alkali basalts or the tholeiites of the Deccan province.

Chapter V summarises the major findings and suggests lines for future work.

ACKNOWLEDGEMENTS

I am greatly indebted to Professor K. Gopalan who suggested this project to me and guided me throughout the course of this work and to Dr.T.R. Venkatesan with whom I worked closely in the development of the Ar-Ar dating technique in our laboratory. I am extremely grateful to Dr. P. Krishnamurthy of the Atomic Minerals Division. Hyderabad, for guidance in the field work and several useful discussions.

Part of this work was carried out at the Scripps Institution of Oceanography, La Jolla,USA.I am grateful to Prof. J.D. Macdougall and Dr. G.W. Lugmair for introducing me to high precision isotopic analysis.I have benefitted greatly from their continued advice and support.I thank Chris MacIssac,Ron LaBorde and Roy Fujita for helping me in the analytical techniques required in my work at SIO and Patti Hey for help in solving crossword puzzles.Grateful thanks to Alan Volpe for all his help during my stay at La Jolla. I thank Dr. A.V. Murali,Johnson Space Centre,Houston, U.S.A.,for providing the Rare Earth Element data.

I have had the good fortune to work with a number of colleagues at PRL who have helped me in numerous ways.I wish to record my sincere thanks to Dr. Ramesh who spent considerable time to teach me various aspects of scientific research and to Mrs. Rashmi Jadeja,who helped me with data reduction for Ar-Ar work.I enjoyed the stimulating company

of fellow graduate students,Sarkar,Birendra Pande,Beig,Pal, Ranjan, Jha, Ajai, Sunil, Rathore, Mathew,Krishnakumar,Raju, Maqbool, Vijayshankar, Subramanian, Vinodkumar, Debi Prasad, Banerjee,Sishir Deshpande and Ajai Singh.

I express my deep sense of gratitude to Prof. K.S. Valdiya of Kumaun University,Nainital and to Prof. D. Lal for their sustained encouragement. Other members of our group, Profs. B.L.K. Somayajulu,S. Krishnaswami,M.N. Rao,N. Bhandari and Drs. J.N. Goswami,R.K. Pant,P.N. Shukla,M.M. Sarin, S.V.S. Murthy and S.K. Bhattacharya have always extended their assistance and encouragement. Kurup, Shivashankaran, J.R. Trivedi, J.T. Padia and Dr. Sheela Kusumgar offered innumerable help during this work. I sincerely thank them all.

I gratefully acknowledge the financial assistance from the National Science Foundation, USA for my work at SIO under SFC Grant INT 8207391.

I thank Nambiar and Viswanathan for typing the thesis neatly.

Finally I wish to thank my parents and family members for encouragement.

(Kanchan Pande)

LIST OF FIGURES

1.1 Diagramatic scheme showing relationship between various types of upper-mantle peridotites.

1.2 Map showing the worldwide distribution of mantle xenolith bearing alkali basalts.

2.1 Schematic of the complete mass spectrometer, gas extraction-purification system.

2.2 Section through gas extraction, furnace and purification line.

2.3 Middle section of the S-S block with only one valve assembly shown.

2.4 Typical Argon spectrum.

2.5 Age spectra of four samples from different elevation of the Mahabaleshwar section of the Deccan Province.

3.1 Map of India showing the Deccan Traps and area of study.

3.2 Geological map of Kutch, Western India.

3.3 Map of Dhrubia hill.

3.4 Map of Vethon hill.

3.5 Generalised geological cross-section of Dhrubiya and Bhujia hills.

3.6 Olivine compositions for nodules and basalts.

3.7 Pyroxene compositions for spinel peridotites and basalts.

3.8 Spinel composition.

3.9 Alkali-silica diagram for basalts from Kutch.

3.10 Age spectrum for BHUJ-F.

3.11 Isochron plot for BHUJ-F.

3.12 Age spectrum for KB85-58.

3.13 Isochron plot for KB85-58.

3.14 Age spectrum for KB83-13.

3.15 Isochron plot for KB83-13.

3.16 Age spectrum for KB83-11A.

3.17 Isochron plot for KB83-11A.

3.18 Age spectrum for BHUJ-A.

3.19 Isochron plot for BHUJ-A.

3.20 Age spectrum for KB85-54A.

3.21 Isochron plot for KB85-54A.

4.1 Map of Western India showing Major Rift zones, positive gravity anomalies and the plugs.

4.2 Chondrite normalised REE pattern for BN-B.

4.3 Chondrite normalised REE pattern for BN-C.

4.4 Chondrite normalised REE pattern for BN-D.

4.5 Chondrite normalised REE pattern for DN-A.

4.6 Chondrite normalised REE pattern for DN-B.

4.7 Chondrite normalised REE pattern for Cpx and Opx BN-A.

4.8 Chondrite normalised REE pattern for Cpx and Opx BN-B.

4.9 Chondrite normalised REE pattern for Cpx and Opx BN-C.

4.10 Chondrite normalised REE pattern for Cpx and Opx DN-1.

4.11 Chondrite normalised REE pattern for Cpx KB85-13.

4.12 Chondrite normalised REE pattern for basalts.

4.13 Sr-Nd isotopic variation in nodules and basalts from Kutch.

4.14 Isotopic composition of spinel peridotites from alkali basalts.

4.15 Nd and Sr isotopic composition for co-existing Cpx and Opx.

4.16 $^{87}Sr/^{86}Sr$ versus $(La/Sm)_n$ in Cpx and Opx.

4.17 ϵ_{Nd} versus $^{87}Sr/^{86}Sr$ in Cpx and Opx.

4.18 ϵ_{Nd} versus Sr/Nd in Cpx and Opx.

4.19 $^{87}Sr/^{86}Sr$ versus $Sm/^{86}Sr$ in Cpx and Opx.

4.20 $^{143}Nd/^{144}Nd$ versus $^{147}Sm/^{144}Nd$ for mineral separates.

4.21 $^{87}Sr/^{86}Sr$ versus $^{87}Rb/^{86}Sr$ for mineral separates.

LIST OF TABLES

2.1 Accuracy and precision of XRF data.

2.2 Isotopic fractionation corrections, estimated precisions, standard reference and decay constants for mass-spectrometric analyses.

2.3 Principal neutron reactions leading to the production of Ar isotopes.

2.4 Typical ^{40}Ar system blank contribution.

2.5 Irradiation parameters.

2.6 Argon isotopic composition and apparent ages of MB81-1/1.

2.7 Argon isotopic composition and apparent ages of MB81-1/2.

2.8 Argon isotopic composition and apparent ages of MB81-3.

2.9 Argon isotopic composition and apparent ages of MB81-10.

2.10 Argon isotopic composition and apparent ages of MB81-24.

3.1 Representative olivine compositions.

3.2 Representative Orthopyroxene compositions.

3.3 Representative Clinopyroxene compositions.

3.4 Representative spinel compositions.

3.5 Chemical composition of basalts from Kutch.

3.6 Argon isotopic composition and apparent ages of BHUJ-F.

3.7 Argon isotopic composition and apparent ages of KB85-58.

3.8 Argon isotopic composition and apparent ages of KB83-13.

3.9 Argon isotopic composition and apparent ages of KB83-11A.

3.10 Argon isotopic composition and apparent ages of BHUJ-A.

3.11 Argon isotopic composition and apparent ages of KB85-54A.

3.12 Plateau-, Isocrhon- and Integrated ages for samples from Kutch.

4.1 REE data for spinel peridotites, mineral separates and basalts.

4.2 Nd and Sr isotopic composition and mineral separates.

4.3 Nd and Sr isotopic composition of basalts.

4.4 Initial Nd and Sr isotopic composition of minerals and basalts.

CHAPTER I

INTRODUCTION

1.1. PERSPECTIVE

It is a well documented fact that the earth is a dynamic system which has evolved today into a chemically structured and heterogeneous planet. However, while some of these structures, like the core, the mantle and the crust are relatively well constrained and their gross chemical compositions deduced from a combination of geophysical and geochemical methods, the finer details and subdivisions of these structures are far less understood primarily due to their inaccessibility. In recent years a wealth of useful information on the composition and evolution of the earth has been inferred by considering it as a geochemical system comprising of a relatively simple set of reservoirs and by using trace elements and/or radiogenic isotopes as tracers of chemical processes which control the exchange of elements within these reservoirs (Allegre, 1987; 1982; Allegre

et al., 1983; Anderson, 1982; De Paolo, 1980; Jacobson and Wasserburg, 1979; O'Nions and Hamilton,1981;O'Nions et al., 1979;Turcotte and Kellogg (1986);Zindler and Hart,1986).

A precise knowledge of the composition of the bulk silicate earth can be used to constrain the chemical dynamics and evolution of the crust mantle systems.The earth's mantle constitutes approximately two thirds the mass of the earth.Except for the most incompatible elements for which the contribution of the crust (0.59% of the mass of the mantle) becomes important,the mantle determines the chemistry of the earth for all oxyphile elements (Wanke et al., 1984). Therefore in evaluating bulk earth composition and compositional evolution of the crust mantle system,it is important to know the composition of the mantle.The upper mantle part of the continental lithosphere,the part of the upper mantle below the Moho which is mechanically coupled to the overlying continental crust is one of the least well known geochemical reservoirs in the outer portion of our planet.

Much of our knowledge regarding mantle composition is based on indirect approaches like (i) analogy with chondritic meteorities (ii) geophysical data,principally seismic and heat flow, and (iii) study of basalts derived from the mantle by partial melting (Gast,1968).Each of these approaches has severe shortcomings. For example, chondritic meteorites are not uniform in composition and the earth apparantly has non-chondritic abundances of volatile elements (Ganpathy and Anders, 1974;Wanke,1981;

Wanke et.al., 1984); geophysical data are not sensitive indicators of composition; our knowledge regarding the degree of melting and liquid/solid partitioning is far from complete to infer unambiguously the nature of mantle composition.

Most of the continental flood basalts are believed to be derived from sources situated in the sub-continental lithosphere and their chemical and isotopic compositions have been used to infer the nature and composition of their mantle sources (BVSP,1981;Brooks et al.,1976;Menzies et al. 1983; 1984;McDounough et al.1985).However,there is a serious difficulty in assessing the chemical nature of their sub-continental mantle sources because their isotopic and trace element abundances are overprinted during the magma transport through the chemically distinct, large ion lithosphile (LIL) enriched continental crust and the upper sub-continental lithospheric mantle prior to eruption and it is not always possible to assess the degree and type of such contamination (Carlson et al., 1981; De Paolo,1981; Mahoney et al., 1982). On the other hand, ultramafic nodules/xenoliths, believed to be fragments of the sub-continental lithosphere, brought up by rapidly transported Kimberlitic and alkali basaltic melts provide a random but more direct and less altered samples of the upper mantle.

Majority of the ultramafic nodules occurring in the alkali basalts are spinel bearing lherzolites and harzburgites, commonly called spinel peridotites.They appear

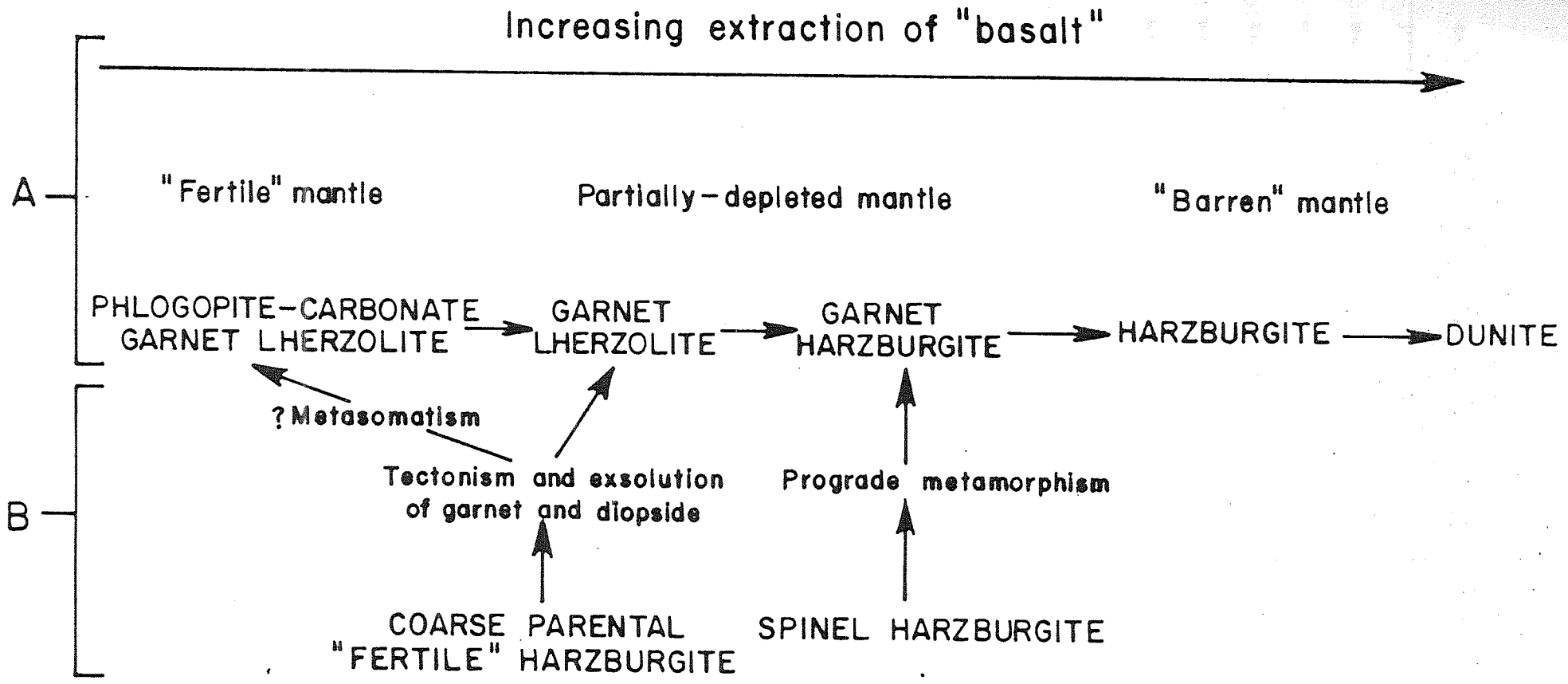


Fig. 1.1 Diagrammatic scheme showing relationship between various types of upper-mantle peridotite. The melting/residue/basalt extraction relationships are shown in horizontal band A. Additional more complex relationships are shown by band B. (After DAWSON, 1984)

to have come from the lithosphere and equilibrated at pressures of about 10-25 kbars. They probably represent major constituents of the continental lithosphere.In view of the differentiated and heterogeneous nature expected for the lithosphere,geochemists have considered models by which mantle fragments may be related to the desired average mantle composition,for example,Fig.1.1 (after Dawson,1984).

Several pioneering papers have attempted to estimate the composition of the primitive upper mantle by comparing the chemistry of the upper mantle lherzolites with the chemistry of meteorites (Hutchinson et al.,1970;Jagoutz et al.1979;Loubet et al.,1975,Hart and Zindler,1986).

The origin and significance of peridotite inclusions in basaltic rocks have been debated for more than a hundred years (summarised in Forbes and Kuno,1965;Menzies,1983). Several models have been proposed for their origin,the most notable being

(i) A cognate origin as cumulates from their host magmas (O'Hara and Mercy, 1963)

(ii) An accidental origin relative to their host magmas (Basu, 1975; Basu and Murthy, 1977, Forbes, 1963; Kushiro and Kuno, 1963, Menzies; 1983.

The complex thermal history and equilibrated textures make the first hypothesis less tenable and,although the second hypothesis is now generally accepted,the question of their exact origin remains. Several choices exist for the origin of mantle peridotites like (a) a parental upper mantle (b) mantle residue after melt extraction by partial

melting (c) ancient cumulates (d) conduit precipitates (e) any of these modified by passage of basaltic magmas (Basu, 1975,Brooks et al.,1976;review by Menzies,1983).

In recent years trace element and isotopic studies on mantle derived spinel peridotites have led to better understanding of their origin and a variety of processes which are recorded in them.Isotopic studies,mainly Sm-Nd and Rb-Sr, have shown that xenoliths have preserved their own intrinsic and varied geochemistry, distinct from the host magma, and represent a multistage evolution over much of the earth history (Basu and Murthy 1977;Chen and Frey, 1981; Dasch and Green, 1979;Jagoutz et al.,1980;MacDonough and McCulloch, 1987; Richardson et al.,1985;Stosch et al., 1986;Stosch et al.,1986,1980;Stueber and Ikramuddin 1974).

Another important observation is that some spinel peridotites believed to be 'fertile' on the basis of major and minor element chemistry are devoid of the crucial inventory of incompatible elements necessary for the trace-element enriched magmas (Griffin and Murthy,1968). This observation led to the concept of mantle metasomatism (Bailey,1970,1972,1982).

The idea of 'mantle metasomatism' was first introduced by Bailey (1970, 1972) to account for certain features of alkaline magmatism but since then it has been observed that metasomatic changes in mantle rocks are common and play a key role in determining the chemical and isotopic characteristics of mantle derived materials. Mantle metasomatism generally refers to the enrichment process

whereby abundances of incompatible trace-elements,like K,Rb, Sr, Ba, light rare earth elements (LREE),Ti,Nb,Zr,P,U and Th are increased relative to the presumed primitive (Sun,1982) and or depleted (Jagoutz et al.1979) mantle precursor.This enrichment process is called 'Patent metasomatism' (Dawson, 1984) if it is texturally evident and is synonymous with 'Modal metasomatism' (Harte, 1983). In contrast, "Cryptic metasomatism" (Dawson, 1984) does not display any textural and modal mineralogical signatures. However the chemical signature seen requires a metasomatic enrichment process.As an important process which determines the chemistry of upper mantle rocks, mantle metasomatism has stimulated a number of studies on metasomatised xenoliths (Erlank et al., 1982; Francis, 1976; Menzies et al.,1985,1987;McDonnough and McCulloch, 1987; Stosch et al.,1986,1980;Stosch and Lugmair, 1986) and several reviews on the subject (Bailey,1982,1984; Dawson, 1980; 1984; Frey,1984,Harte,1983,Hawkesworth et al., 1983, Menzies 1983, Menzies and Hawkesworth,1987,Roden and Murthy, 1985; Wilshire, 1984).Isotopic studies,mainly Sm-Nd, have been carried out on metasomatised xenoliths to infer the timing of metasomatism. Such studies indicate that metasomatism occurred relatively recently. For example,at Nunivak, less than 200 My ago (Menzies and Murthy,1980;Roden et al., 1984), at San Carlos,less than 500 Mys ago (Zindler and Jagoutz, 1988) at Dreiser Weiher less than 200 My ago (Stosch et al., 1980) at Geronimo Volcanic field,less than 500 Myr ago (Kempton et al.,1984).

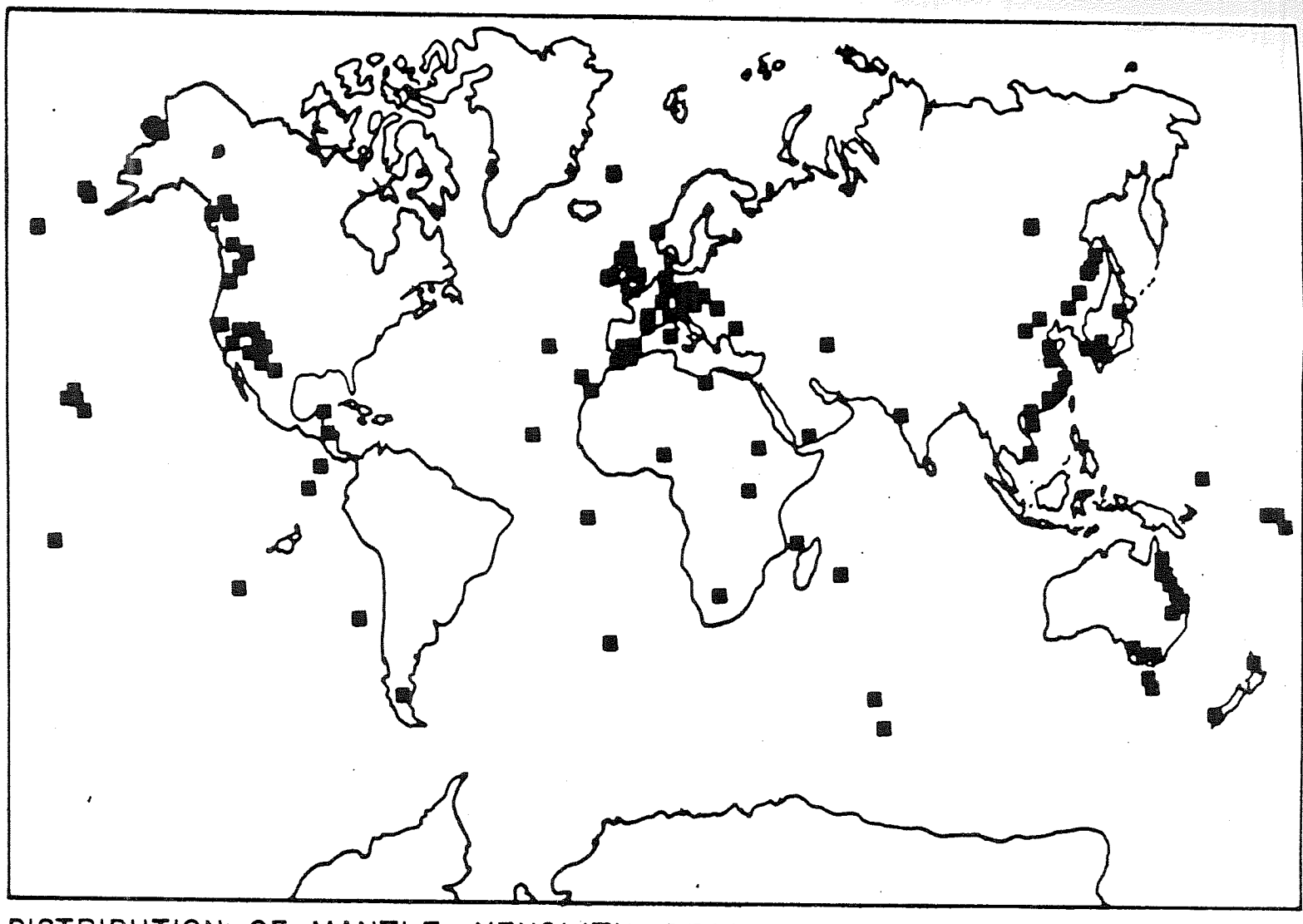


Fig. 1.2 DISTRIBUTION OF MANTLE-XENOLITH-BEARING ALKALI BASALTS. SOME SQUARES REPRESENT MORE THAN ONE VOLCANOE. ATLANTIC LOCATIONS ARE OFF MAP. (AFTER BOETTCHER, 1984)

1.2. REGIONAL DISTRIBUTION OF XENOLITHS

The worldwide occurrence and distribution of peridotities has been described by Boettcher (1983) Forbes and Kuno (1965) Kushiro and Kuno (1963), Menzies (1983) and Ross et al (1954). Inclusion bearing basalts occur in oceanic, circumoceanic and intracontinental settings (Fig. 1.2) but the distribution clearly shows that the oceanic and circumoceanic settings predominate. A very significant observation made by Forbes and Kuno (1965) is that most of the inclusion bearing basalts are of Cenozoic age. They suggested that the mechanism which produces peridotite bearing basalts may have become more active during the Cenozoic as Palaeozoic and Mesozaic inclusion-bearing basalts are extremely rare or nonexistent. It is possible that nodule bearing basalts may have occurred as frequently in the Pre-Cenozoic but that alteration, deformation and recrystallisation have obscured the evidence. Another significant feature is that continental peridotite inclusion bearing basalts occur as pyroclastic cones, breccia pipes and/or flows of rather limited area and most Pre-Cenozoic occurrences may not have survived destructional processes over long periods of geologic time.

Forbes and Kuno (1965) for the first time focused on the comparative petrology of the host rocks and the inclusions. It was observed by them and other workers (Forbes and Kuno, 1967; White, 1966) that most ultramafic inclusions occur in alkaline and undersaturated rocks and that their presence in tholeiitic basalts is very rare.

Another notable feature is the similarity in the bulk chemical composition of the host alkali basalts from varied tectonic settings. There is also an apparent tectonic association of rift zones and xenolith bearing basalts in both continental and oceanic settings.These observations led to the suggestion that peridotite inclusions are related to the genesis of alkali basaltic magmas in these zones. Comparison of the chemistry of alkali olivine basalts all over the world from both the oceans and the continents indicates that there is no difference in the major element composition of these basalts from varied tectonic environments. This prompted Schwarzer and Rogers (1974) to suggest that alkali olivine basalts are generated at sufficient depths in the upper mantle under the continents and oceanic areas with the result that its major element chemistry is unaffected by chemical or thermal differences between the continental and oceanic upper mantle. Basu (1975) suggested that there is a close relationship between the mantle plumes, hot spots and ultramafic xenoliths in alkaline magmas. He observed that the world wide occurrence of xenoliths in alkali basalts from both the continents and the oceans is restricted to tectonic settings which generally encompass Wilson-Morgan hot spots. Mantle metasomatism as a precursory process to the genesis of alkaline magmas hosting ultramafic nodules has been advocated by many workers (Boettcher et al.,1979,Menzies and Murthy,1980;Wass and Rogers,1980).

1.3. PETROGRAPHIC AND CHEMICAL OVERVIEW

The most commonly encountered xenoliths in alkaline lavas are peridotites,pyroxenites,eclogites and megacrysts. Generally these deep seated inclusions are divided into the following two groups (i) cognate (ii) accidental. The cognate xenoliths are related to the host basalts whereas the accidental xenoliths are not.The latter may be either fragments of upper mantle or portions of residual peridotite resulting from an earlier partial melting event in upper mantle material.

Although peridotite inclusions in basalts are present in a variety of petrologic types,they can be conveniently classified into two contrasting groups primarily on the basis of their major element chemistry.These correspond to the Cr-diopside (or green clinopyroxene) and Al-augite (or black clinopyroxene) groups of Wilshire and Shervais (1975), Groups I and II of Frey and Prinz (1978) and Type I and II of Menzies (1983) which are mutually equivalent chemically. Type I inclusions are rich in Cr and Mg compared to Type II inclusions and the latter are richer in Fe and Ti.Type I inclusions contain predominantly the phases olivine, orthopyroxene, clinopyroxene and spinel in decreasing order of abundance (the lherzolite series) with a complete gradation to harzburgite (<5% cpx) and dunite but pyroxene rich varieties such as orthopyroxenites and olivine clinopyroxenites are also fairly common.In addition major amounts of paragasitic amphibole and minor phlogopite may also occur. (Lloyd and Bailey,1975;Menzies and Murthy 1980;

Menzies, 1983). The textures of Type I inclusions are generally metamorphic with equilibrated grain boundaries, although minor deformation is often preserved.By contrast, Type II inclusions contain a more varied mineralogy and mode that consists mostly of clinopyroxene olivine, amphibole, spinel and orthopyroxene with accessory plagioclase, Fe-Ti oxides, apatite and phlogopite. Relict igneous textures partly or wholly recrystallised are common. In addition, incipient partial melting is more common than in Type I.

Veining and discordant planar contacts are common within ultramafic xenoliths but generally Type I series never crosscut Type II (Kempton et al.,1984;Wilshire and Shervais, 1975). On the basis of chemical and textural and crosscutting relationship it has been inferred that Type II series postdate the predominant processes responsible for the observed chemistry and mineralogy of Type I peridotites (Wilshire and Shervais (1975).The observation that Type II inclusions have radiogenic isotope composition which generally overlap with those of host basalts (Frey and Prinz, 1978; Menzies 1983),whereas this is not so for Type I inclusions, lends support to this notion. It has been suggested that Type II veins represent precipitates on the walls of conduits at depth,through which basaltic magma was flowing (Irving,1980).

The processes recorded in the chemistry of ultramafic xenoliths are complex and varied (Frey,1984;Frey and Green, 1974;Frey and Prinz,1978;Irving 1980,Menzies 1983).

1.4. BACKGROUND TO THE PRESENT STUDY

The present study focuses on the field occurrence, chemical, mineralogical and isotopic studies of upper mantle derived ultramafic nodules occurring in alkali basalts in the Deccan volcanic province of northwestern India with implications to their continental lithospheric mantle source regions.

The late Cretaceous to early Eocene Deccan Traps of India represent one of the largest manifestations of volcanism in the last 200 Ma.Extensive isotopic,trace and major element studies on the predominantly tholeiitic basalts carried out earlier (Mahoney,1984) as part of an Indo-US project have provided an average,though indirect, picture of their mantle source regions.This source is a widespread isotopically homogeneous and depleted one with ϵ_{Nd} ~+8 similar in nature to the source of Indian Ocean Mid Ocean Ridge Basalts (MORB). A volumetrically minor but important constituent of this province is the alkaline rocks, some of which as at Kutch host ultramafic nodules.The presence of small peridotite xenoliths in the basalts of Kutch was first noted by De (1964) who,however,gave only brief and generalised descriptions. Details of their location, mode of occurrence and chemical compositions were lacking. In view of the potential importance of such rare samples for understanding the sub Deccan lithosphere and to complement the findings from studies of the tholeiitic

basalts, the present work was undertaken.

CHAPTER II

EXPERIMENTAL TECHNIQUES

This chapter describes the experimental techniques employed during the course of this work.The first section outlines briefly the procedures for rock crushing,mineral separation, sample preparation and chemical separation adopted for major and trace element determination by X-Ray fluorescence spectrometry and electronmicroprobe and mass-spectrometric measurement of the concentration and isotopic composition of Sm,Nd,Rb and Sr carried out at the Scripps Institution of Oceanography,La Jolla,USA.The second section describes in detail the development of the $^{40}Ar-^{39}Ar$ dating technique for the first time in India using the Indian nuclear reactors, Apsara and Cirus at Bhabha Atomic Research Centre,Bombay.This method was used to establish the temporal relationship between the alkali basalts from Kutch and the Deccan tholeiitic basalts.The rare earth element determinations were made by Dr. A.V. Murali at Johnson Space Centre, Houston, U.S.A. by Instrumental Neutron Activation Analysis.

2.1.1. ROCK CRUSHING AND MINERAL SEPARATION

A. WHOLE ROCK BASALT SAMPLES

Fresh basalt samples, weighing about 2 Kg were sawn using a diamond saw into thin slices free from any altered or contaminated surface material like hammer marks. Slices free from any visiible nodule/phenocryst material were selected. These thin slices, about less than 5 mm in thickness, were then polished on coarse diamond (600 m) laps to remove saw marks. Polished slices were subsequently cleaned with deionised water in ultrasonic cleaners repeatedly to remove all the fines and then rinsed finally with methanol.

The dried slices were crushed using a small jaw crusher into less than 5 mm size fragments. These fragments, along with fines were coned and quartered to obtain about 300 g of representative sample. This fraction was further ground to less than 200 mesh in a Spex-ball mill using tungsten carbide vials for both XRF and mass-spectrometric analyses. All the equipment used in the process were thoroughly cleaned and precondtioned with a small amount of sample being processed.

B. ULTRAMAFIC NODULES

The cores of spinel peridotite nodules were preferentially sampled and crushed to about one mm size

with a steel hammer. An aliquot of a few samples at this stage was taken for whole rock REE analyses. For all other REE and mass spectrometric analyses high purity, inclusion free mineral separates were used.

Clean clinopyroxenes and orthopyroxenes were hand-picked under a binocular microscope. Inclusion-free grains were selected under the microscope with high intensity horizontal illumination in an alcohol-water medium. Particular attention was paid to separate grain free of visible inclusions of other minerals as well as fluid inclusions.

The clean inclusion free separates were ultrasonicated in 2N HCl for about 10 minutes followed by 5% HF for about 10 minutes and then again by 2N HCl for about 10 minutes. Finally they were cleaned in high purity double-distilled water in ultrasonic cleaners for 10 minutes, rinsed a few times with double-distilled water and dried. Aliquots of these 'leached' mineral separates were used for both REE and isotopic determinations.

2.1.2. X-RAY FLUORESCENCE AND ELECTRON MICROPROBE STUDIES

Major and trace element concentrations of whole rock basalt samples were made on XRF and mineral chemical compositions were determined on electron microprobe following the techniques adopted at the Scripps Institution of Oceanography, U.S.A.

The major element measurements were made on fused glass disc prepared from a 1:5 mixture of sample powder (0.500 g)

Table 2.1. Accuracy and Precision of XRF Data

	Accuracy %	Precision %
SiO_2	0.39	1.17
TiO_2	0.03	0.09
Al_2O_3	0.31	0.33
FeO	0.29	0.19
MnO	0.02	0.01
MgO	0.11	0.10
CaO	0.08	0.07
Na_2O	0.14	0.05
K_2O	0.03	0.06
P_2O_5	0.02	0.01
	(ppm)	(ppm)
Sr	5	3
Zr	9	5
Ni	4	3
V	4	6
Ba	3	1
Rb	6	5
Y	2	1
Nb	4	1

and spectroflux-105, and trace elements were measured on pressed pellets using a mixture of 3.000 g sample powder and 1 g of cellulose as binder.

Glass discs and pressed pellets were analysed in a Philips 1410 X-ray fluoroscence spectrometer.Major elements were determined against calibration curves based on eight international rock standards of widely different compositions. BCR-1 was used as an internal standard to minimize errors due to instrumental drift.Nine replicate samples were prepared to check the reproducibility.Accuracy of concentration determination was obtained from the deviation of the calculated concentration from the recommended values for the standards and the precision was calculated from the results on the replicate samples (Table 2.1). For trace element determinations the X-ray intensity ratios were modified by the mass absorption coefficient to correct for matrix effects.

Mineral chemical compositions were obtained on both polished thin sections and grain mounts using an automatic CAMECA microprobe Smithsonian mineral standards and pure metal oxides were used as standards.

Thin sections were mapped prior to analysis on a micrometer stage to locate the minerals of interest. Corrections for mass absorption (A),fluorescence (F) and atomic number (Z) were carried out on line using the programs available at the Scripps Institution of Oceanography. The accuracy of concentration determination was obtained by analysis of standard minerals.

2.1.3. MASS SPECTROMETRY

The sample dissolution and spiking procedures were the same for whole rock and mineral samples.About 30 mg of representative sample powder (the high purity 'leached' mineral separates ranged from 10 mg clinopyroxenes to 60 mg orthopyroxene samples) was weighed accurately into a 15 ml teflon vial. It was moistened with a few drops of high purity double distilled water.A few cc of 2:1 HF and HNO_3 acid mixture were added and the copped teflon vials were ultrasonicated for about two hours. Samples were considerably dissolved after this ultrasonic agitation. Samples were then evaporated to dryness and redissolved in about 1 cc of HNO_3 and dried again.This step was repeated. The dried samples were dissolved in about 3 cc of 2N HCl.

The sample solution in 2N HCl was totally spiked with a mixed Sm-Nd and Rb and Sr tracers.

Chemical separation of Rb, Sr,Sm and Nd in the sample employed a two column cation exchange procedure.Rb and Sr were eluted in the first column (primary column) which used DOWEX AG 50W-X8 resin and 2N HCl as eluant.The REE were eluted as a batch using 6N HCl after the separation of Rb and Sr in this column. From this fraction Sm and Nd were separated from each other and the other REE in a second column (micro column) using AG 50W-X8-200-400 mesh resin and α-HIBA (alpha hydroxyisobutyric acid) elution.

The concentration and isotopic composition of Sm,Nd,Rb

Table 2.2. Isotopic fractionation corrections, estimated precisions, standard reference values and decay constants.

Isotopic fractionation corrections were made using

$^{86}Sr/^{88}Sr = 0.1194$

$^{148}Nd/^{144}Nd = 0.242436$

$^{143}Nd/^{144}Nd = 0.511859$ for La Jolla Nd standard

$^{143}Nd/^{144}Nd = 0.512566$ and

$^{147}Sm/^{144}Nd = 0.1936$ for present day Juvinas.

$\lambda_{^{147}Sm} = 6.54 \times 10^{-12}\ Yr^{-1}$

$^{87}Sr/^{86}Sr = 0.71025$ for NBS 787 Sr

$\lambda_{^{87}Rb} = 1.42 \times 10^{-11}\ Yr^{-1}$.

Sm and Nd determinations are accurate within 0.2%.

and Sr were determined on a VG 54E Spectrometer at the Scripps Institution of Oceanography,La Jolla following the procedures described in detail by Carlson (1980).

Isotopic fractionation corrections,estimated precisions, standard reference values and decay constants are given in Table 2.2.

2.2.1. ^{40}Ar-^{39}Ar TECHNIQUE

The development of the ^{40}Ar-^{39}Ar technique for dating igneous rocks, in particular, the Deccan basalts for the first time in India is described below.This development was taken up in 1983 using the Indian nuclear reactor Apsara at the Bhabha Atomic Research Centre,Bombay.

2.2.2. PRINCIPLE

The ^{40}Ar-^{39}Ar technique is a modern variant of the conventional K-Ar method. In the conventional method,the daughter to parent ratio is obtained from two independent experiments. The quantity of radiogenic ^{40}Ar in a rock or mineral is measured by isotope dilution mass spectrometry in one aliquant of the sample and potassium is measured in a separate aliquant by flame-photometry or atomic absorption spectrophotometry. In the Ar-Ar method, the daughter to parent ratio is measured in a single experiment on the same sample aliquant in terms of the isotopic ratio ^{40}Ar-^{39}Ar thereby avoiding the problems of sample inhomogeneity. Also, since age determination relies on the measurement of isotopic abundance ratios rather than

elemental abundance ratio, the method is capable of greater precision than the conventional K-Ar method.

Samples to be dated are irradiated in a nuclear reactor to convert some of ^{39}K to ^{39}Ar by the fast neutron reaction $^{39}K(n, p)^{39}Ar$ which has a threshold of 0.22 MeV. After irradiation the sample is fused and the argon isotopic composition is measured in a mass-spectrometer. If the fraction of ^{39}K converted to ^{39}Ar by irradiation were known exactly, then the age can be determined directly from $^{40}Ar_{rad}/^{39}Ar_K$ using the equation

$$T = \frac{1}{\lambda} \ln\left[\frac{^{40}Ar_{rad.}}{^{39}Ar_K}\left(\frac{\lambda}{\lambda_\epsilon}\right)+1\right]$$

where $\lambda\epsilon$ is the decay constant for electron capture, the decay constant for λ_β emission, $\lambda = \lambda_\epsilon + \lambda_\beta$, and constant C includes the factors for both the fraction of ^{39}Ar produced from ^{39}K and the fraction of ^{40}K in potassium.

The evaluation of ^{39}K to ^{39}Ar conversion factor is, however, not easy by direct methods. A monitor of known age is used for this purpose. The monitor sample is irradiated along with the sample so that both receive the same neutron fluence. The age of the unknown sample is then calculated from

$$T_u = \frac{1}{\lambda} \ln\left[\frac{\left(^{40}Ar_{rad.}/^{39}Ar_K\right)_u (e^{\lambda t_m} - 1)+1}{\left(^{40}Ar_{rad.}/^{39}Ar_K\right)_m}\right]$$

where subscripts u and m refer to the unknown and monitor samples respectively.

Table 2.3: Principal neutron reactions leading to the production of argon isotopes (after Brereton (1970)).

Target	Argon isotopes produced				
	^{36}Ar	^{37}Ar	^{38}Ar	^{39}Ar	^{40}Ar
Calcium	$^{40}Ca(n,n\alpha)$	$^{40}Ca(n,\alpha)$	$^{42}Ca(n,n\alpha)$	$^{42}Ca(n,\alpha)$ $^{43}Ca(n,\alpha)$ $^{43}Ca(n,n\alpha)$ $^{44}Ca(n,n\alpha)$	
Potassium			$^{41}K(n,\alpha)^{38}Cl\xrightarrow{\beta}$	$^{39}K(n,nd)$ $^{41}K(n,d)$ $^{39}K(n,p)$	$^{40}K(n,p)$ $^{40}K(n,d)$ $^{41}K(n,d)$
Argon	$^{36}Ar(n,\gamma)$	$^{40}Ar(n,nd)^{38}Cl\xrightarrow{\beta}$	$^{38}Ar(n,\gamma)$ $^{40}Ar(n,d)^{39}Cl\xrightarrow{\beta}$		
Chlorine	$^{36}Cl(n,\alpha)^{38}Cl\xrightarrow{\beta}$	$^{37}Cl(n,\gamma)^{38}Cl\xrightarrow{\beta}$			

The above equation is simplified by defining a quantity J as

$$J = \frac{e^{\lambda t_m} - 1}{(^{40}Ar_{rad}/^{39}Ar_K)_m}$$

The age equation can then be written as

$$T_u = \frac{1}{\lambda} \ln \left[J . (^{40}Ar_{rad}/^{39}Ar_K)_u + 1 \right]$$

The above age equation requires the determination of $^{40}Ar_{rad}/^{39}Ar_K$ ratio. If the only contaminants present were atmospheric argon, then $^{40}Ar_{rad}/^{39}Ar_K$ could be calculated from the measured $^{40}Ar/^{39}Ar$ and $^{36}Ar/^{39}Ar$ ratios using

$$\frac{^{40}Ar_{rad.}}{^{39}Ar_K} = \left(\frac{^{40}Ar}{^{39}Ar}\right)_m - \left(\frac{^{40}Ar}{^{36}Ar}\right)_{Atm} \left(\frac{^{36}Ar}{^{39}Ar}\right)_m$$

where atm and m refer to atmospheric and measured ratios, respectively.

However, several interfering argon isotopes are produced during the irradiation. These sources of interference have been discussed in detail by Mitchell (1968), Brereton (1970) and Turner (1971). Of the various possible reactions (Table 2.3) the following four reactions produce significant interferences

$^{40}Ca(n,n\alpha)^{36}Ar$

$^{42}Ca(n,\alpha)^{39}Ar$

$^{40}K(n,p)^{40}Ar$

$^{41}K(n,d)^{40}Ar$

Consequently, to determine the quantity $^{40}Ar_{rad}/^{39}Ar_K$ for use in the age equation, the $^{40}Ar/^{39}Ar$ ratio measured in the mass-spectrometer needs to be corrected for atmospheric, Ca- and K-derived Ar isotopes. The correction for Ca- and K-derived Ar isotopes is made using the fact that ^{37}Ar is also produced in the reactor by the $^{40}Ca(n,\alpha)^{37}Ar$ reaction.

If there were no Ca-derived ^{36}Ar then the only other component, besides the sample, would be atmospheric. However, part of ^{36}Ar is derived from ^{40}Ca and therefore this contribution is to be subtracted. Similarly, the ^{40}Ar generated by neutron reactions with potassium and ^{39}Ar generated by neutron reactions with Ca must be subtracted from measured $^{40}Ar/^{39}Ar$. After incorporating these corrections the expression for $^{40}Ar_{rad}/^{39}Ar_K$ becomes

$$\frac{^{40}Ar_{rad}}{^{39}Ar_K} = \frac{\left(\frac{^{40}Ar}{^{39}Ar}\right)_m - \left(\frac{^{40}Ar}{^{36}Ar}\right)_{Atm}\left[\left(\frac{^{36}Ar}{^{39}Ar}\right)_m - \left(\frac{^{36}Ar}{^{37}Ar}\right)_{Ca}\left(\frac{^{37}Ar}{^{39}Ar}\right)_m\right]}{1-\left(\frac{^{39}Ar}{^{37}Ar}\right)_{Ca}\left(\frac{^{37}Ar}{^{39}Ar}\right)_m} - \left(\frac{^{40}Ar}{^{39}Ar}\right)_K$$

where

$$\left(^{36}Ar/^{37}Ar\right)_{Ca}, \left(^{39}Ar/^{37}Ar\right)_{Ca}, \left(^{40}Ar/^{39}Ar\right)_K$$

are reactor constants related to the production of Ar isotopes from K and Ca. These constants are determined from analysis of high purity CaF_2 and K_2SO_4 irradiated along with the samples.

The ^{37}Ar produced from $^{40}Ca(n,\alpha)^{37}Ar$ is radioactive, with a half life of 35.1 days. Consequently, the measured $(^{36}Ar/^{37}Ar)_{Ca}$ and $(^{39}Ar/^{37}Ar)_{Ca}$ need to be corrected for

the decay of ^{37}Ar. The decay factor used for segmented irradiation of samples is given by

$$\text{Decay Factor} = \lambda \sum_{i=1}^{n} t_i \Big/ \left[\sum_{i=1}^{n} \left(1 - e^{-\lambda t_i}\right) e^{-\lambda t_i'} \right]$$

where t_i is the duration of irradiation of segment i, t_i' is the time elapsed since the cessation of irradiation segment i and the measurement of the sample. A segment of irradiation is preceded and followed by a reactor shut down or removal of sample for a brief period during which no production takes place.

2.2.3. EXPERIMENTAL DETAILS

A. IRRADIATION OF SAMPLES

Two reactors, namely, Apsara and Cirus, situated at BARC, Bombay, were available for the irradiation of samples for Ar-Ar work. Apsara is a light-water moderated reactor with total neutron flux of about $10^{12} n/cm^2 S$ with the fast flux representing about 10-15% of the total. Cirus is a heavy water moderated reactor with a total neutron flux of about $5 \times 10^{13} n/cm^2 S$ with flux at 5-10% of the total. Though Cirus has a higher total neutron flux than Apsara, the former is not suitable for the Ar-Ar irradiation because of its higher thermal neutron component which results in higher thermal neutron-produced Ar isotopes (Tetley et. al., 1980). The irradiations were therefore carried out mainly in the

Apsara despite its much smaller fast neutron flux (~ $1x10^{11}$ n/cmS) in the positions available for irradiation [Compare with $1.7x10^{13}$ n/cms in GSTR (Dalrymple et al 1981)]. This necessitated longer irradiation times, about two weeks, for adequate production of ^{39}Ar isotope. Compounded with the problem of low fast neutron flux is the large flux variation in the peripheral positions available for these experiments. Our initial results indicated that the neutron fluence variation in the irradiation can volume as determined by ^{58}Co activity of the irradiated Ni monitors, is about 25% in the vertical direction over a height of 5 cm and 8-20% in the horizontal direction over a distance of 2.5 cm. To take care of such a large variation in the fluence over the irradiation volume, in all subsequent experiments high purity Ni wire was included in each sample vial to determine the fluence seen by each sample relative to that of the monitor.

B. SAMPLE PREPARATION FOR IRRADIATION

For all our studies, fresh whole rock basalt chips were powdered in a stainless steel mortar and pestle to about 100-150 m size. About 500-700 mg aliquots of homogenised powders were used. For the first irradation a 18.70 $\pm$ 0.66 Ma (Kaneoka, 1980) old muscovite monitor was used. In all subsequent irradiations the 520.3$\pm$1.8 Ma Minnesota Hornblende-M Hb (Samson and Alexander, 1986) was used as the monitor.

The rock samples and monitor along with high purity

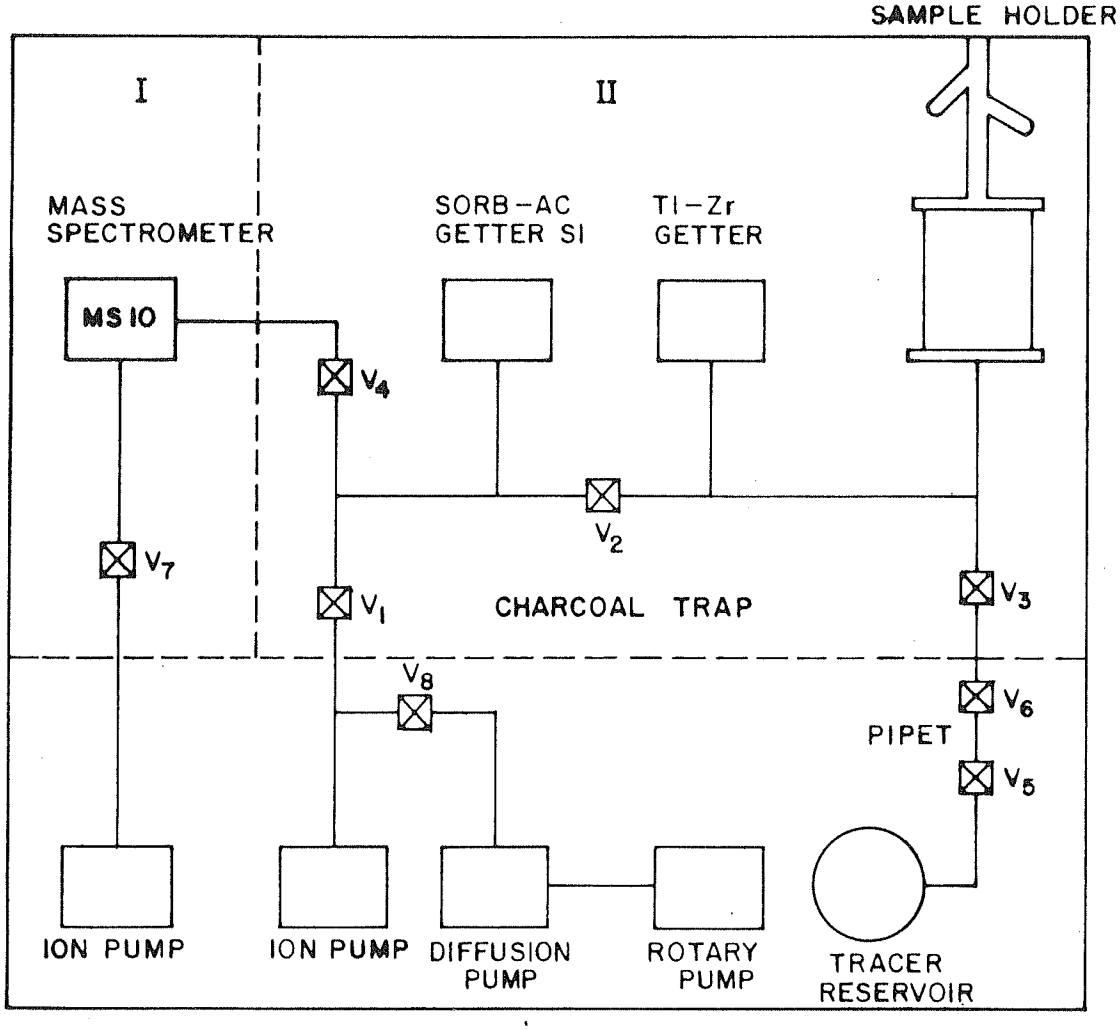


Fig. 2.1 SCHEMATIC OF THE COMPLETE MASS SPECTROMETER GAS EXTRACTION-PURIFICATION SYSTEM

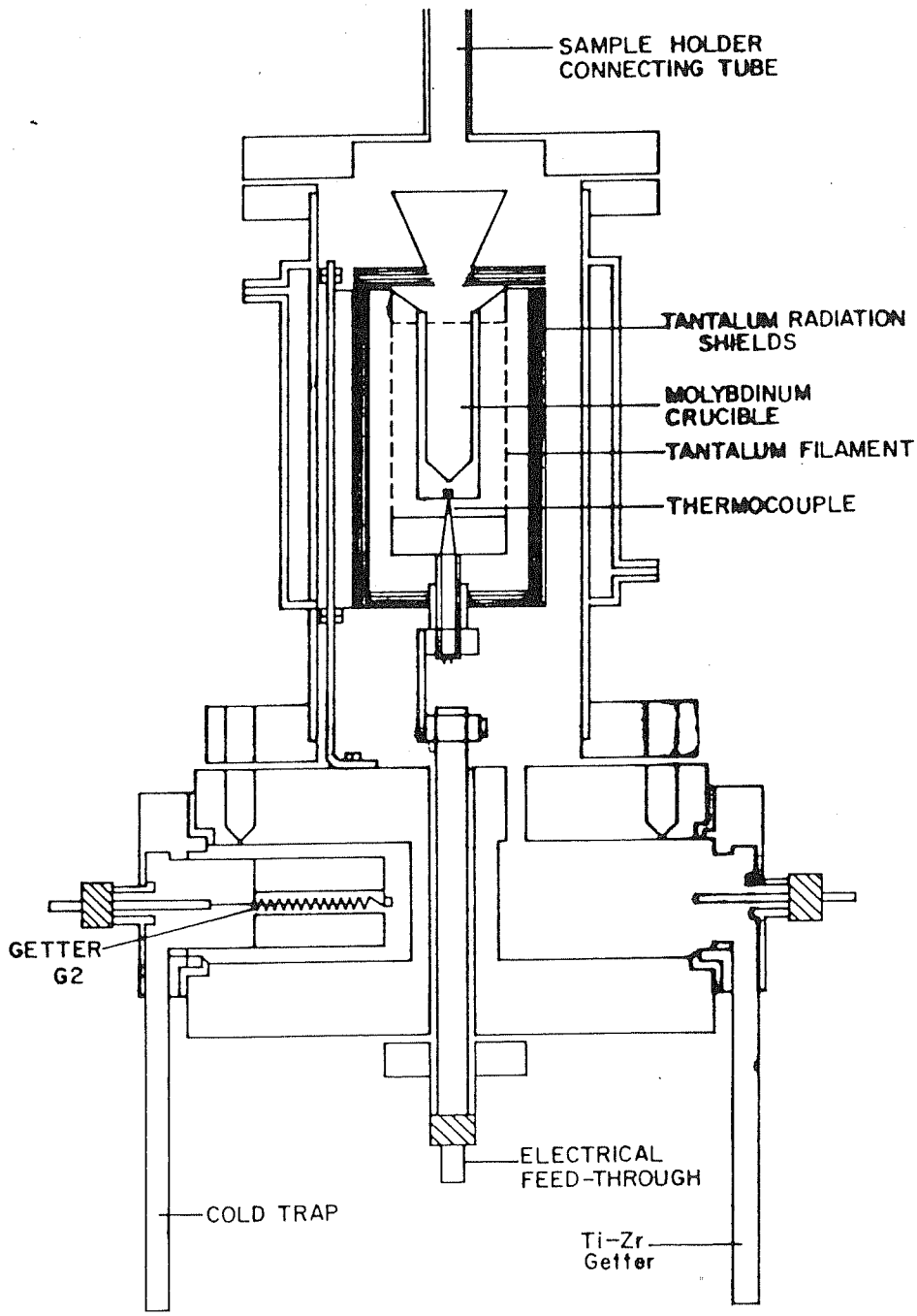


Fig. 2.2 SECTION TRROUGH GAS EXTRACTION FURNACE AND PURIFICATION LINE

CaF_2 and K_2SO_4 were taken in flat-bottomed quartz vials. Sample amounts were adjusted so that all samples stood at the same level, including the monitor, CaF_2 and K_2SO_4 so as to intercept the same fast neutron flux. This minimises the effect of vertical flux variation. To monitor the fluence variation, high purity Ni wire, of the same height as the sample, was placed in each vial.

Sample vials were sealed taking care to avoid overheating of samples. The sealed vials were then placed in an aluminium can and irradiated for two to three weeks.

The irradiated samples were allowed to 'cool' for a few weeks to reduce the activity of the samples for safe handling. Samples were then wrapped in aluminium foils and stored in the sample holder of the argon extraction system.

C. ARGON EXTRACTION AND PURIFICATION

Argon extraction and purification carried out in an all-metal, compact UHV furnace and purification system developed in our laboratory by Prof. Gopalan. Fig. 2.1 shows the schematic of the complete system.

The furnace of the extraction unit (fig. 2.2) consists of a molybdenum crucible electrically heated by a concentric, tantalum mesh filament surrounded by tantalum radiation shields in a stainless steel vacuum chamber. The temperature of the crucible is measured with a 95% Pt+5%Rh - 80%Pt+20%RH thermocouple. The temperature measurements are reliable to within 10^{o}-20^{o}C. A variac controlled transformer supplies current through the copper feed-through to the

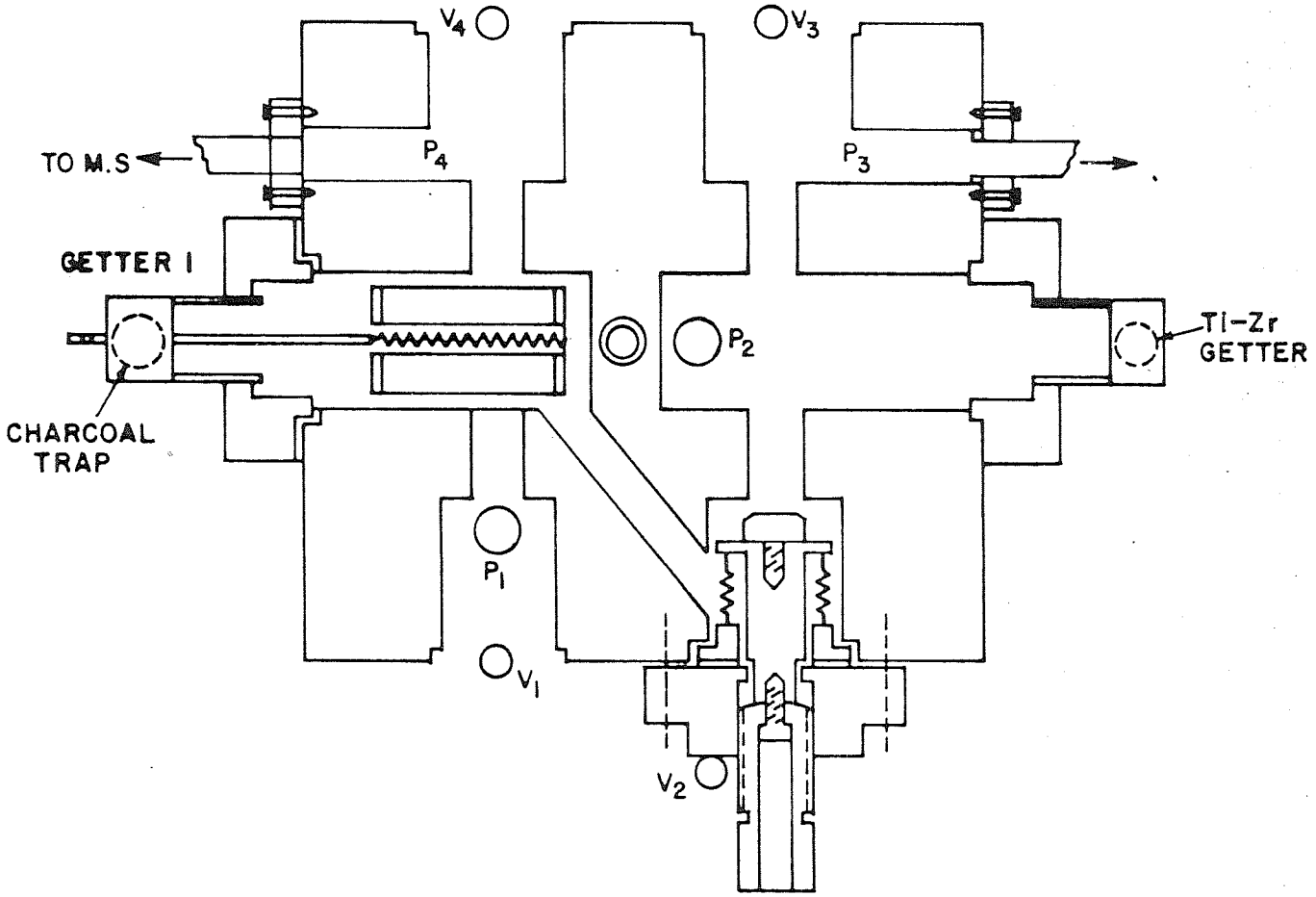


Fig. 2.3 MIDDLE SECTION OF THE SS-BLOCK WITH ONLY ONE VALVE ASSEMBLY SHOWN

heater raising the crucible to about 1500°C.Samples are dropped into the crucible from a glass sample holder connected to the top flange.

The gas purification system consists of four valves V_1-V_4 and two getter volumes, all interconnected and machined into a single rectangular stainless steel block. Middle section of this block is shown in fig. 2.3.

The furnace volume and the block are pumped through port P_1 of the valve V_1.Gas released from the crucible at any one temperature is continually cleaned by a Ti-Zr alloy getter at 800°C through port P_2.A tracer can be added to this gas, if required through port P_3 of valve V_3.The semi-cleaned gas, accumulated over about 40 min - typical duration of a temperature step - is transferred to the getter space G_2 by opening V_2 and with liquid nitrogen on charcoal trap. V_2 is closed after 15 minutes to raise the temperature for the next step.The gas is further purified in G2 by a SAES getter. It is then admitted into the mass-spectrometer after 10 minutes through port P_4 of valve V_4. After a brief equilibration period,V_4 is closed.V_1 is opened to pump out the remaining gas long before the next increment of gas is ready for second purification and mass-spectrometric analysis.

The experiment consists of degassing the sample at successively higher temperature steps, usually fifteen, beginning at 400°C until fusion.The monitors,K_2SO_4 and CaF_2 are however degassed in single step.The gas,in each step,is purified and then administered into a MS10S

Table 2.4: Typical Percentage of System Blanks (KB85-58).

Temperature ^{o}C	Ar-40 %
380	8.41
470	4.13
540	5.04
605	4.54
670	5.62
740	7.07
770	2.96
820	2.27
870	2.70
900	3.67
1000	2.94
1060	6.18
1135	5.19
1310	12.56
1410	36.51

PRINTED IN INDIA

OmniScribe

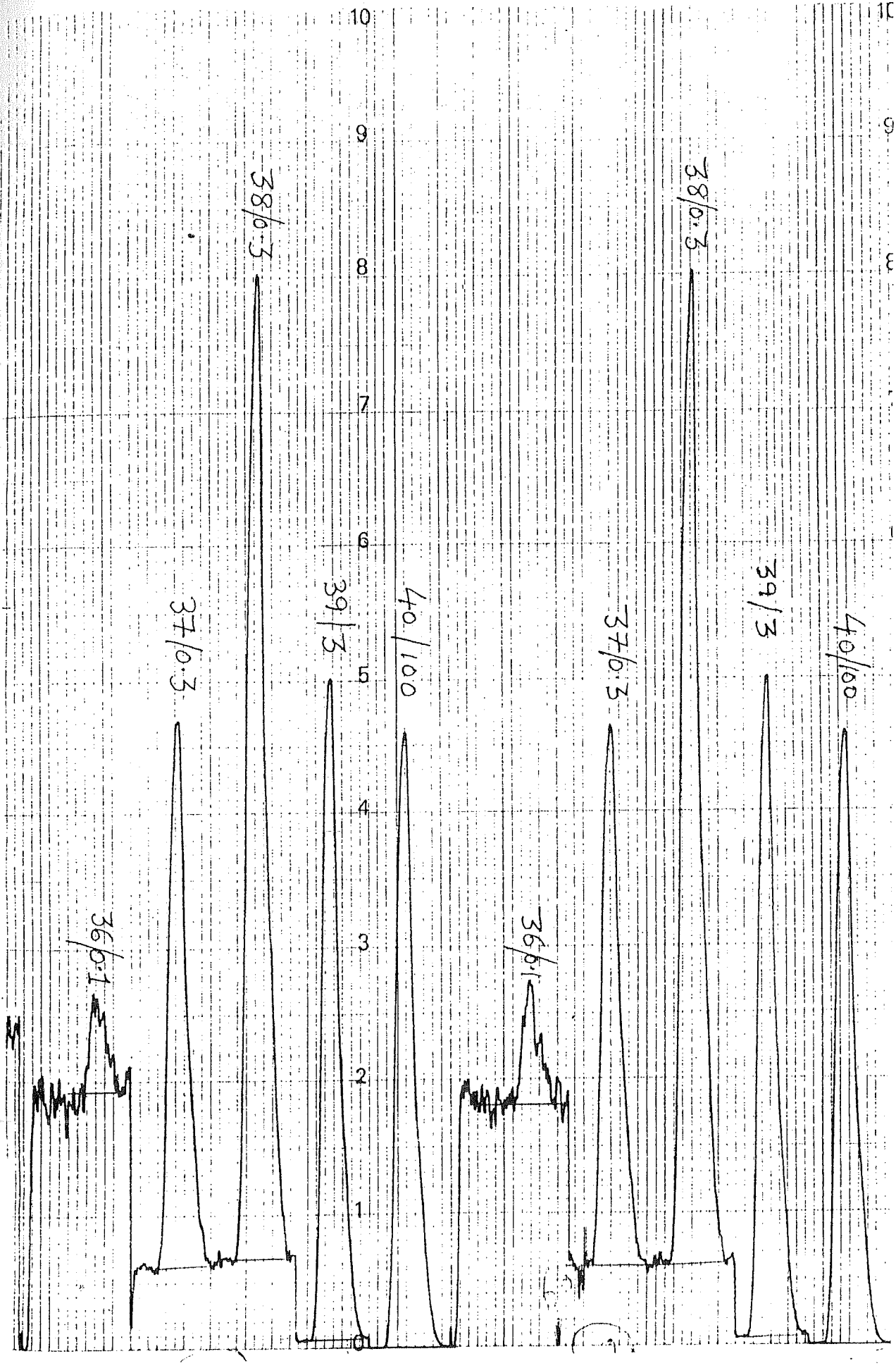


Fig. 2.4 Typical Argon spectrum.

mass-spectrometer operated in the static mode.Using voltage scanning, the ion currents at masses 40,39,38,37 and 36 are sequentially recorded on a chart paper (fig. 2.4).Peak heights and relative timing of peak measurements from the time of sample introduction are used for a curve-fit routine (Bevington, 1969) to compute the required isotopic ratios corresponding to zero time.

Each sample was preceded and followed by system blank measurement. System-blanck estimation consists of measuring the argon concentration at every temperature step by following the same procedure as for samples but without any sample in the crucible.

The absolute ^{40}Ar blanks during the present work were about $1x10^{-8}$cc STP for the 1500°C step,comparable with the blanks in a similar extraction system (Turner,1972).The blank contributions to the sample gas were very small for temperatures upto about 1200°C,varying from 2 to 10% of the ^{40}Ar signal but increase to about 20% and occasionally to 40% in the fusion step (Table 2.4).

Mass discrimination corrections were determined based on analysis of air argon. Errors were computed by quadratically compounding errors from statistics,blanks and interfering isotopes. Errors for apparent ages include the error in J but the error boxes (2σ level) in age spectra plots do not include the error in J (Roddick et al. 1980). Isochron ages were obtained by linear regression (Williamson, 1968) of data points corresponding to plateau steps. The plateau ages are weighted means of the apparent

Table 2.5 Irradiation parameters for the eight irradiations

IRRN #	$(36/37)_{Ca}$	$(39/37)_{Ca}$	$(40/39)_{K}$
2 (Apsara)	0.000347	0.000818	0.098230
3(Apsara)	0.000289	0.000451	0.034309
4 (Cirus)	0.000362	0.000892	0.568640
5 (Cirus)	0.000386	0.000770	0.438320
6 (Apsara)	0.000283	0.000672	0.021111
7 (Apsara)	0.000213	0.000688	0.044450
8 (Apsara)	0.000385	0.000581	0.023867

ages of steps forming the plateau.the total or integrated age is computed by summing the isotopic computations of all temperature fractions.

2.2.4. RESULTS

During our preliminary studies,using Apsara (and Cirus when Apsara was shut down due to technical reasons) basalt samples from different elevations of the thickest exposed Deccan lava sequence at Mahabaleshwar were analysed. Replicate samples were measured over seven different irradiations - five in Apsara and two in Cirus - to check the reproductivity of results.

All the irradiations were carried out in different reactor positions and for varying duration ranging from two to three weeks. Consequently, for each irradiation, the reactor constants $(36/37)_{Ca}$, $(39/37)_{Ca}$ and $(40/39)_{K}$ were determined. Table 2.5 details the variation in these parameters during the seven irradiations. For Apsara, $(36/37)_{Ca}$ vary by 44.7% and 44.9% respectively and $(40/39)_{K}$ exhibit a much larger variation of about 73%.The $(36/37)_{Ca}$ and $(39/37)_{Ca}$ in Cirus are comparable with Apsara whereas $(^{40}Ar/^{39}Ar)K$ values are much higher. The much larger variation in K produced $(^{40}Ar/^{39}Ar)$ ratio is probably due to large thermal neutron flux variations (Tetley et. al., 1980).

Results on only five samples are reported at this stage to illustrate the quality and reproductivity of ^{40}Ar-^{39}Ar data. Three of these samples, namely MB81-1/1,MB81-3 and

Table 2.6. Argon Isotopic Composition and Apparent Ages of MB81-1/1

Sample No.	Step Temp. °C	36-Ar 39-Ar	37-Ar 39-Ar	40-Ar 39-Ar	Cumulative release of 39-Ar%	Apparent age (Ma)
MB81-1/1 50m above Mean Sea Level	400	0.6974 0.0008	88.50 0.09	202.89 1.83	1.4	64.5 1.2
	450	0.0357 0.0008	17.27 1.09	20.18 1.09	6.9	154.7 0.2
	500	0.0094 0.0004	7.32 0.36	9.56 0.04	21.4	103.9 1.8
	550	0.0078 0.0002	13.20 0.05	5.15 0.04	35.6	56.7 1.1
	650	0.0054 0.0005	17.84 0.65	4.67 0.06	45.5	65.5 2.5
	700	0.0029 0.0004	6.42 0.30	5.23 0.05	57.6	70.1 1.7
	750	0.0045 0.0003	9.48 0.18	5.40 0.04	73.0	69.3 1.3
	800	0.0038 0.0004	9.24 0.96	5.27 0.08	81.6	70.0 2.4
	850	0.0056 0.0008	13.96 0.56	5.52 0.13	87.2	72.0 3.0

Table 2.6 contd.

950	0.0131 0.0012	20.11 1.33	6.23 0.30	90.6	58.4 6.6
1100	0.0174 0.0014	26.40 0.72	5.74 0.39	94.3	41.0 8.3
1300	0.0998 0.0022	151.31 1.21	19.66 0.67	100.0	47.2 1.4

$J = 0.0080 \pm 0.0001$

Table 2.7. Argon Isotopic Compositions and Apparent Ages of MB81-1/2

Sample No.	Step Temp. °C	36-Ar 39-Ar	37-Ar 39-Ar	40-Ar 39-Ar	Cumulative release of 39-Ar%	Apparent age (Ma)
MB81-1/2 5·0m above Mean Sea Level	400	0.0741 0.0025	1.69 0.22	32.21 0.08	1.9	112.2 7.9
	450	0.0126 0.0005	1.55 0.06	11.29 0.02	12.8	82.0 1.6
	500	0.0045 0.0001	2.16 0.01	7.51 0.02	25.4	67.5 0.3
	550	0.0044 0.0002	3.75 0.04	7.29 0.01	40.8	67.6 0.1
	650	0.0079 0.0002	9.01 0.02	3.18 0.02	58.7	73.1 0.6
	700	0.0025 0.0003	6.42 0.02	6.69 0.01	73.9	70.7 0.9
	750	0.0039 0.0003	9.67 0.01	6.59 0.1	86.3	69.4 1.0
	800	0.0051 0.0007	11.64 0.14	6.71 0.03	91.7	69.4 2.3
	850	0.0084 0.0010	14.15 0.14	8.01 0.05	94.5	76.3 3.5

13934

Table 2.7 contd.

950	0.0108 0.0003	24.29 0.09	6.87 0.08	97.1	69.1 1.4
1300	0.0678 0.0014	114.32 0.52	13.96 0.15	100.0	81.1 5.3

$$J = 0.0064 \pm 0.0001$$

Table 2.8. Argon Isotopic Composition and Apparent Ages of MB81-3

Sample No.	Step Temp. °C	36-Ar 39-Ar	37-Ar 39-Ar	40-Ar 39-Ar	Cumulative release of 39-Ar%	Apparent age (Ma)
MB81-3 225m above Mean Sea Level	400	0.1076 0.0025	3.69 0.02	34.01 0.04	2.1	31.5 9.3
	500	0.0095 0.0005	1.54 0.02	4.85 0.2	7.1	27.2 1.8
	600	0.0029 0.0002	1.84 0.02	6.55 0.05	23.2	72.7 0.9
	650	0.0023 0.0002	2.53 0.01	5.99 0.01	39.2	68.5 0.6
	700	0.0030 0.0002	4.44 0.04	5.70 0.01	52.8	64.8 0.8
	750	0.0021 0.02	4.81 0.02	5.57 0.01	66.5	66.7 0.8
	800	0.0022 0.0003	4.78 0.03	5.61 0.01	75.7	66.8 0.9
	850	0.0019 0.0001	4.35 0.03	5.71 0.03	83.0	68.5 0.6
	900	0.0029 0.0003	4.48 0.02	5.80 0.02	88.3	66.3 1.1

Table 2.8 contd.

1000	0.0057 0.0004	4.41 0.05	5.74 0.02	93.8	55.1 1.6
1100	0.0261 0.0009	67.79 0.58	5.80 0.04	97.0	49.8 3.6
1300	0.0602 0.0013	94.87 0.19	12.99 0.35	100.0	43.0 6.8

$$J = 0.0071 \pm 0.0001$$

Table 2.9. Argon Isotopic Composition and Apparent Ages of MB81-10

Sample No.	Step Temp. °C	36-Ar 39-Ar	37-Ar 39-Ar	40-Ar 39-Ar	Cumulative release of 39-Ar%	Apparent age (Ma)
MB81-10 580m above Mean Sea Level	400	0.0512 0.0009	1.46 0.05	15.29 0.07	6.8	3.2 3.6
	500	0.0184 0.0003	2.14 0.03	8.14 0.03	19.9	35.8 1.1
	600	0.0067 0.0010	6.15 0.02	6.53 0.02	44.4	63.3 0.4
	650	0.0046 0.0001	9.11 0.02	5.66 0.02	62.8	63.4 0.6
	700	0.0066 0.0001	17.75 0.22	5.69 0.03	74.2	65.7 0.5
	750	0.0062 0.0001	12.36 0.04	5.64 0.04	81.1	60.9 0.5
	800	0.0081 0.0002	13.96 0.07	5.76 0.04	85.4	57.2 0.9
	850	0.0084 0.0004	15.79 0.05	5.79 0.07	89.2	58.3 1.7
	900	0.0113 0.0003	19.16 0.04	6.34 0.13	91.5	58.4 1.9

Table 2.9 contd.

1000	0.0217	28.89	7.01	93.7	38.7
	0.0017	0.06	0.23		7.1
1100	0.0610	164.79	6.85	96.8	39.2
	0.0013	0.64	0.20		5.8
1300	0.2428	147.95	67.72	100.0	113.8
	0.0066	0.38	1.68		33.0

$$J = 0.0071 \pm 0.0001$$

Table 2.10. Argon Isotopic Composition and Apparent Ages of MB81-24.

Sample No.	Step Temp. °C	36-Ar 39-Ar	37-Ar 39-Ar	40-Ar 39-Ar	Cumulative release of 39-Ar%	Apparent age (Ma)
KB81-24	400	0.0183	2.58	10.27	3.5	49.9
1250m		0.0007	0.19	0.08		2.4
above						
Mean	450	0.0069	3.43	8.03	11.5	62.8
Sea		0.0003	0.12	0.04		0.9
Level						
	500	0.0054	5.09	7.62	21.4	65.1
		0.0005	0.65	0.03		1.8
	550	0.0044	6.42	7.11	32.5	64.4
		0.0001	0.11	0.03		0.5
	650	0.0044	8.36	6.90	45.7	64.6
		0.0001	0.05	0.02		0.3
	700	0.0052	8.98	6.70	56.1	60.9
		0.0001	0.12	0.04		0.6
	750	0.0051	11.67	6.66	70.1	64.1
		0.0001	0.04	0.03		0.4
	800	0.0078	14.20	6.82	78.5	60.5
		0.0001	0.12	0.02		0.5
	850	0.0091	13.69	7.65	85.4	64.5
		0.0002	0.10	0.04		0.7

Table 2.10 contd.

950	0.0225	26.08	8.99	89.7	52.7
	0.0001	0.17	0.06		3.2
1100	0.2252	112.76	62.84	97.1	99.9
	0.0038	0.16	0.27		12.9
1300	0.4666	78.41	133.10	100.0	42.3
	0.0125	4.93	2.83		42.1

$$J = 0.0059 \pm 0.0001$$

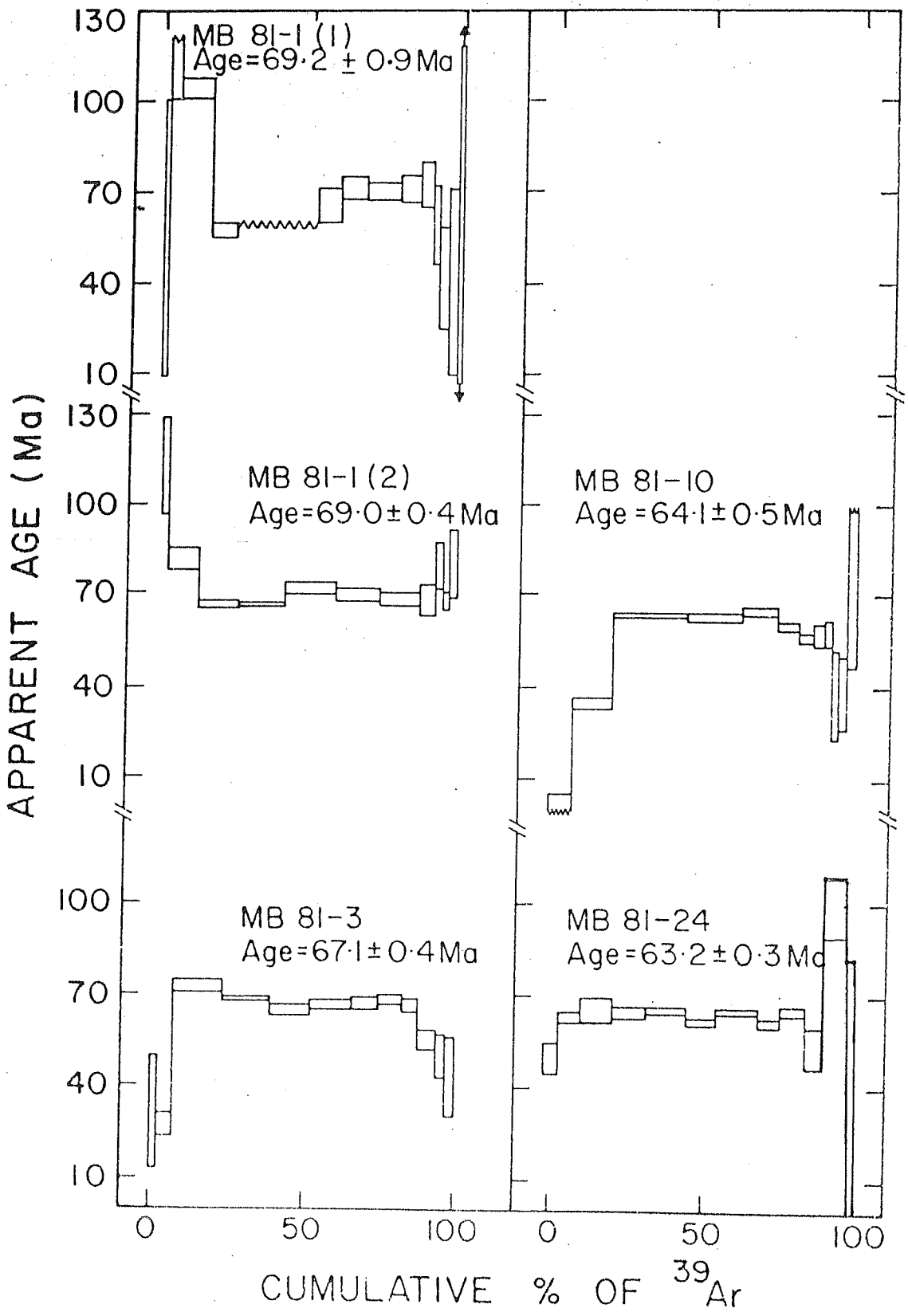


Fig. 2.5 Age spectra of four samples from different elevation of the Mahabaleshwar section of the Deccan Province.

MB81-10 were irradiated in one batch in Apsara reactor whereas the other two,MB81-1/2 and MB81-24 were irradiated together in Cirus.For both these irradiations the 520.3±1.8 Ma Minnesota Hornblende monitor and replicate sample (MB81-1/1 and MB81-1/2) were used. The J values for the three samples irradiated in Apsara varies from 0.0070 to 0.0080 and for those irradiated in Cirus it varies from 0.0059 to 0.0063 .

The argon isotopic compositions and abundances of these samples are given in Tables 2.6 and 2.10.Their age spectra are shown in fig.2.5. For sample MB81-1/1,irradiated in Apsara, 600^{o}C fraction was lost due to experimental failure. For this fraction the ^{39}Ar was computed using the ^{39}Ar/K.J values of MB81-3 and MB81-10.

The release curves for all the five samples shown good plateaus within experimental errors (2σ) comprising more than 50% of ^{39}Ar released.The plateau ages corresponding to these plateau regions are 69.2±0.9 Ma,69.0±0.4 Ma,67.1±0.4 Ma,64.1±0.5 Ma and 63.2±0.3 Ma for MB81-1/2,MB81-1/2,MB81-3, MB81-10 and MB81-24,respectively.

These plateau ages are consistent with the flow stratigraphy (Tables 2.6-2.10),varying from 69.2±0.4 Ma for the lowest elevation sample to 63.2±0.3 Ma for the highest elevation one. Also replicate analyses of MB81-1 in two different reactors are in excellent agreement.These results demonstrate that satisfactory Ar-Ar ages can be obtained on basalt samples using our system.

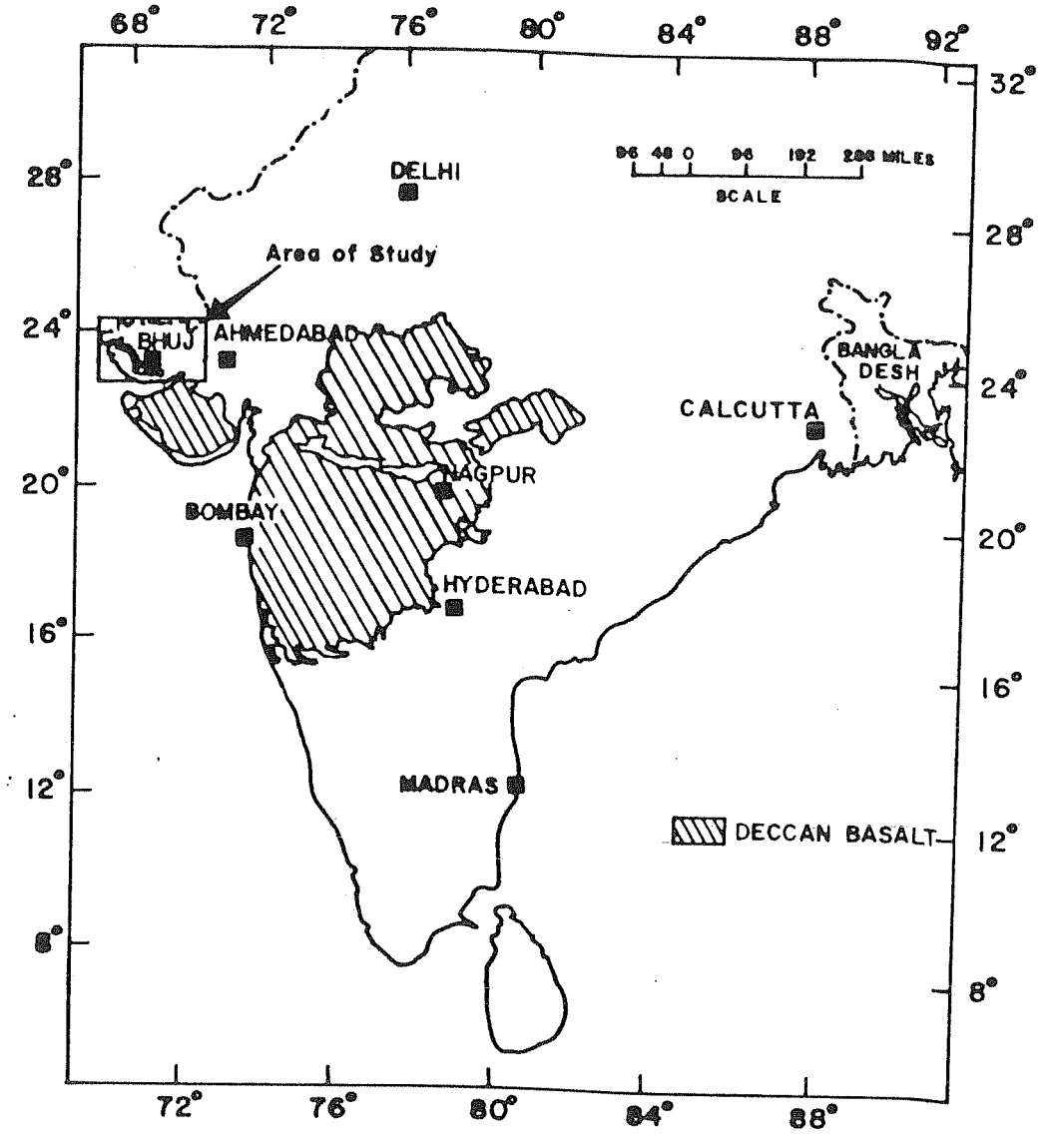


Fig. 3.1 Map of India showing the Deccan Traps and area of study.

CHAPTER III

FIELD, PETROGRAPHIC, CHEMICAL AND GEOCHRONOLOGICAL STUDIES

3.1 INTRODUCTION

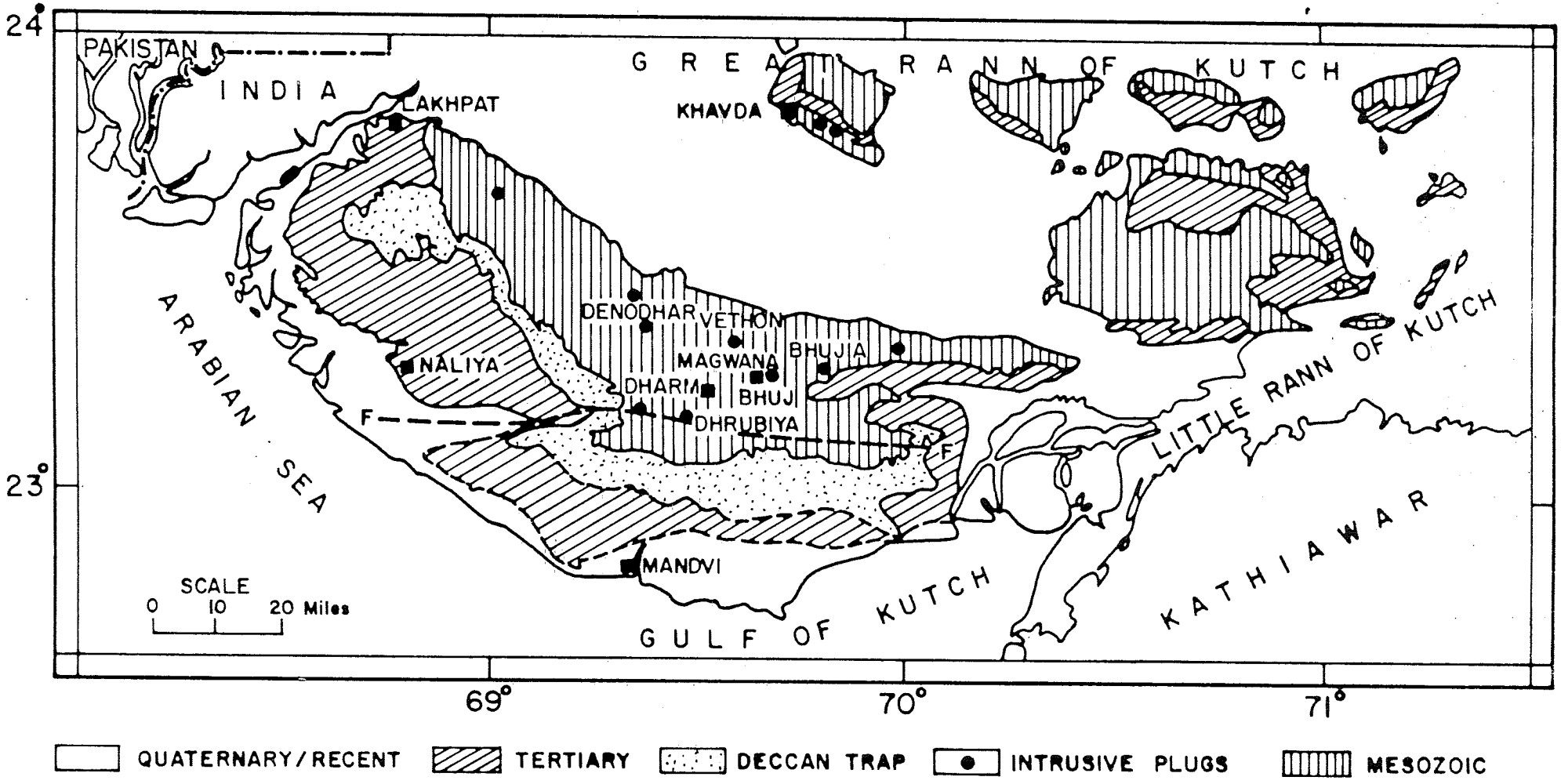
The Deccan Traps presently cover about 500,000 km^2 of the Indian subcontinent and are predominantly tholeiitic in composition. Besides their occurrence in the western and central parts of Peninsular India, where they form a vast plateau, the Deccan lavas of tholeiitic composition also outcrop as isolated patches in Saurashtra and Kutch in Gujarat state (Fig.3.1). Bowen (1927) first reported nephelinite basalt from Kutch. The occurrence of alkali basalts hosting peridotite nodules from Kutch was first reported by De (1964) and in a subsequent work (De,1981) he demonstrated the presence of different magma types, such as tholeiites, alkali olivine basalts and olivine nephelinites from this region. He suggested that these alkaline magmas represent the closing phases of the predominantly

tholeiitic Deccan activity.Published information pertaining to the peridotite nodules and host basalts were,however, brief and generalised. Details regarding their exact locations, mode of occurrence, petrography and mineralogy were lacking. This being the only area in the Deccan Basaltic Province where such nodules have been reported and considering that the occurrence of xenolith bearing basalts in continental flood basalt provinces is rare,(the only other report being from the Patagonian Plateau Basalts, Brazil), it is surprising that these nodules remained unstudied for almost twenty years until this work was initiated in 1983.

The first phase of my work involved a reconaissance survey of most of the Kutch Peninsula with Dr. P. Krishnamurthy to identify target areas for intensive search for alkali basaltic plugs and nodules. The area covered (about 200 km across) falls between latitude $23^{o}2' - 23^{o}26'$ N and longitude $69^{o}13' - 69^{o}45'$ E represented in the survey of India toposheets. 41-E/2, 3, 6, 7,8,10,11 and 12 and is easily approachable from Bhuj by road.

Though the alkali basalt plugs form prominent hills in the low-lying landscape there are quite a few hills composed of only sedimentary rocks. However, it was soon realised that the alkali basalt bodies are or were being quarried for construction or road material.This observation helped us greatly in locating many alkali basalt bodies.A

Fig. 3.2 GEOLOGICAL MAP OF KUTCH, WESTERN INDIA
(MODIFIED AFTER BISWAS 1970)



generalised geologic map,based on our reconnaissance survey and published work by Biswas (1970) is given Fig. 3.2.

Our initial efforts helped us to narrow down the area for detailed investigation to about 30km across,around Bhuj and Magwana, where most of alkaline bodies are exposed. Identification and collection of ultramafic nodules was, however, not very successful. We collected a few weathered samples which were suspected to be spinel peridotites. Preliminary studies by Dr. Krishnamurthy at Scripps Institution of Oceanography confirmed that while a few were in fact upper mantle derived nodules,there were also some dunites probably of cognate origin (Krishnamurthy et al. 1988)

3.2 FIELD RELATIONS

Detailed fieldwork was carried out subsequently with a view to identify the nodule bearing alkali basalt bodies and to study their (alkali basalt) field relationship with the surrounding country rocks.Alkali basalts which host the spinel peridotite nodules occur as plugs or sheet like bodies at Bhujia, Dhrubiya and Vithon hills and dunites occur at Dharam and Dhenodhar and intrude flat lying to gently dipping Jurassic sandstones. All these five bodies are fairly well exposed because of quarrying for road material. While Dhrubiya, Dharam,Dhenodhar and Vethon hills are easily accessible and are currently being mined,the

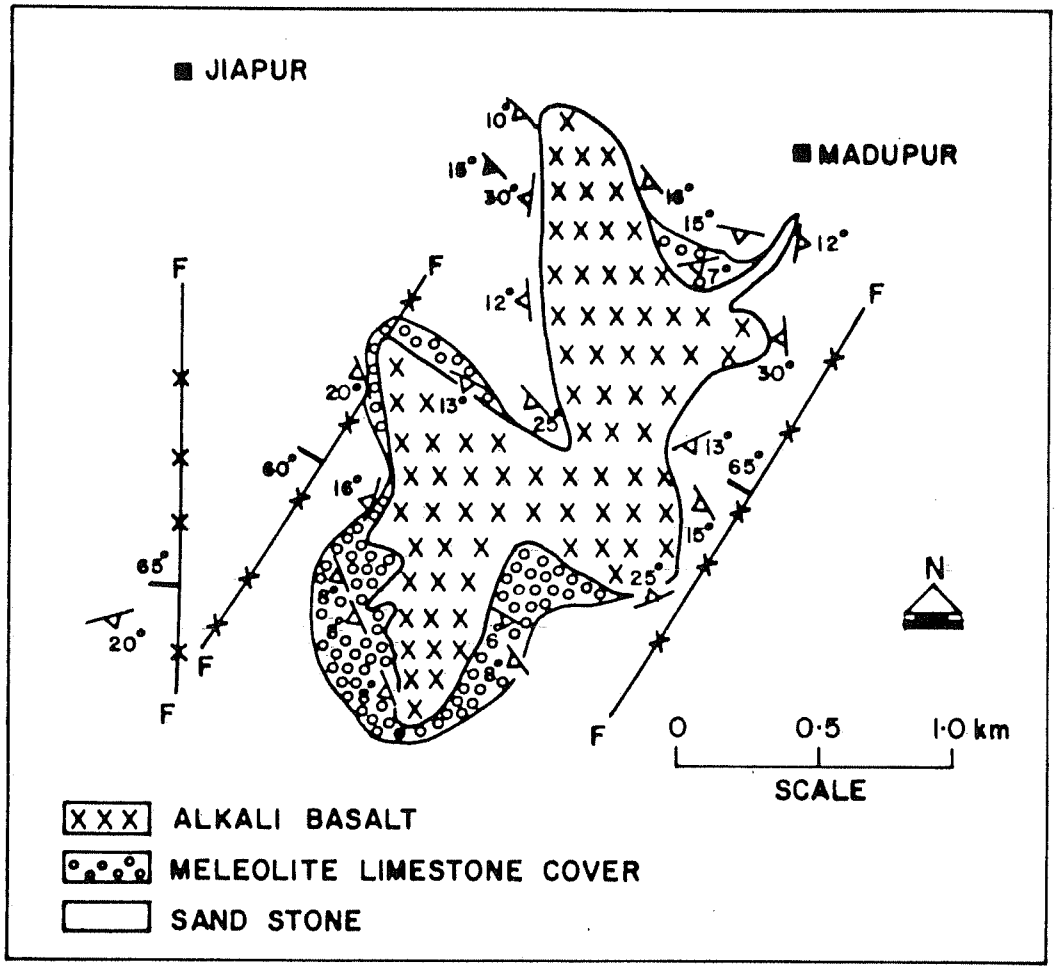


Fig. 3.3 GEOLOGIC MAP OF DHRUBIYA HILL

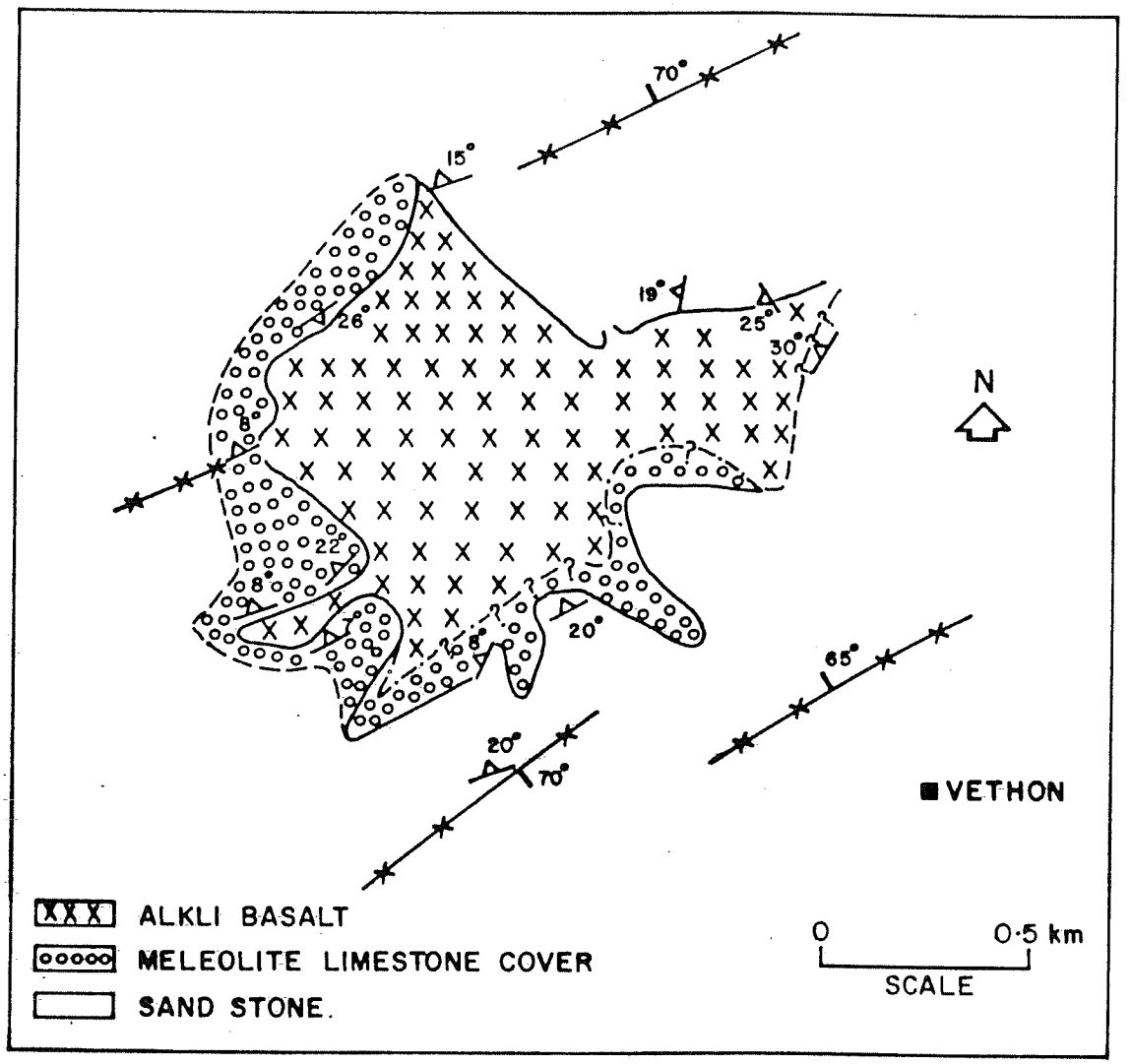
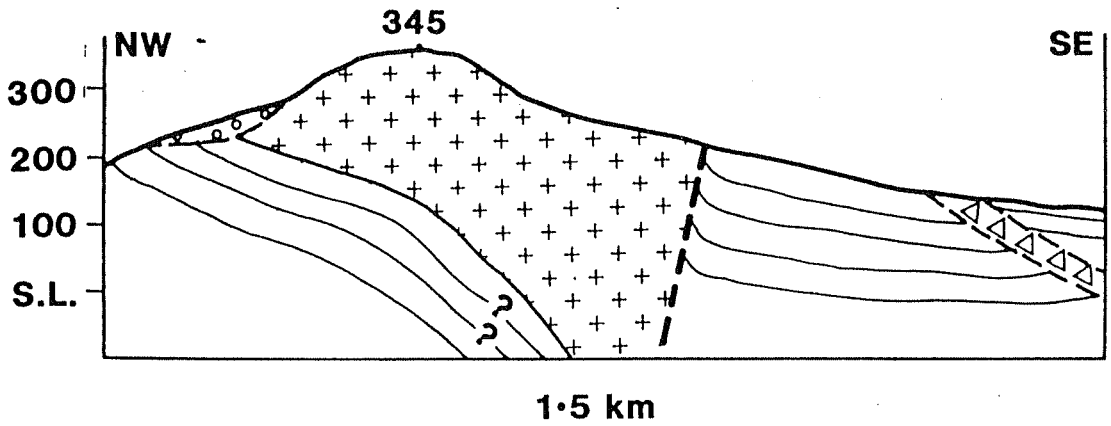
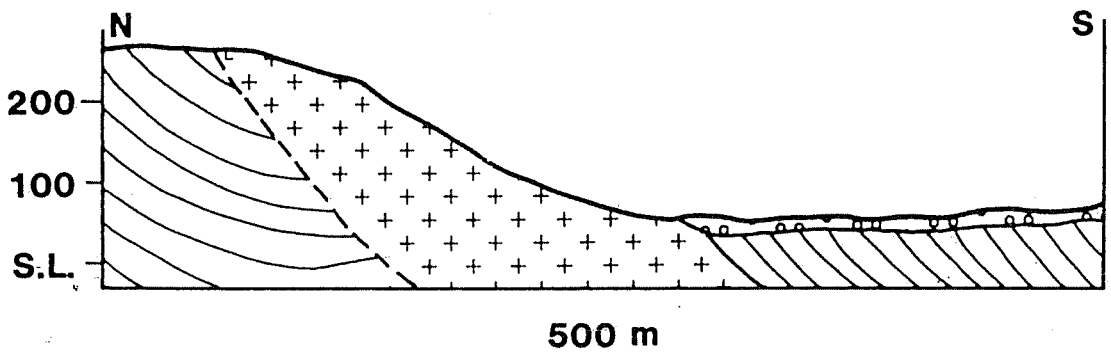


Fig. 3.4 GEOLOGIC MAP OF VITHON HILL

A. DHRUBYA HILL



B. BHUJIA HILL



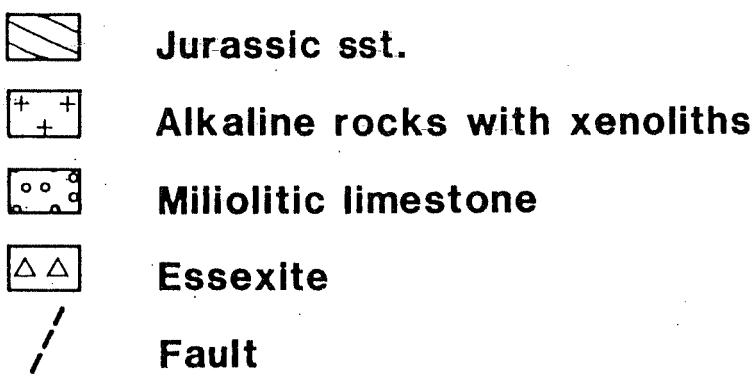


Fig. 3.5 Generalised geological cross-section of Dhrubiya and Bhujia hills.

Bhujia hills have been closed to public due to military presence. The geologic maps of Dhrubiya and Vethon hills are shown in Fig. 3. 3 and 3.4 and the generalised geologic crossection for Bhujia and Dhrubiya,hills is given in Fig. 3.5. The contact zones between the alkali basalt bodies and the sandstones which they intrude in many places are concealed by an overlying apron of Tertiary meliolitic limestone. But at places where the contacts are exposed,like in Dhrubiya and Vethon hills, the Jurassic strata are upturned, exhibiting steep dips and have become quartzitic with intricate veining of silica. Both at Dhrubiya and Vethon, which are spinel peridotite bearing localities,and at Dhram which is a dunite bearing body,there are prominent NE - SW fracture zones in the Jurassic sandstones bordering these intrusive bodies. These fractures may be related to the en-echelon pattern of emplacement of some of the sheet like occurrences like at Dharam and Vethon hills.In all these alkaline bodies there is evidence for both explosive and relatively quiescent volcanism.At Dhrubiya and Vethon hills, for example, there are occurrences of zeolitised volcanoclastic rocks comprising fragments of basic rocks, spinel peridotite xenoliths and Jurassic sandstones in a tuffaceous matrix. At Bhujia,Vethon and Dharam hills these alkaline bodies have well developed prominent columnar joints and amygdaloidal horizons which suggest surface or near surface lava flow.

The relation between these alkali basalt bodies and the Deccan tholeiites cannot be evaluated in the field as these

two are nowhere seen in contact. The nearest tholeiite outcrop is some 30 Km to the south.Precise ^{40}Ar-^{39}Ar dating of these alkali basalts and tholeiites from this area was carried out to determine their temporal relationship.

3.3 MODE OF OCCURRENCE OF NODULES:

Spinel peridotite nodules were found in the alakaline rocks at Dhrubiya, Vethon and Bhujia hills whereas dunites of a probable cognate origin were collected from Dharam.In all the cases the nodules are small,averaging only 1-2 cm in diameter,although a few larger xenoliths,upto about 4 cm in diameter were recovered from Bhujia and Dhrubiya hills. The spinel peridotites are subangular to rounded or elongated and both granular and non granular types.The non-granular types tend to exhibit preferred mineral orientation. At two places, Bhujia and Dhrubiya hills,the nodules show a preferential concentration:at Bhujia hill, they are concentrated in the central part of the sheet like intrusion with the long axis oriented parallel to the strike of the body,and at Dhrubiya there is a preponderance of nodules at the lower or neck levels of the plug compared to the upper portions. These observations refer only to xenoliths larger than about 0.5 to 1 cm;below this size it is difficult to distinguish between phenocrysts and the xenoliths in the field.

3.4 PETROGRAPHY AND TEXTURE OF NODULES:

Thin section, grain mount and electron microprobe studies of these nodules show that there are two types: dunites and peridotites/lherzolites.

The dunites which occur at Dharam hill and Dhenodhar are comprised wholly of olivines with very minor opaques and scarce clinopyroxenes. The olivines show undulose extinction and/or strain shadows and exhibit fluid inclusions. Microprobe analyses (Fig. 3.6) show them to be iron rich averaging Fo_{79} and distinct from those found in the spinel peridotite. Their iron rich compositions are similar to those found in host basalts (Table 3.1,Fig. 3.6). Some of the olivine crystals of nodules are jacketed by clinopyroxenes which show strong marginal zoning. These features result from reaction of olivines with the host alkalic liquid. The close similarity of the olivine compositions of the nodules and host rocks strongly suggests that they are most probably cognate.

The spinel peridotites, on the other hand,are closely analogous to mantle derived nodules found in alkali basalts from southwestern U.S.,central Europe,eastern and southern Africa, southern Australia amongst others (Boyd and Meyer, 1979;Menzies,1983;Hawkesworth et al.,1983).

The spinel peridotites can be divided into the two

textural classes of Mercier and Nicolas (1975) and Harte (1977) (i) Equigranular or tabular granuloblastic and (ii) Porphyroclastic. The former have grain sizes generally less than 1 mm and show feeble mineral orientation whereas the latter have large (3-4 mm) olivine and orthopyroxene crystals showing marginal granulation The porphyroclastic variety sometimes has regions of roughly equigranular texture suggesting an affinity with the equigranular types.

The small size and relative rarity of nodules in Kutch basalts precluded a meaningful evaluation of mineral modes. However, a qualitative abundance estimate is olivine > orthopyroxens > clinopyroxene > spinel.Spinel occurs only in rather small amounts along intercrystal boundaries.No other minerals could be seen in all the nodules during the course of this study.They can be classified as Cr-diopside group of Wilshire and Shervias (1975) Group I of (Frey and Prinz,1978) and Type I (Menzies,1983).

3.5 MINERAL COMPOSITIONS

3.5.1.SPINEL PERIDOTITES

The representative major element chemistry of the various phases from the nodules is given in Tables 3.1 to 3.4 and compositional variations are presented in Figs. 3.6 to 3.8. Mineral compositions were determined using a Cameca electron microprobe at the Scripps Institution of

Table 3.1. Representative Major Element Composition of Olivines in the Nodules and Basalts from Kutch.

Oxide Wt.%	BHUJ-A	BHUJ-B	BHUJ-E	BN-1	DHRUB -A	DHRUB -B	KB83-11	KB83-11
SiO_2	40.51	40.38	40.69	40.52	40.56	38.96	40.38	40.69
TiO_2	0.02	0.01	0.02	0.02	0.03	0.07	0.01	0.02
Al_2O_3	0.00	0.01	0.00	0.00	0.01	0.01	0.00	0.00
Cr_2O_3	0.01	0.01	0.02	0.02	0.03	0.02	0.01	0.02
FeO	9.09	10.08	10.28	10.54	9.16	18.90	10.08	10.28
MnO	0.13	0.04	0.17	0.17	0.14	0.35	0.04	0.17
MgO	50.11	48.98	49.25	49.78	50.27	42.51	48.98	49.25
CaO	0.04	0.05	0.11	0.03	0.03	0.24	0.05	0.11
Na_2O	0.00	0.00	0.00	0.00	0.00	0.02	0.00	0.00
K_2O	0.01	0.00	0.00	0.01	0.01	0.00	0.00	0.00
NiO	0.30	0.35	0.28	0.29	0.28	0.19	0.35	0.28
Total	100.29	99.91	100.83	101.41	100.54	100.29	99.91	100.89
Fo	90.4	89.3	89.1	88.96	90.35	79.08	89.30	89.11
Fa	9.6	10.7	10.9	11.04	9.65	20.92	10.70	10.89

Table 3.1 contd.

Oxide Wt.%	KB85-54	KB83-11	KB83-11	KB83-11	KB83-13	KB83-16	KB83-17
SiO_2	38.52	38.66	38.69	38.52	38.64	38.86	39.40
TiO_2	0.04	0.01	0.08	0.00	0.03	0.04	0.04
Al_2O_3	0.00	0.00	0.02	0.00	0.01	0.03	0.02
Cr_2O_3	0.04	0.00	0.05	0.01	0.03	0.01	0.03
FeO	19.45	19.04	19.31	18.52	19.17	19.02	16.36
MnO	0.08	0.12	0.07	0.14	0.09	0.33	0.25
MgO	40.91	41.60	41.48	41.94	41.23	42.16	44.31
CaO	0.49	0.11	0.42	0.11	0.33	0.29	0.26
Na_2O	0.00	0.00	0.00	0.00	0.00	0.03	0.00
K_2O	0.00	0.00	0.00	0.00	0.00	0.01	0.01
NiO	0.10	0.22	0.12	0.27	0.14	0.15	0.19
Total	99.63	99.77	100.23	99.56	99.68	100.93	100.91
Fo	78.79	79.29	79.14	79.80	79.09	79.39	82.41
Fa	21.29	20.71	20.86	20.20	20.91	20.61	17.58

Table 3.1 contd.

Oxide Wt.%	KB85-18	KB85-21	KB85-59	KB85-58
SiO_2	40.04	39.26	39.57	37.17
TiO_2	0.03	0.04	0.04	0.04
Al_2O_3	0.02	0.01	0.04	0.00
Cr_2O_3	0.07	0.05	0.04	0.01
FeO	14.28	18.38	15.64	27.31
MnO	0.23	0.26	0.24	0.54
MgO	45.95	42.81	44.80	35.26
CaO	0.32	0.23	0.31	0.37
Na_2O	0.00	0.00	0.00	0.00
K_2O	0.00	0.01	0.01	0.00
NiO	0.22	0.18	0.19	0.09
Total	101.19	101.25	100.90	100.82
Fo	84.76	80.21	83.21	69.21
Fa	15.25	19.79	16.79	30.79

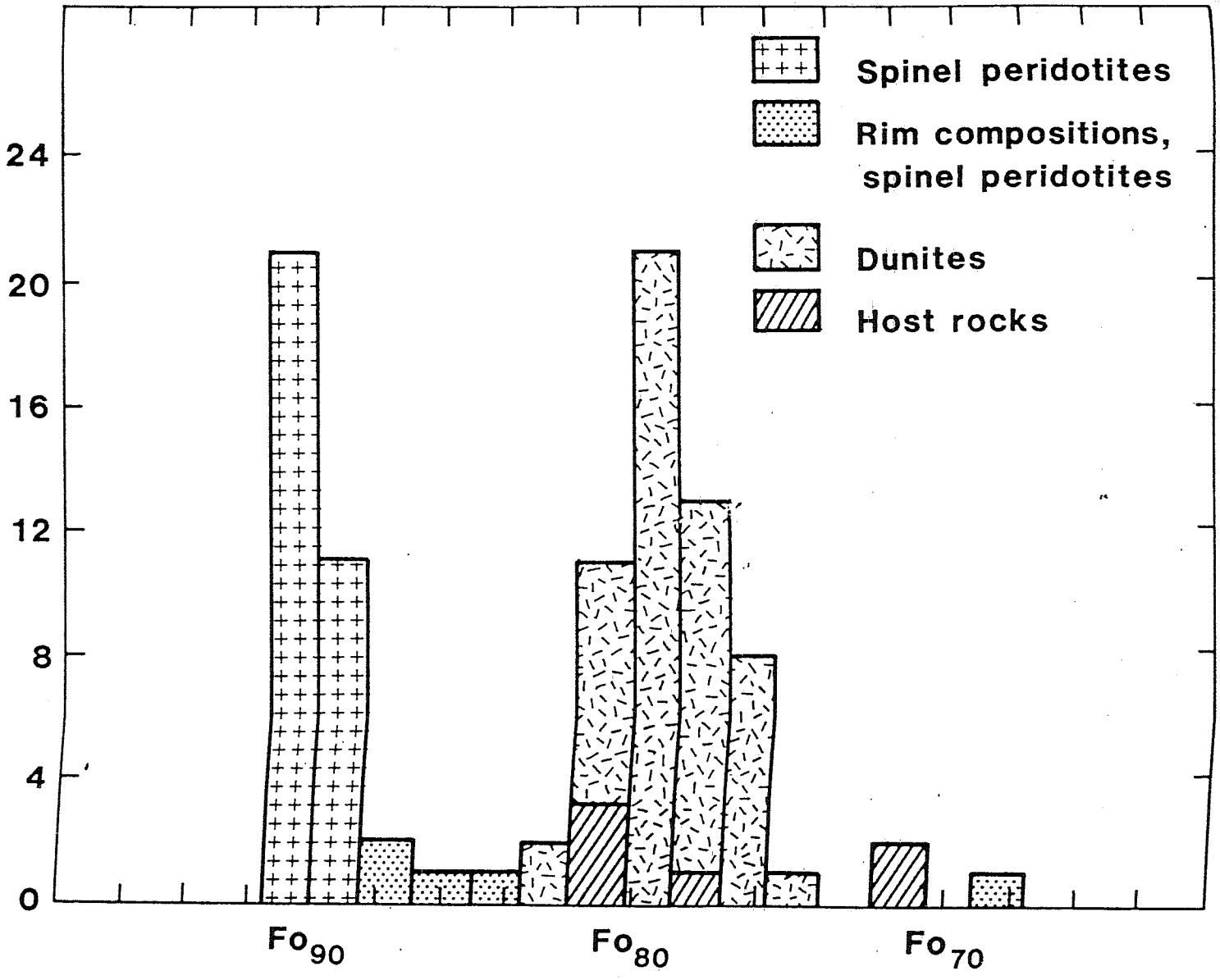


Fig. 3.6 **OLIVINE COMPOSITION**

Oceanography. Reference mineral standards supplied by the Smitsonian Institution were used as standards. Detailed analyses were carried out on nodules from Bhujia, Dhrubiya and Vethon hills. For each grain, a number of measurements was made to check homogoneity, and where appropriate, several spots were averaged to give the final composition. Compositional variations between core, rim and the intergranular material (neoblasts) were examined in the porphyroclastic nodules. Interaction between xenolith minerals and host rock was also studied by careful analysis of nodule minerals abutting the host matrix. Altogether over 700 individual spots were analysed.

Olivine Compositions

The olivines in the analysed nodules are quite homogeneous in composition averaging Fo_{90} (table 3.1 and Fig. 3.6). Minor element abundances (Ni, Ca, Mn, Fe) are normal for olivines of this composition (Simkin and Smith, 1970) Only grains in contact with the host liquid show compositional variability, ranging down to Fo_{65} (Fig. 3.6) and such compositional differences are restricted to the outer 50 μm or less of individual crystals. Fluid inclusions are common.

Table 3.2. Representative Orthopyroxene Compositions.

Oxide Wt.%	BHUJ-A		BHUJ-B		BHUJ-H		BN-C	
SiO_2	55.68	55.03	55.01	55.14	55.12	55.41	55.31	55.40
TiO_2	0.18	0.20	0.16	0.17	0.16	0.06	0.04	0.05
Al_2O_3	3.70	3.80	3.79	3.96	3.92	2.83	3.00	2.91
Cr_2O_3	0.35	0.43	0.30	0.36	0.38	0.43	0.45	0.41
FeO	5.83	5.70	5.75	5.78	5.75	5.84	5.92	5.66
MnO	0.13	0.18	0.16	0.18	0.19	0.18	0.18	0.17
MgO	34.23	34.01	34.04	34.13	34.27	34.34	34.40	34.32
CaO	0.42	0.48	0.44	0.47	0.44	0.50	0.57	0.49
Na_2O	0.04	0.06	0.03	0.04	0.04	0.03	0.03	0.02
K_2O	0.03	0.01	0.00	0.03	0.01	0.00	0.03	0.01
NiO	0.06	0.07	0.11	0.11	0.07	0.12	0.06	0.05
Total	100.67	99.99	99.82	100.37	100.35	99.72	99.92	99.51
En	90.36	90.32	90.34	90.26	90.37	90.19	90.08	90.46
Fs	8.83	8.76	8.81	8.85	8.80	8.86	8.96	8.61
Wo	0.8	0.92	0.85	0.89	0.83	0.95	0.96	0.93

Table 3.2 contd.

Oxide Wt. %	KB83-13		DN-1		DN-2	
SiO_2	55.08	55.3	55.32	55.21	54.59	55.29
TiO_2	0.08	0.10	0.03	0.11	0.11	0.15
Al_2O_3	3.02	2.6	2.76	2.70	4.03	3.68
Cr_2O_3	0.49	0.46	0.47	0.48	0.25	0.35
FeO	5.87	5.89	5.88	5.70	6.58	6.37
MnO	0.18	0.15	0.15	0.15	0.16	0.16
MgO	34.02	34.44	34.28	34.58	32.86	34.05
CaO	0.48	0.46	0.56	0.32	0.36	0.40
Na_2O	0.06	0.09	0.05	0.05	0.03	0.03
K_2O	0.02	0.02	0.02	0.00	0.00	0.01
NiO	0.03	0.02	0.04	0.08	0.08	0.06
Total	99.36	99.23	99.57	99.38	99.06	100.53
En	90.10	90.26	90.02	90.78	89.10	89.60
Fs	8.99	8.88	8.90	8.61	10.20	9.60
Wo	0.91	0.86	1.08	0.60	0.70	0.80

Table 3.3. Representative Major Element Composition of Clinopyroxenes

Oxide Wt.%	BHUJ-A		BHUJ-B		BN-H		BHUJ-C		KB85-13			DN-1
SiO_2	51.57	50.91	51.75	51.53	52.32	52.61	52.33	52.32	51.96	52.28	51.25	52.14
TiO_2	0.83	0.82	0.67	0.81	0.05	0.08	0.07	0.11	0.38	0.36	0.40	0.34
Al_2O_3	5.87	3.97	5.18	5.52	3.75	3.73	3.54	3.75	5.37	5.57	5.26	5.48
Cr_2O_3	0.96	1.08	0.82	0.84	1.10	1.12	1.03	1.23	1.61	1.70	1.70	1.66
FeO	1.81	2.11	1.82	1.92	2.03	2.12	2.01	1.99	2.54	2.52	2.36	2.50
MnO	0.10	0.10	0.12	0.11	0.07	0.10	0.11	0.11	0.07	0.02	0.12	0.10
MgO	15.34	16.71	15.57	15.46	16.31	16.20	16.25	16.08	14.48	14.25	14.02	14.44
CaO	22.07	23.09	22.07	22.18	22.53	22.37	22.41	22.36	20.51	20.54	20.45	20.35
Na_2O	1.75	0.64	1.63	1.71	1.49	1.46	1.44	1.52	3.01	3.11	3.15	2.99
K_2O	0.02	0.01	0.00	0.01	0.01	0.02	0.00	0.01	0.00	0.01	0.01	0.00
NiO	0.07	0.08	0.07	0.01	0.03	0.08	0.05	0.06	0.04	0.04	0.03	0.00
Total	100.46	99.6	99.7	100.15	99.69	99.93	99.26	99.58	100.94	100.45	98.77	100.03
Wo	49.15	48.06	48.77	49.00	48.08	47.96	48.00	48.23	48.05	48.51	48.82	47.92
En	47.52	48.36	47.87	47.51	48.41	48.32	48.44	48.24	47.18	46.81	46.55	47.30
Fs	3.33	3.58	3.36	3.50	3.51	3.72	3.55	3.53	4.77	4.68	4.62	4.78

Table 3.3 contd.

Oxide Wt.%	DN-2		BHUJ-E		BN-1	
SiO_2	51.51	51.56	51.87	52.04	51.57	51.97
TiO_2	0.23	0.35	0.16	0.25	0.53	0.55
Al_2O_3	4.44	4.80	4.53	4.48	7.28	3.32
Cr_2O_3	1.15	1.16	1.28	1.13	0.71	1.24
FeO	1.99	2.10	1.95	2.11	2.37	2.91
MnO	0.06	0.11	0.10	0.10	0.09	0.12
MgO	15.77	15.36	15.33	15.56	14.07	14.14
CaO	22.42	22.36	22.11	22.32	28.97	22.09
Na_2O	1.57	1.65	1.68	1.66	2.63	0.68
K_2O	0.00	0.02	0.01	0.02	0.02	0.02
NiO	0.04	0.03	0.01	0.09	0.02	0.07
Total	99.19	99.50	99.03	99.76	100.27	100.09
Wo	48.77	49.20	49.08	48.86	49.40	45.70
En	47.74	47.01	47.35	47.36	46.10	49.40
Fs	3.48	3.79	3.57	3.77	4.50	4.90

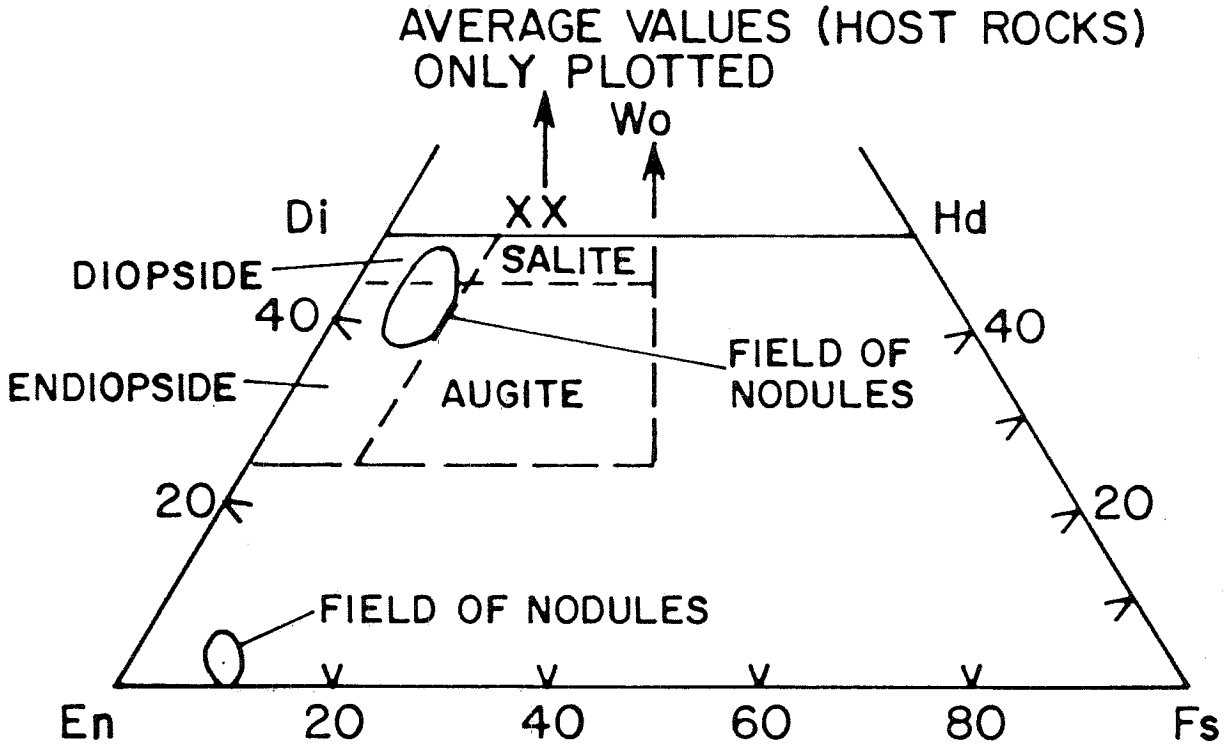


Fig. 3.7 PYROXENE COMPOSITIONS FOR SPINEL PERIDOTITES AND HOST BASALTS.

Orthopyroxene Compositions

Like the olivines, the orthopyroxenes (enstatites) are also fairly uniform in composition, averaging $En_{89.6}$ $Fs_{9.7}$ $Wo_{0.7}$ (Table 3.2, Fig. 3.7. Al_2O_3 contents are relatively low, varying from 3 to 4%. Transitional compositions appear at xenolith margins presumably due to orthopyroxene - host liquid or orthopyroxene-clinopyroxene reactions. Such features may also be related to the small size and hence rapid temperature equilibration of the xenoliths with the host basalts during ascent. Compositional variability due to exsolution could not be observed at the scale of our analyses (beam size ~1 μm).

Clinopyroxene Compositions

Clinopyroxenes in these xenoliths are chrome diopsides with very little variation (Table 3.3 Fig. 3.7). The observed compositional range is En_{48-49} Wo_{46-49} Fs_{4-5}. Granulose and some sieve structured crystals tend to be poorer in Al_2O_3, Cr_2O_3 and Na_2O than other varieties.

Spinel Compositions

Spinels exhibit maximum chemical variation among the nodule minerals. In some there is a strong marginal zoning, leading to compositions similar to those in the host

Table 3.4. Representative major element composition of spinels from both the nodules and hosts.

	BHUJ-A				BHUJ-B			
SiO_2	0.00	0.00	0.00	0.00	0.01	0.00	0.00	0.00
TiO_2	0.06	0.07	0.04	0.06	0.15	0.16	0.15	0.14
Al_2O_3	43.56	42.35	43.10	42.97	57.05	56.66	55.85	57.03
Cr_2O_3	25.28	26.25	26.55	26.34	12.51	12.48	13.53	12.30
FeO	12.21	12.05	11.77	12.06	9.72	9.25	8.75	9.41
Fe_2O_3	1.40	2.13	1.82	1.71	0.37	0.79	1.78	0.36
MnO	0.13	0.15	0.14	0.16	0.13	0.10	0.12	0.15
MgO	17.42	17.55	17.90	17.61	20.60	20.82	21.30	20.67
CaO	0.00	0.00	0.02	0.01	0.01	0.00	0.02	0.01
Na_2O	0.00	0.01	0.00	0.00	0.00	0.00	0.00	0.00
K_2O	0.01	0.00	0.00	0.01	0.01	0.00	0.01	0.01
NiO	0.20	0.18	0.19	0.18	0.35	0.32	0.28	0.29
Total	100.28	101.65	101.54	101.12	100.93	100.63	101.79	100.35

Table 3.4 contd.

	DN-1				KB85-13			
SiO_2	0.00	0.00	0.00	0.00	0.00	0.00	0.00	0.00
TiO_2	0.14	0.12	0.17	0.13	0.11	0.11	0.10	0.11
Al_2O_3	40.89	41.87	40.34	41.19	46.82	47.91	46.69	47.38
Cr_2O_3	26.96	25.96	27.81	26.54	21.31	20.83	22.32	21.42
FeO	13.69	13.59	13.94	13.76	11.51	11.72	12.11	11.59
Fe_2O_3	2.73	2.78	2.71	2.59	2.08	1.58	1.46	1.56
MnO	0.21	0.21	0.23	0.18	0.11	0.14	0.19	0.14
MgO	16.34	16.52	16.23	16.29	18.28	18.31	17.95	18.33
CaO	0.02	0.03	0.04	0.02	0.03	0.00	0.00	0.01
Na_2O	0.00	0.01	0.00	0.00	0.00	0.00	0.00	0.00
K_2O	0.02	0.02	0.00	0.01	0.01	0.02	0.00	0.01
NiO	0.11	0.13	0.17	0.16	0.23	0.25	0.17	0.21
Total	101.10	101.24	101.65	100.88	100.48	100.87	101.00	100.77

Table 3.4 contd.

	KB/13/ 83N	KB/1/ 83N2	KB/1/83/N1			KB/13/83		
					Core	Rim	Host	
SiO_2	0.00	0.00	0.00	0.00	0.00	0.13	0.24	0.03
TiO_2	2.69	0.10	0.10	0.02	0.17	15.75	17.73	24.61
Al_2O_3	34.78	50.24	50.92	60.36	48.80	8.75	7.61	3.07
Cr_2O_3	28.05	16.42	15.21	7.90	16.73	9.19	3.00	0.05
FeO	13.96	11.96	12.14	10.83	11.92	40.10	40.03	51.21
Fe_2O_3	4.27	4.32	4.07	1.22	4.75	20.64	25.12	17.91
MnO	0.24	0.17	0.16	0.04	0.14	0.67	0.61	0.76
MgO	17.01	18.60	18.39	20.19	18.33	4.12	5.23	1.41
CaO	0.10	0.02	0.02	0.04	0.02	0.08	0.13	0.05
Na_2O	0.00	0.00	0.00	0.00	0.00	0.00	0.00	0.00
K_2O	0.00	0.01	0.00	0.00	0.01	0.01	0.02	0.02
NiO	0.28	0.26	0.23	0.34	0.17	0.05	0.07	0.01
Total	101.43	102.12	101.27	100.95	101.06	99.49	99.80	99.15

Table 3.4 contd.

	KB/1/83	
SiO_2	0.01	0.07
TiO_2	8.85	22.01
Al_2O_3	13.84	3.97
Cr_2O_3	21.17	2.65
FeO	35.48	66.75
Fe_2O_3	17.15	--
MnO	0.45	0.68
MgO	4.18	3.30
CaO	0.00	0.13
Na_2O	0.01	0.00
K_2O	0.00	0.00
NiO	0.01	0.07
Total	101.20	99.64

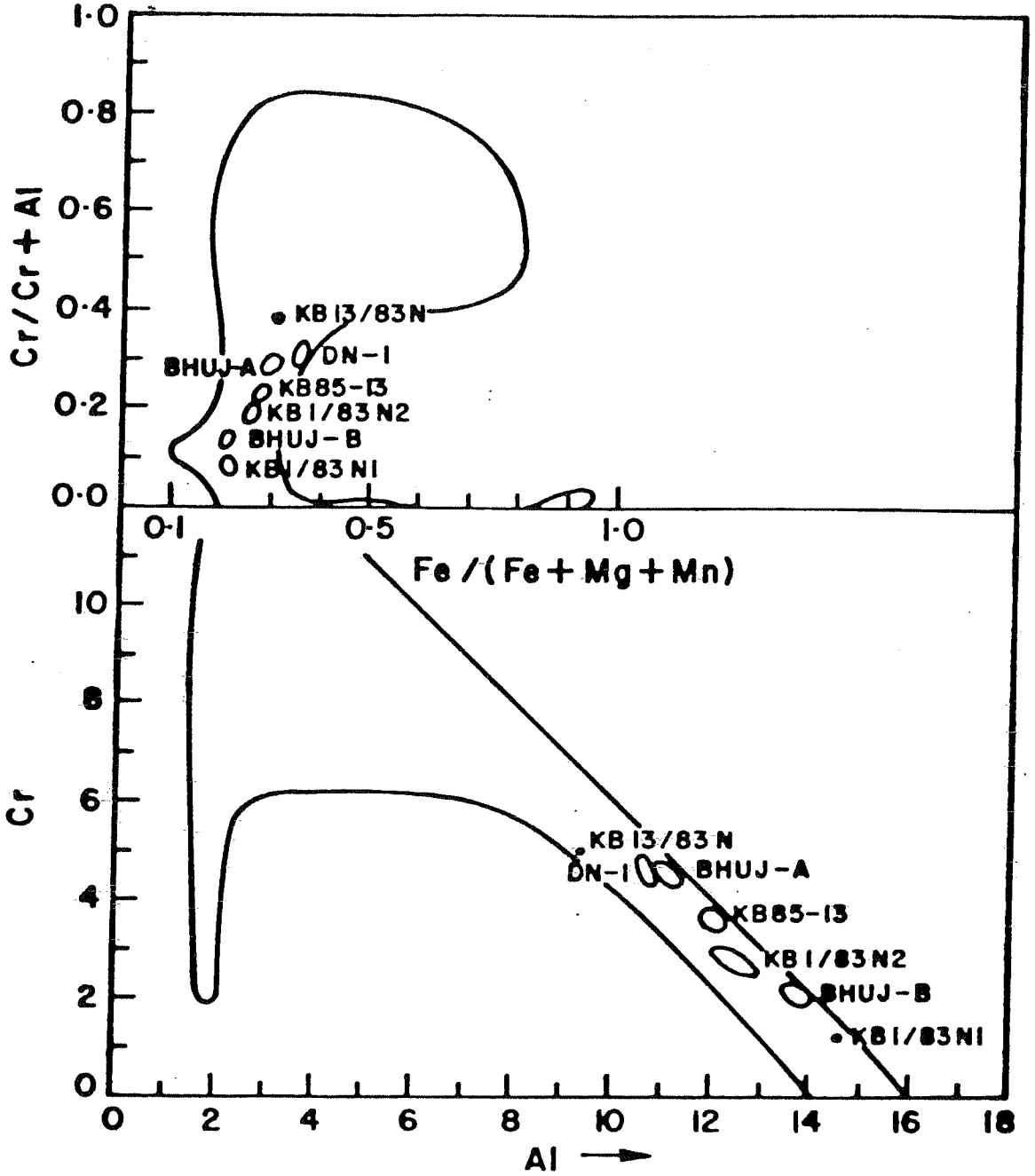


Fig. 3.8 **Spinel Composition for Spinel Perodotites (Field boundaries after Haggarty, 1979)**

basalts (Table 3.4 Fig. 3.8). In terms of their average composition, however, these spinels are quite similar to those found in upper mantle derived spinel peridotites (Haggerty,1979).

The spinel peridotites from Kutch have a mineralogy and composition similar to Type I (Menzies,1983).Though it is not possible to distinguish between the two possibilities, namely (1) Type 1 inclusions represent accumulates from basalt melt, and (2) they are residue from variable degree of partial melting of more fertile lherzolite composition, because all textural evidences have been obliterated,the nodules from Kutch most probably represent the second possibility.

3.6 BASALTS FROM KUTCH

As mentioned earlier (section 3.2), both alkali and tholeiite basalts occur in Kutch.The alkali basalts,some of which host nodules,were studied in detail to determine the nodule-host rock relationship.

A.MINERALOGY

The alkali basalts are dense,fine to medium grained and only sparsely porphyritic with mainly olivine and occasional clinopyroxene phenocrysts.Thin sections of these basalts reveal that larger phenocrysts have marginal embayment and corrosion and may in fact be xenocrysts.The groundmass is fine grained,less than 0.1 mm and composed of

olivine, clinopyroxene, lathes of plagioclase and opaque oxides with occasional patches of analcite.

Representative mineral analyses are given in table 3.1-3.3 and plotted in figs. 3.6-3.7.

The phenocryst composition of olivines range from Fo_{75} to Fo_{81}, averaging Fo_{79} whereas the rims of zoned crystals and groundmass olivines reach values upto Fo_{64} (see table 3.1 and fig. 3.6). These phenocryst olivines differ from the olivine compositions of spinel peridotites not only in being less forsteritic (see Fig. 3.6) but also in their higher C_aO and lower Ni contents.

The clinopyroxenes vary from titanium-augites to salites in composition (fig. 3.7). Their composition is similar to those found in alkali basalts in general. Many crystals show strong marginal zoning. Margins have higher Al_2O_3 and lower SiO_2 contents than the cores.

Feldspars occur as microlites and anhedral plates in the groundmass and comprise of both plagioclase and Na-K feldspars. The alkali basalts which host spinel peridotites contain only labrodorite (An_{50}) while the dunite bearing basalts contain both the types.

Opaque oxides which occur as inclusions in olivines, phases bordering olivines and indivisual crystals, show wide variation in Al_2O_3, TiO_2 and Cr_2O_3 contents indicating complex crystallisation histories.

The tholeiites are fine grained, dense rocks. Their olivine compositions are more iron rich (Fo_{69}) and the clinopyroxenes are distinctly richer in E_n molecule

Table 3.5. Chemical Composition of Basalts from Kutch

Oxide Wt. %	BH-A	BH-B	BH-C	BH-D	BH-E	BH-F
SiO_2	42.74	42.59	42.44	42.84	44.02	44.06
TiO_2	3.65	3.66	3.68	3.65	3.17	3.23
Al_2O_3	8.03	8.28	8.25	8.26	13.20	13.50
FeO	13.38	13.32	13.04	12.99	13.96	13.84
MnO	0.17	0.17	0.17	0.16	0.17	0.17
MgO	14.88	14.35	14.78	14.70	10.39	9.95
CaO	12.11	11.88	12.11	12.18	10.48	10.54
Na_2O	3.03	3.63	3.38	3.04	3.33	3.69
K_2O	0.79	0.94	1.03	1.07	0.72	0.93
P_2O_5	0.93	0.98	0.95	0.92	0.46	0.43
Total	99.71	99.80	99.83	99.81	99.90	100.34
Sr (ppm)	960	871	1085	1248	764	682
Zr	271	284	279	259	203	201
Ni	446	416	423	418	205	199
V	275	283	289	269	323	341
Ba	1398	1435	1356	2113	602	549
Rb	54	52	58	66	18	16
Y	27	28	30	28	24	24
Nb	130	123	123	108	51	42

Oxide Wt. %	KB83-11(B)	KB-85-54(A)	KB85-54(B)	KB85-57	SK-15/83	KB85-58
SiO_2	42.59	43.44	42.59	49.69	47.14	50.29
TiO_2	2.55	3.32	3.21	2.31	2.30	2.94
Al_2O_3	11.67	13.21	11.98	14.31	13.19	13.17
FeO	12.62	13.42	13.91	13.81	11.56	14.36
MnO	0.18	0.18	0.19	0.17	0.17	0.18
MgO	13.33	10.81	12.76	6.15	10.66	5.65
CaO	11.44	10.79	11.24	10.12	11.60	10.19
Na_2O	3.34	2.91	2.34	1.84	2.18	1.91
K_2O	1.29	2.10	1.61	0.53	0.63	0.77
P_2O_5	0.52	0.42	0.34	0.28	0.34	0.33
Total	99.53	100.60	100.27	99.21	99.72	99.79
Sr (ppm)	615	704	593	225	507	215
Zr	201	200	175	162	196	188
Ni	352	221	265	97	317	70
V	312	367	399	314	322	383
Ba	519	526	403	139	403	406
Rb	51	56	48	13	15	17
Y	23	27	27	36	28	45
Nb	53	52	39	21	54	21

Oxide Wt. %	BN-12 (1)	BN-12 (2)	BN-12 (3)	DH-A	DH-B	KB83-13	KB-83-11(A)
SiO_2	42.43	42.96	42.82	43.64	43.78	43.16	41.93
TiO_2	3.73	3.67	3.54	3.17	3.21	3.09	2.60
Al_2O_3	8.56	8.69	7.94	13.37	13.50	11.91	11.31
FeO	13.09	13.04	12.66	13.80	13.58	13.67	12.70
MnO	0.17	0.16	0.17	0.17	0.18	0.20	0.19
MgO	13.82	14.02	95.70	9.45	9.32	11.90	14.07
CaO	12.05	12.13	11.69	10.24	10.14	11.25	12.02
Na_2O	3.75	3.58	3.38	4.10	3.79	2.85	2.75
K_2O	1.09	1.14	1.06	1.40	1.49	1.43	0.81
P_2O_5	1.00	0.98	0.90	0.44	0.48	0.56	0.55
Total	99.68	100.37	99.86	99.78	99.47	100.02	98.93
Sr (ppm)	1029	1027	1114	739	741	822	781
Zr	297	293	257	204	272	266	197
Ni	391	386	494	184	186	278	378
V	284	289	275	327	336	336	312
Ba	1431	1499	1804	562	596	468	603
Rb	73	75	72	60	57	45	27
Y	32	28	28	24	23	34	24
Nb	106	100	110	49	62	81	56

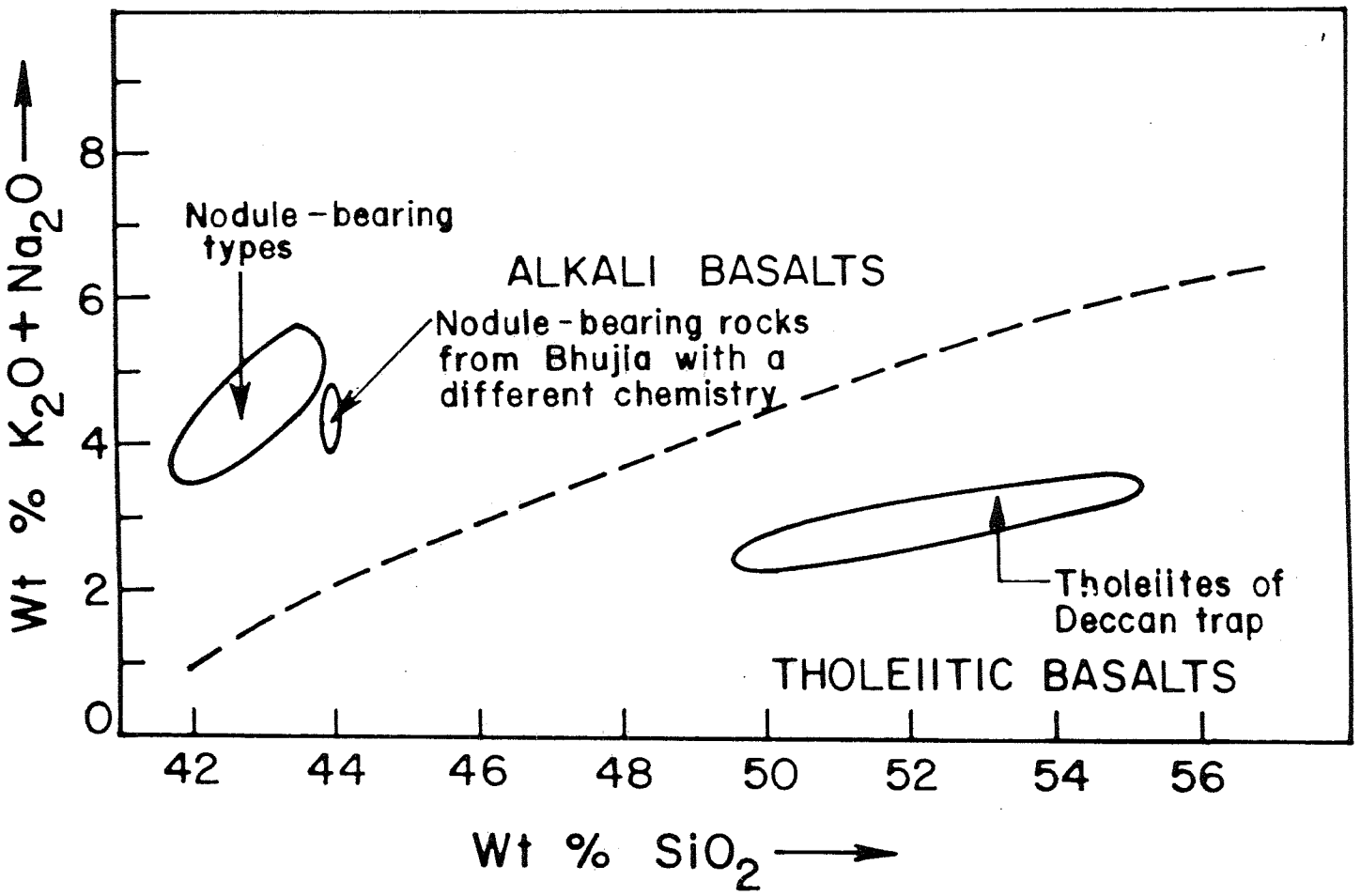


Fig. 3.9 ALKALI-SILICA DIAGRAM FOR BASALTS FROM KUTCH

(averaging $Wo_{39}En_{47}Fs_{14}$) than those in the alkali basalts. Plagioclase feldspars are of labrodorite (An_{60}) composition.

B.CHEMISTRY

The chemical composition of basalts is given in table 3.5. Major and trace-element concentrations were determined by X-ray fluorescence spectrometry. The accuracy and precision were determined by using international rock standards and replicate analyses and are shown in the table 2.1. Rb and Sr analyses were carried out by both isotope dilution and XRF and generally agree within 2%.In the analyses, where both the methods were used,isotope dilution values were preferred.

The undersaturated and alkaline nature of the basalts hosting the nodules is evident from the chemical composition (Table 3.5). Fig. 3.9 is an alkali silica diagram for these rocks showing that these are typical of alkali basalts from other regions of the world (Schwarzer and Rogers, 1974). At Bhujia hill, however, two distinct compositions are observed, distinguished particularly by differences in Al_2O_3,MgO and Ni contents.These differences are reflected in their Nd and Sr isotopic compositions,as will be discussed in Chapter 4.These samples could either represent two different magma types in Kutch or the range of variation in basalts from Kutch, the absence of intermediate values being due to sampling bias. The tholeiites from Kutch have a chemistry typical of the tholeiites from the main Deccan sequence (Mahoney,1984).

3.7. $^{40}Ar-^{39}Ar$ GEOCHRONOLOGY

The temporal relationship between the alkali and tholeiite basalts of Deccan province is still a subject of debate primarily due to absence of direct field relationship in many places, like Kutch, and lack of radiometeric age data for alkaline rocks.It is generally believed that the alkaline magmatism occurred towards the end of the Deccan igneous activity,although some workers suggest an earlier alkaline phase (Walker,1969;Bose,1980).A third view considers these two types to be contemporaneous (Chatterjee,1961).

To establish the temporal relationship between the rare, nodule-bearing alkali basalts and the main phase of Deccan volcanism precise 40/39 Ar dating of these samples was undertaken following the procedure described in Chapter II. Five fresh alkali basalt samples (BHUJ-A,BHUJ-F,KB83-11A, KB85-54 AND KB83-13) representing various nodule bearing localities and one fresh tholeiite (KB85-58) from the nearest Deccan Trap outcrop were dated.Sample BHUJ-A and BHUJ-F are from Bhujia hill, KB83-11A from Dharam hill, KB83-13 from Vethon hill, KB85-54A from Denodhar hill and KB85-58 from near Magwana (fig. 3.2).BHUJ-A and BHUJ-F are samples representing basalts with differing chemistry from Bhujia. The argon isotopic compositions and abundances along with fractions of radiogenic argon and apparent ages for each temperature fraction are given in tables 3.6-3.11.The

Table 3.6. Argon Isotopic Composition and Apparent Ages of BHUJ-F

Sample No.	Step Temp. °C	36Ar / 39Ar	37Ar / 39Ar	40Ar / 39Ar	40Ar* / 39Ar	Fraction of 39Ar released	Apparent Age (Ma)	40Ar* %
BHUJ-F	380	0.2397 0.0044	1.2771 0.0123	99.84 1.28	29.14 1.83	1.56	66.8 0.4	29.16
	470	0.0497 0.0012	0.8965 0.0044	42.04 0.32	37.44 0.47	6.35	63.0 0.1	65.23
	540	0.0188 0.0010	0.7448 0.0027	32.61 0.29	27.12 0.42	7.40	62.3 0.9	83.11
	610	0.0132 0.0020	0.8249 0.0003	32.16 0.27	28.33 0.39	7.96	65.0 0.9	88.05
	670	0.1393 0.0025	0.8824 0.0018	30.64 0.45	26.62 0.88	5.00	61.1 1.9	86.81
	740	0.0178 0.0025	0.9734 0.0006	34.34 0.70	29.17 1.01	3.38	66.9 2.3	84.90
	770	0.0352 0.0028	0.8931 0.0047	38.62 0.77	28.32 1.13	3.06	65.0 2.6	73.30
	820	0.0209 0.0018	0.6326 0.0005	34.23 0.47	28.12 0.71	5.11	64.2 1.6	82.12
	870	0.0139 0.0012	0.5647 0.0010	33.27 0.32	29.21 0.48	7.76	65.0 1.1	87.76

Table 3.6 contd.

900	0.0163	0.6238	35.49	30.74	8.51	70.4	86.59
	0.0011	0.0032	0.29	0.44		1.0	
1000	0.0137	4.8809	32.10	28.66	10.71	65.7	89.02
	0.0012	0.0028	0.26	0.44		1.0	
1060	0.0019	4.0294	27.83	27.78	10.13	63.8	99.59
	0.0011	0.0040	0.28	0.43		1.0	
1310	0.0080	14.7299	29.99	29.58	22.32	67.1	99.19
	0.0011	0.0028	0.32	0.48		1.2	

$$J = 0.001295 \pm 0.000017$$

Table 3.7. Argon Isotopic Composition and Apparent Ages of KB85-58

Sample No.	Step Temp. °C	36Ar / 39Ar	37Ar / 39Ar	40Ar / 39Ar	40Ar* / 39Ar	Fraction of 39Ar released	Apparent Age (Ma)	40Ar* %
KB85-58	380	0.9192	3.1534	314.24	43.04	0.32	104.4	13.70
		0.0199	0.0071	3.51	6.88		16.2	
	470	0.1643	2.7839	69.59	21.36	3.06	52.5	30.60
		0.0021	0.0299	0.57	0.85		2.1	
	540	0.0880	2.4025	52.95	27.21	3.33	66.7	51.30
		0.0023	0.0031	0.28	0.75		1.8	
	600	0.0603	2.0259	47.91	30.32	4.21	74.1	63.20
		0.0016	0.0314	0.24	0.53		1.3	
	670	0.0565	2.3754	43.25	26.82	8.08	65.7	61.90
		0.0014	0.0652	0.46	0.68		1.5	
	740	0.0365	2.6365	37.72	27.26	6.12	66.8	72.20
		0.0015	0.0005	0.29	0.54		1.3	
	770	0.0256	2.3784	34.57	27.28	10.78	66.8	78.80
		0.0005	0.0003	0.11	0.19		0.5	
	820	0.0228	2.3478	33.71	27.24	14.57	66.8	80.70
		0.0004	0.0031	0.08	0.14		0.3	
	870	0.0236	2.1554	33.92	27.22	12.73	66.7	80.10
		0.0004	0.0013	0.10	0.16		0.4	

Table 3.7 contd.

900	0.0287 0.0006	1.9160 0.0026	35.71 0.14	27.45 0.22	9.12	67.2 0.5	76.80
1000	0.0387 0.0005	2.1134 0.0021	38.38 0.12	27.20 0.19	10.76	66.6 0.4	70.80
1060	0.0317 0.0020	5.7563 0.0106	34.29 0.24	25.64 0.37	5.56	62.9 0.9	74.50
1140	0.0371 0.0008	20.7480 0.0004	34.55 0.19	26.22 0.30	6.90	64.3 0.7	75.00
1310	0.1452 0.0018	58.3940 0.0447	62.88 0.90	27.54 1.09	3.71	67.5 2.6	42.30
1410	0.8129 0.0537	54.7760 0.0320	288.03 16.56	55.78 23.69	0.93	134.1 54.9	18.80

$$J = 0.001384 \pm 0.000018$$

TABLE 3.8. Argon isotopic composition and apparent ages of KB83-13

Sample	Temperature °C	36Ar/39Ar	37Ar/39Ar	40Ar/39Ar	40Ar*/39Ar	Fraction of 39Ar released	Apparent age Ma	40Ar* %
KB83-13	380	0.0196 0.0036	0.5469 0.0023	37.33 0.49	31.58 1.18	0.79	74.8 2.7	84.58
	470	0.0042 0.0002	0.3747 0.0002	28.09 0.04	28.87 0.08	15.20	63.8 0.2	95.63
	540	0.0034 0.0002	0.4486 0.0001	27.30 0.02	26.34 0.05	17.33	62.6 0.1	96.46
	610	0.0066 0.0002	0.7263 0.0007	28.91 0.03	27.03 0.08	13.72	64.2 0.2	93.46
	670	0.0059 0.0003	0.7550 0.0004	30.05 0.05	28.38 0.10	9.69	67.4 0.2	94.41
	740	0.0067 0.0002	0.5714 0.0006	29.70 0.05	27.79 0.08	12.51	66.0 0.2	93.51
	770	0.0080 0.0005	0.5003 0.0001	30.17 0.08	27.86 0.15	6.91	66.1 0.4	92.31
	820	0.0153 0.0005	0.5633 0.0007	31.20 0.08	26.74 0.17	6.51	63.5 0.4	85.67
	870	0.0162 0.0009	0.7215 0.0004	31.96 0.16	27.23 0.30	3.79	64.7 0.7	85.16

Table 3.8 contd.

900	0.0197 0.0001	0.9578 0.0022	29.71 0.18	23.99 0.34	3.38	57.1 0.8	80.73
1000	0.0120 0.0011	2.4546 0.0026	28.59 0.20	25.33 0.37	3.51	60.2 0.9	88.47
1060	0.0172 0.0017	13.2920 0.0045	25.89 0.37	22.46 0.63	2.39	53.5 1.5	86.09
1140	0.0396 0.0033	61.5540 0.0114	28.88 0.81	25.06 1.32	1.39	59.6 3.1	83.66
1310	0.0989 0.0029	81.5690 0.0525	46.29 1.12	27.65 1.55	2.67	65.6 3.6	56.90
1410	1.1537 0.0629	81.0010 0.2939	200.24 43.34	137.96 49.49	0.28	368.9 146.3	65.66

J = 0.001341
0.000017

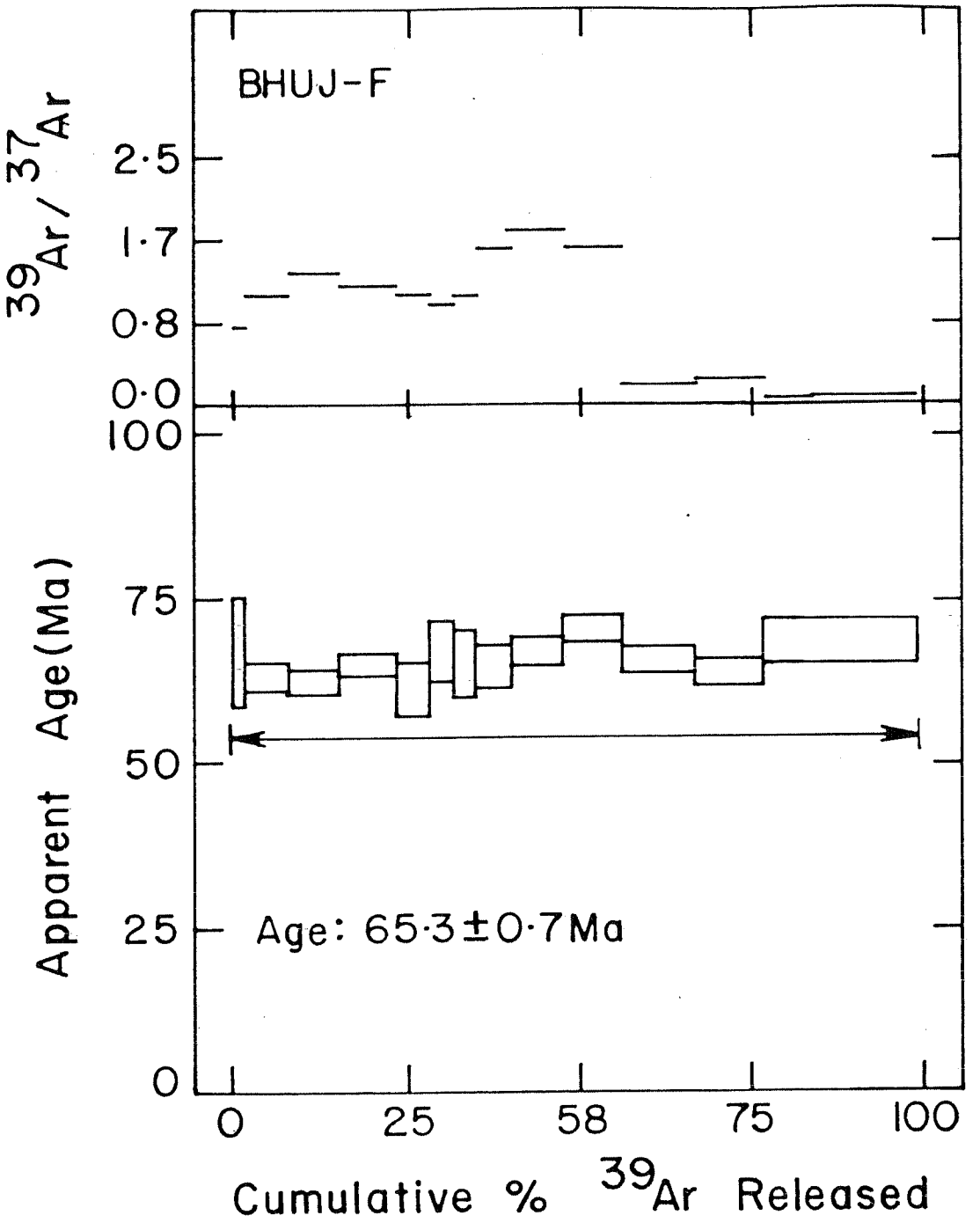


Fig. 3.10 Age spectrum for BHUJ-F.

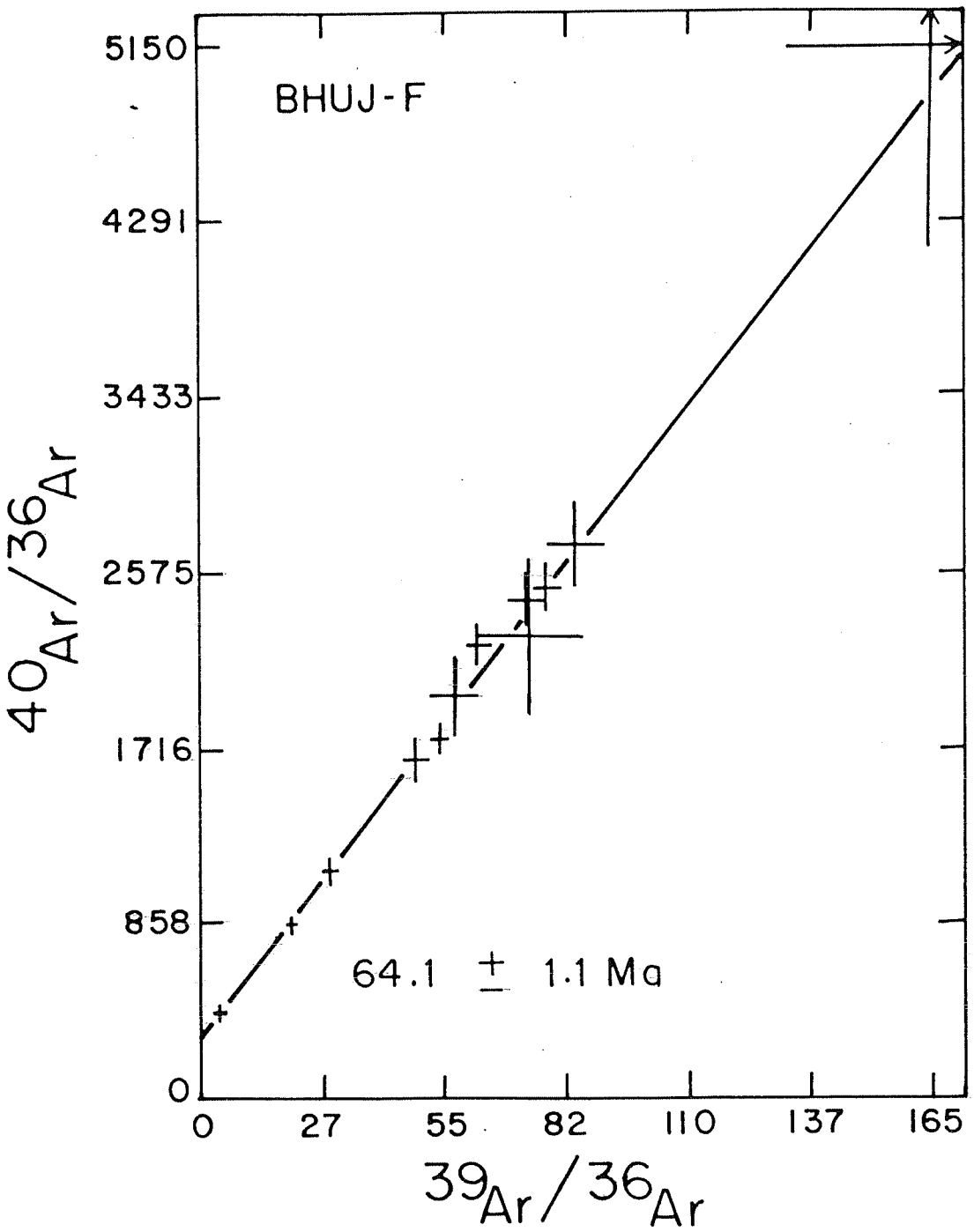


Fig. 3.11 Isochron plot for BHUJ-F.

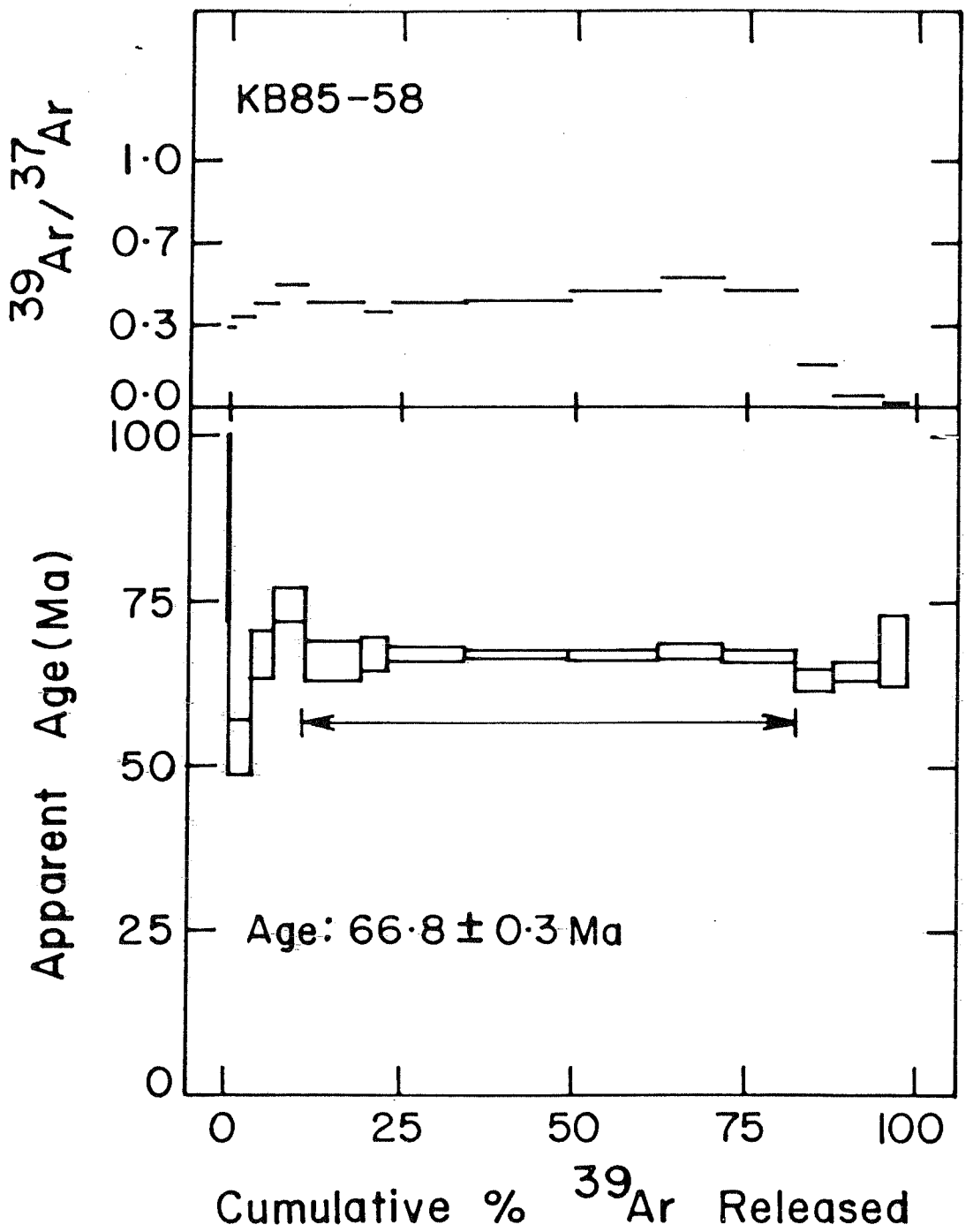


Fig. 3.12 Age spectrum for KB85-58.

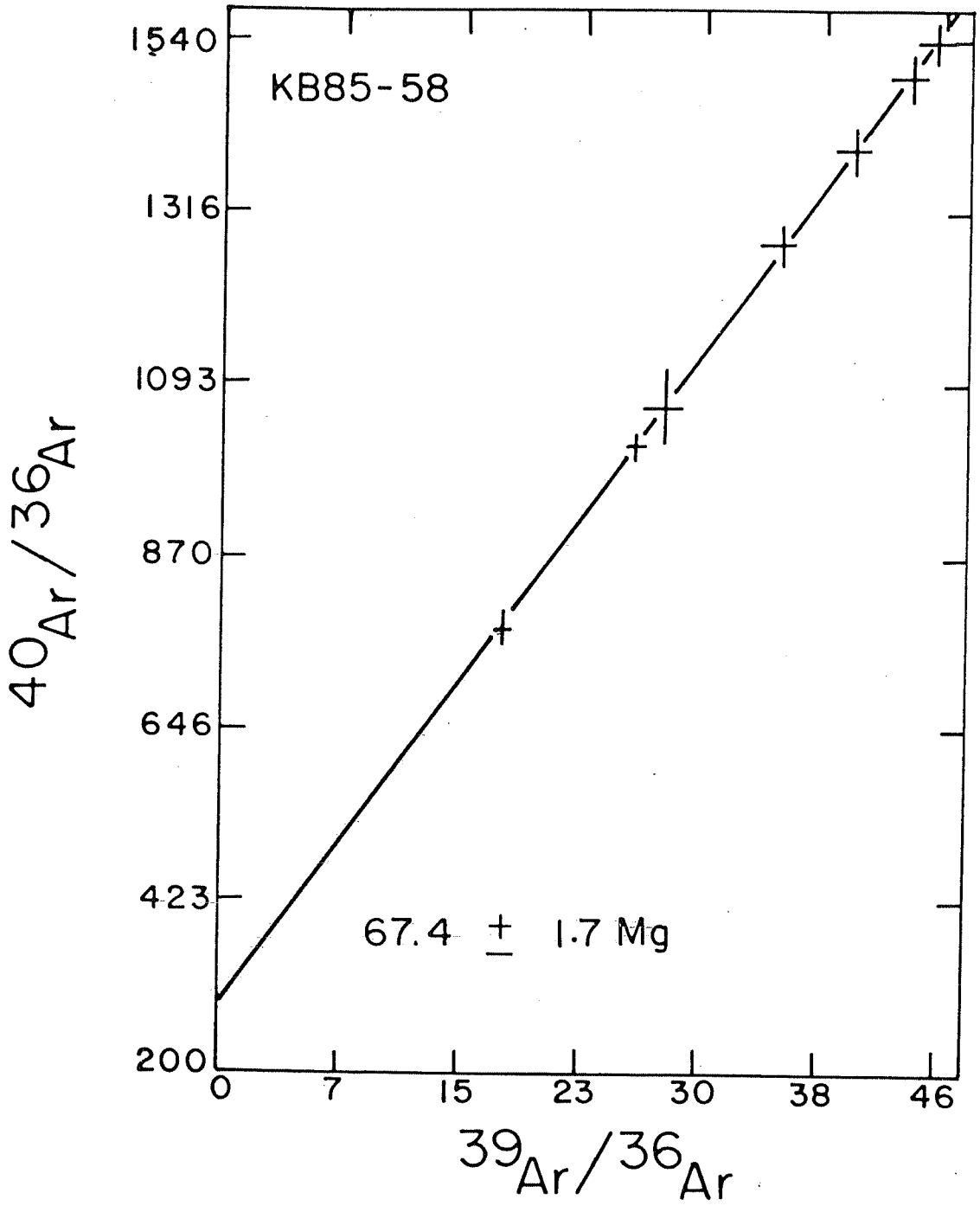


Fig. 3.13 Isochron plot for KB85-58.

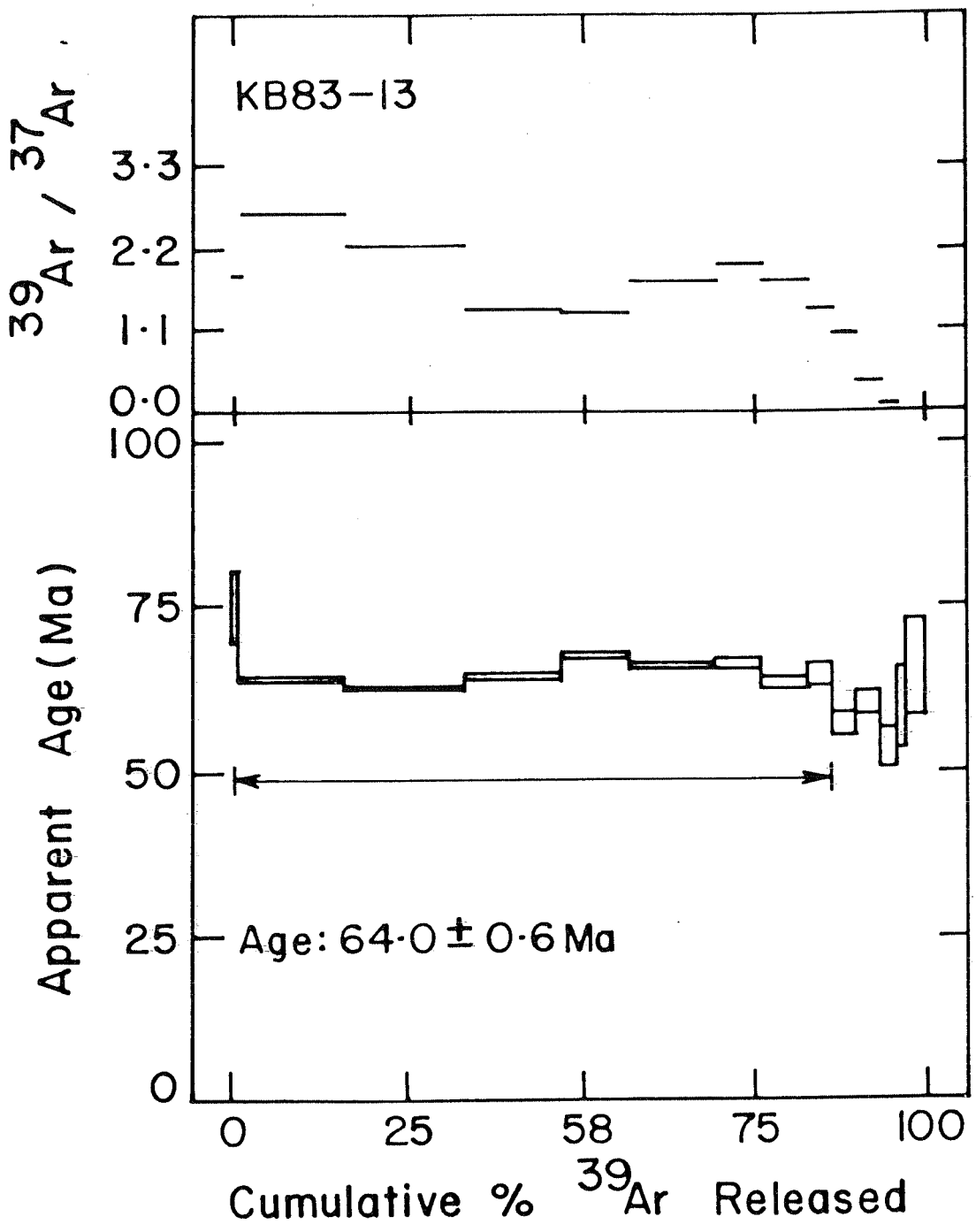


Fig. 3.14 Age spectrum for KB83-13.

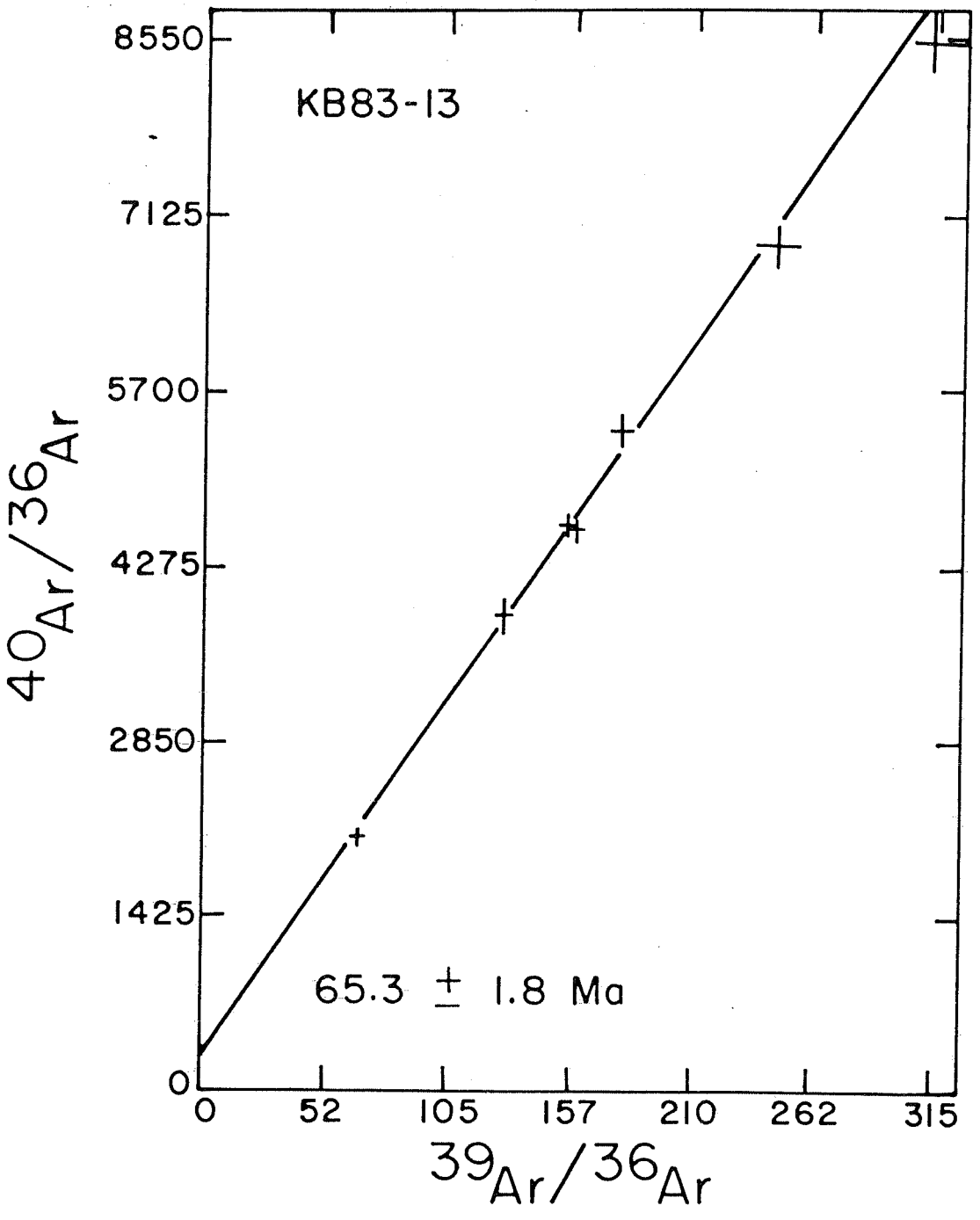


Fig. 3.15 Isochron plot for KB83-13.

modified J factor to allow for inter-sample fluence variations is also given. J values vary from 0.00123 to 0.00148 due to 17% variation of neutron fluence across the irradiation can.

The age spectra along with $^{39}Ar/^{37}Ar$ representing K/Ca ratio in the degassed phases,and the isochron plots for all the samples are shown in figs. 3.10-3.21.The plateau-, isochron- and integrated- or total-ages are summarised in table 3.12.

The ^{39}Ar release patterns for three samples,BHUJ-F, KB85-58 and KB83-13 (figs. 3.10-3.14) define good plateaux within experimental errors (2σ level) comprising 70-90% of ^{39}Ar released yielding weighted plateau ages of 65.3±0.7 Ma, 66.8±0.3 Ma and 64.4±0.7 Ma respectively. (Note all the errors quoted are 1σ level only,unless indicated otherwise). Their isochron ages are 64.1±1.1 Ma, 67.4±1.7 Ma and 65.7±1.8 Ma respectively. There is an excellent agreement between the plateau- and isochron-ages indicating that these samples have not lost any significant amount of radiogenic argon during their history.The initial value of the $^{40}Ar/^{36}Ar$ ratio corresponding to the Y-intercept of the isochrons are about 300 which is very close to the present day atmospheric value (table 3.13).The undisturbed nature of these samples is reflected also in the integrated ages which are 66.8±1.00 Ma, 67.0±0.6 Ma and 63.7±0.5 Ma for BHUJ-F,KB85-58 and KB83-13,respectively.

The concordance of plateau-, isochron- and integrated ages around 66 Ma for these three samples,of which BHUJ-F

TABLE 3.9. Argon isotopic composition and apparent ages of KB83-11A

Sample No.	Step Temp. °C	36-Ar/39-Ar	37-Ar/39-Ar	40-Ar/39-Ar	40-Ar*/39-Ar	Fraction of 39-Ar released	Apparent age Ma	40-Ar* %
KB83-11A	380	0.2248 0.0058	0.7799 0.0002	87.52 1.33	21.18 2.18	1.08	55.8 5.6	24.19
	470	0.0517 0.0005	0.4802 0.0003	37.57 0.11	22.32 0.19	12.67	58.7 0.5	59.41
	540	0.0284 0.0004	0.3809 0.0003	32.32 0.10	23.97 0.16	14.24	63.0 0.4	74.13
	610	0.0196 0.0005	0.4105 0.0005	31.62 0.13	25.86 0.20	11.51	67.9 0.5	81.76
	670	0.0221 0.0007	0.4766 0.001	32.54 0.16	26.06 0.26	9.18	68.4 0.7	80.05
	740	0.0284 0.0011	0.5842 0.0003	34.01 0.25	25.68 0.40	6.56	67.4 1.0	75.48
	770	0.0514 0.0015	0.5396 0.0032	40.42 0.34	25.29 0.55	4.72	66.4 1.4	62.54
	820	0.0714 0.0013	0.3995 0.0007	48.84 0.30	27.77 0.50	5.53	72.8 1.3	56.84

Table 3.9 contd.

870	0.0709	0.3934	47.48	26.57	5.38	69.7	55.95
	0.0014	0.0001	0.32	52.81		1.4	
900	0.0417	0.5219	40.18	27.91	6.08	73.1	69.43
	0.0014	0.0001	0.28	0.50		1.3	
1000	0.0174	1.4308	30.21	25.22	5.73	66.2	83.41
	0.0017	0.0032	0.34	0.61		1.6	
1060	0.0125	4.0120	25.32	22.11	7.02	58.2	87.12
	0.0015	0.0017	0.34	0.56		1.5	
1140	0.0165	30.4610	27.31	26.34	4.58	69.1	94.75
	0.0028	0.0093	0.58	1.03		2.6	
1310	0.2422	83.9140	92.98	32.53	5.51	85.0	33.28
	0.0055	0.1310	1.03	2.00		5.2	
1410	0.3349	71.7810	288.21	206.00	0.23	480.8	68.50
	0.4459	0.1357	119.81	185.84		380.7	

J = 0.001483
0.000019

Table 3.10. Argon Isotopic Composition and Apparent Ages of BHUJ-A

Sample No.	Step Temp. °C	36Ar/39Ar	37Ar/39Ar	40Ar/39Ar	40Ar*/39Ar	Fraction of 39Ar released	Apparent Age (Ma)	40Ar* %
BHUJ-A	380	0.2257 0.0112	1.2367 0.0074	93.88 0.01	27.34 3.61	0.32	66.2 8.5	29.10
	470	0.0266 0.0005	0.8842 0.0035	30.09 0.08	22.32 0.18	6.77	54.2 0.4	74.13
	540	0.0078 0.0002	0.9407 0.0020	25.92 0.03	23.71 0.07	17.52	57.5 0.2	91.42
	610	0.0045 0.0002	0.8190 0.0001	27.16 0.06	25.96 0.09	17.18	62.9 0.2	95.56
	670	0.0044 0.0002	0.6231 0.0044	27.75 0.05	26.51 0.09	15.54	64.2 0.2	95.50
	740	0.0095 0.0005	0.8092 0.0014	29.66 0.08	29.93 0.17	17.71	65.2 0.4	90.76
	770	0.0166 0.0005	0.8189 0.0005	32.16 0.08	27.32 0.17	7.90	66.1 0.4	84.93
	820	0.0154 0.0001	0.6651 0.0026	32.38 0.17	27.90 0.33	3.97	67.5 0.8	86.14
	870	0.0226 0.0013	0.6968 0.0047	36.35 0.19	29.74 0.43	3.43	71.8 1.0	81.80

Table 3.10 contd.

900	0.0205	1.1504	33.82	27.90	2.70	66.5	82.40
	0.0015	0.0005	0.24	0.90		1.2	
1000	0.0084	1.8470	29.48	27.23	5.29	65.9	92.26
	0.0007	0.0057	0.13	0.25		0.6	
1060	0.0203	8.3739	28.83	23.86	6.02	57.9	82.37
	0.0007	0.0056	0.11	0.23		0.5	
1140	0.0498	50.5290	32.71	24.44	2.24	59.3	72.52
	0.0019	0.1061	0.30	0.66		1.6	
1310	0.1038	55.8930	50.71	27.27	3.02	66.0	52.04
	0.0021	0.0381	0.74	1.00		2.4	
1410	0.8277	51.4850	365.58	130.75	0.39	296.5	34.70
	0.0948	0.0266	21.97	36.70		76.8	

$$J = 0.001366 \pm 0.000017$$

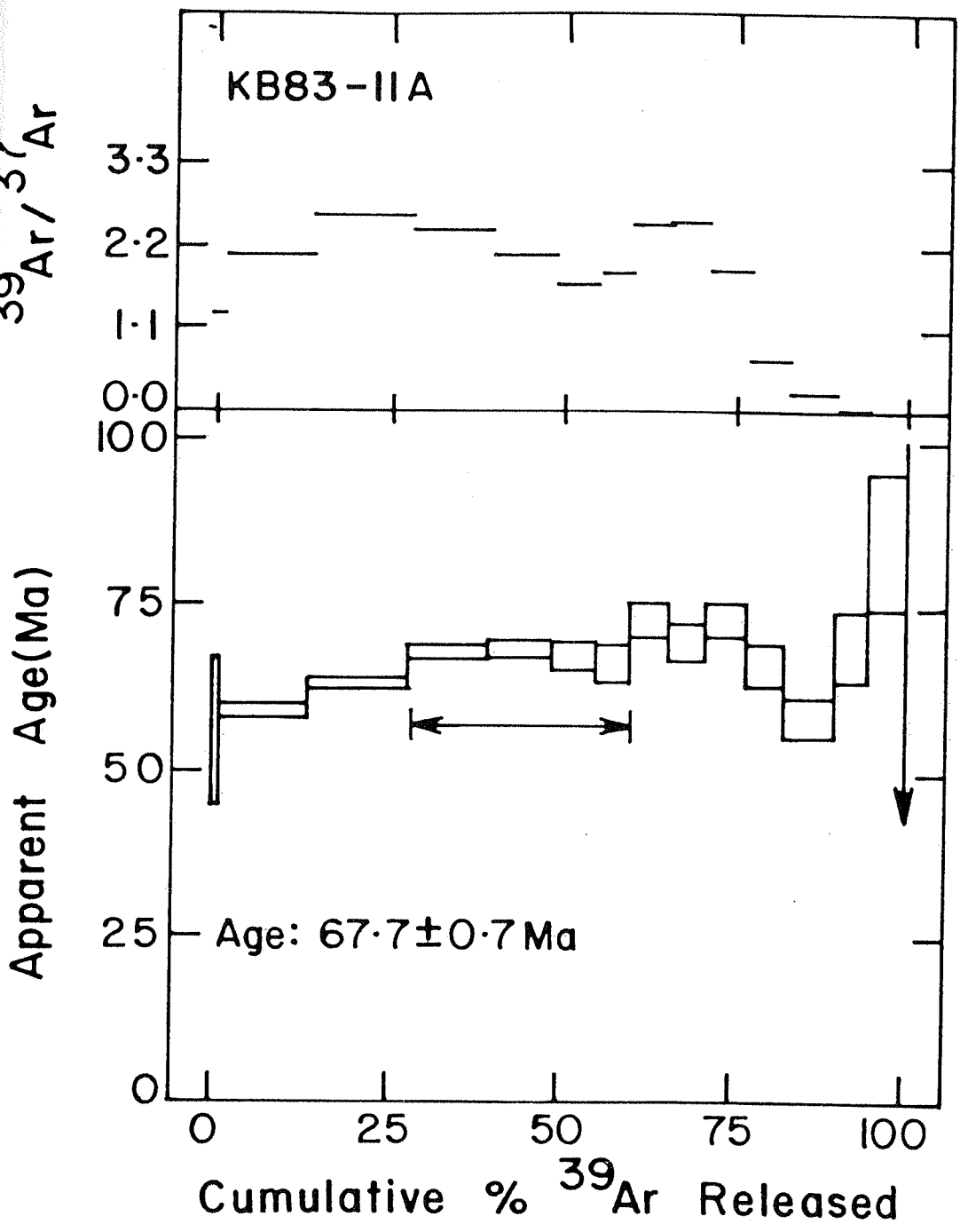


Fig. 3.16 Age spectrum for KB83-11A.

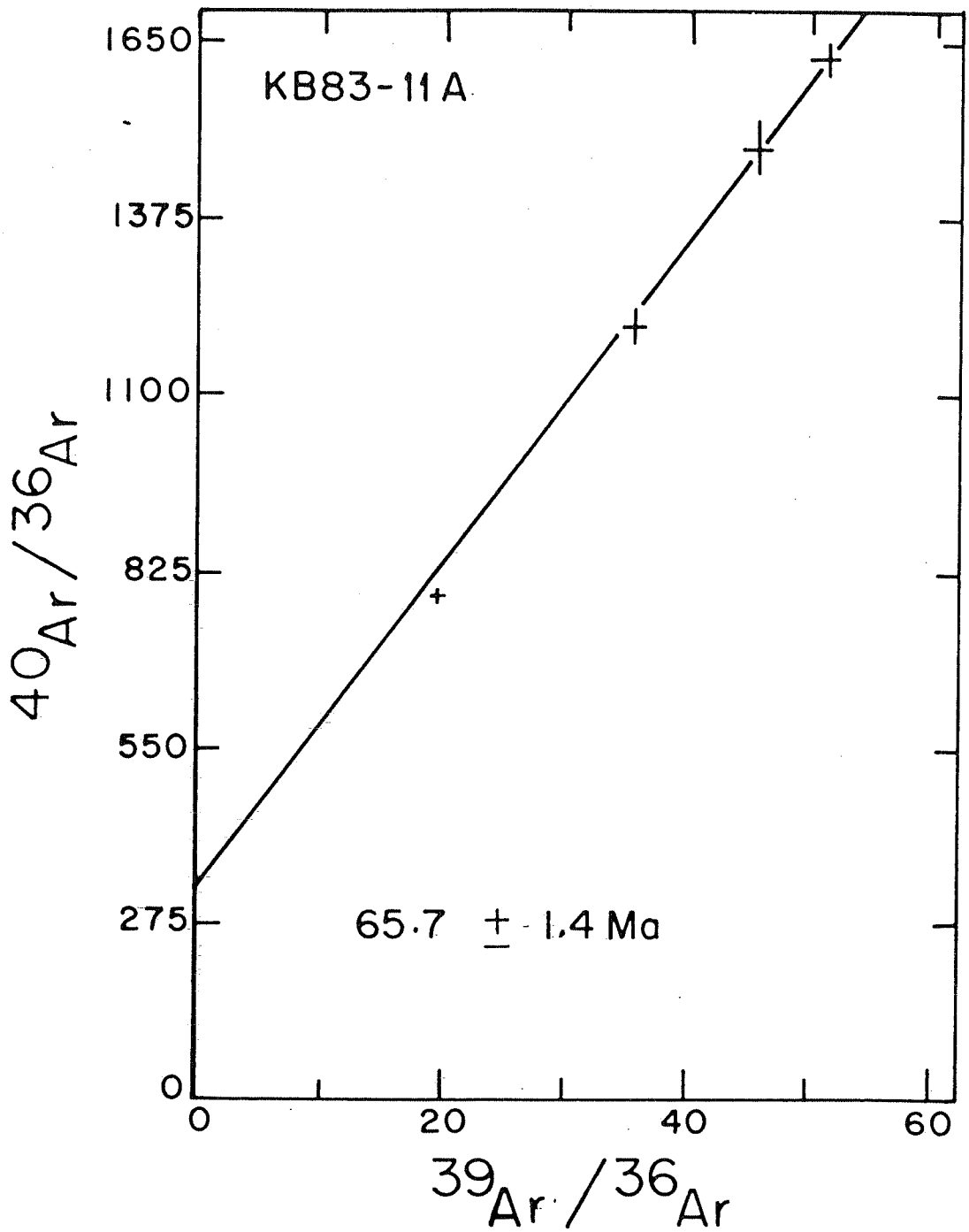


Fig. 3.17 Isochron plot for KB83-11A.

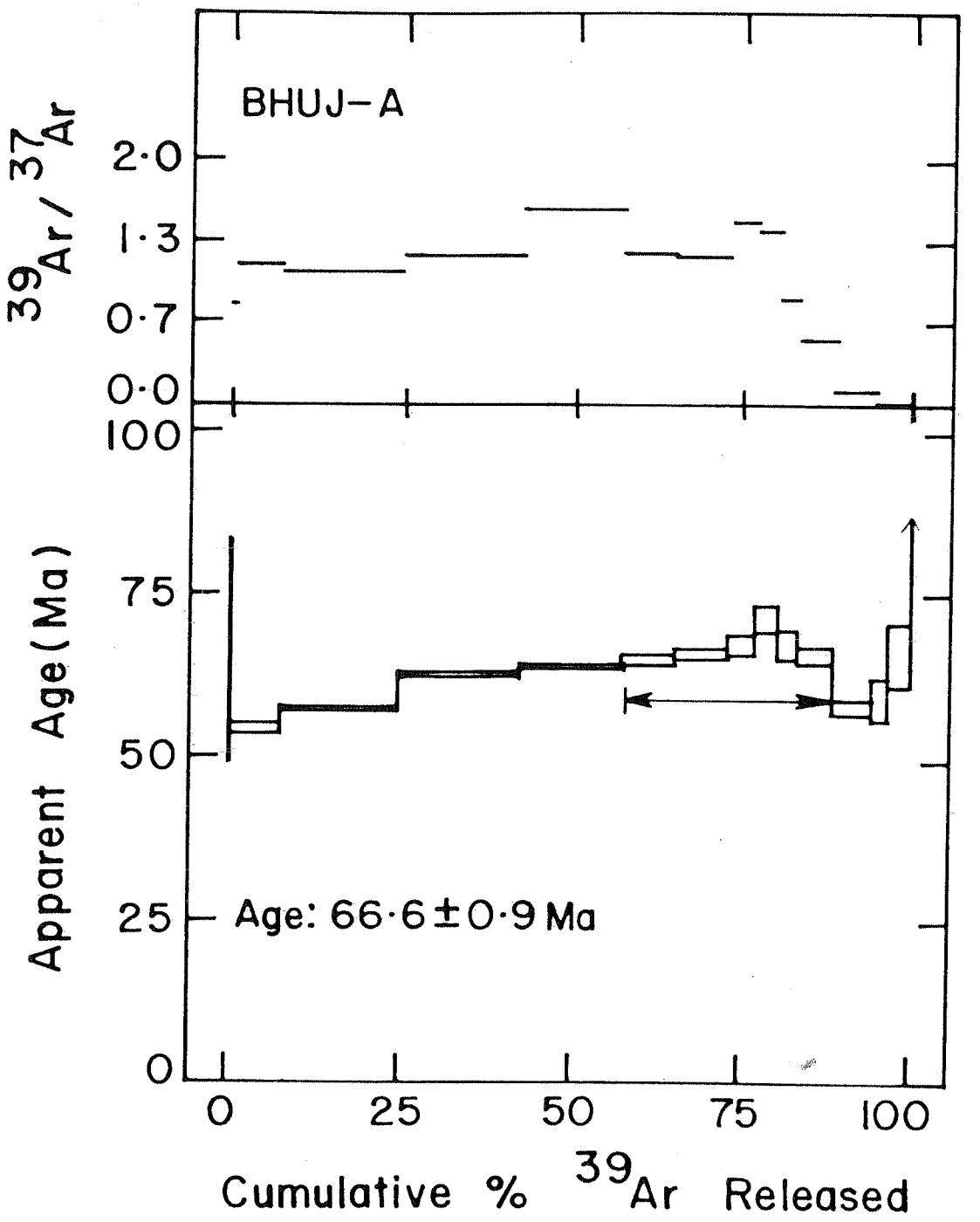


Fig. 3.18 Age spectrum for BHUJ-A.

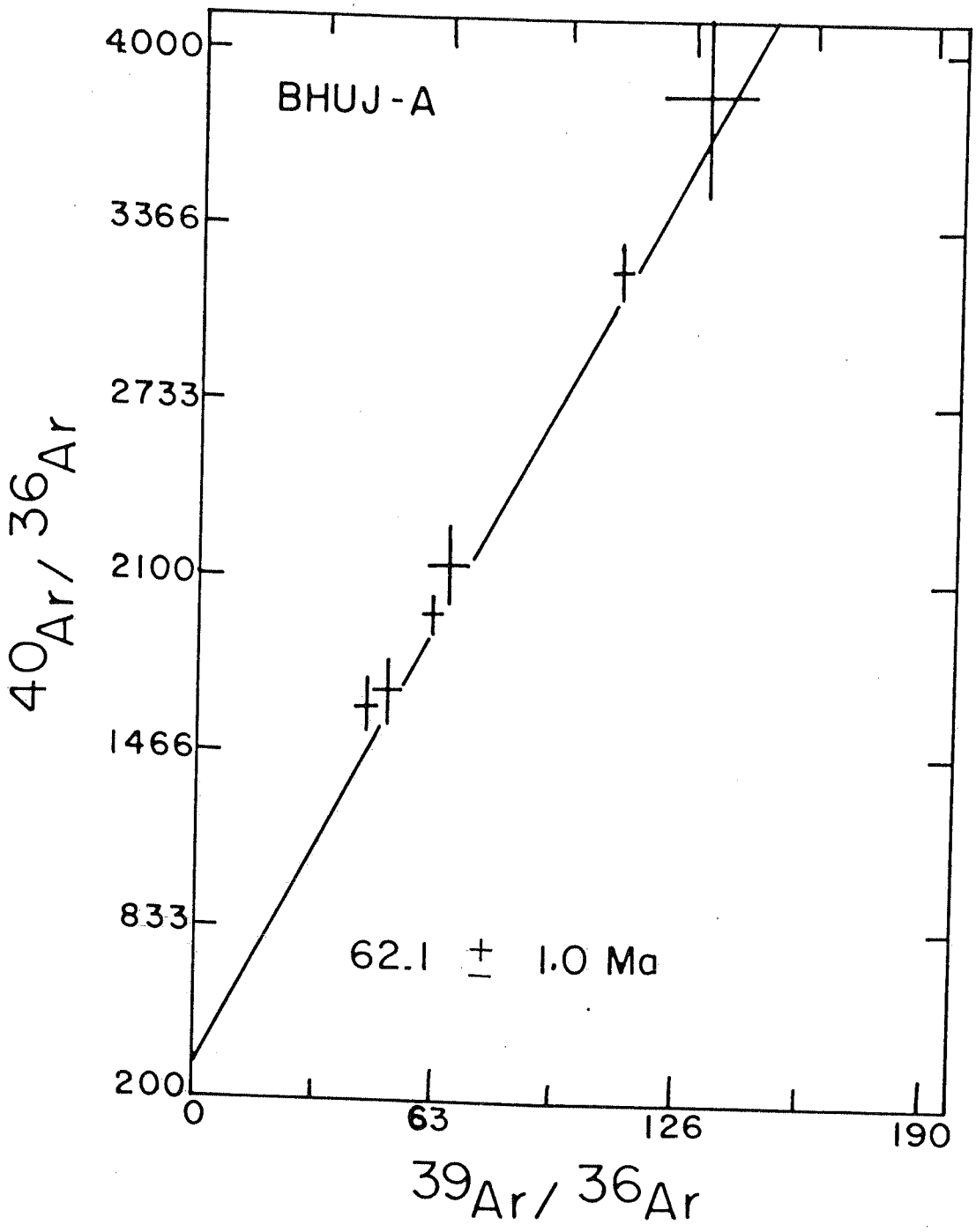


Fig. 3.19 Isochron plot for BHUJ-A.

and KB83-13 are alkali basalts and KB85-58 a tholeiite, suggests that these ages are in fact their formation ages. Moreover, the plateau ages for these samples are indistinguishable at 2σ level indicating that the alkali and tholeiitic basalts in Kutch are contemporaneous.

Two samples, KB83-11A and BHUJ-A have similar ^{39}Ar release pattern (figs. 3.16-3.18).Loss of radiogenic argon in low temperature fractions is evident.However,the release curves show plateau regions comprising about 32% of ^{39}Ar in the higher temperature fractions.these plateaux correspond to an age of 67.7$\pm$0.7 Ma for KB83-11A and 66.6$\pm$0.9 Ma for BHUJ-A.

The isochron age of KB83-11A corresponding to the plateau steps is 65.7$\pm$1.4 Ma and its integrated age is 67.8$\pm$1.2 Ma. These ages agree well with its plateau age of 67.7$\pm$0.7 Ma. Moreover, the weighted mean age of all the higher temperature fractions is 68.1$\pm$1.5 Ma which is not significantly different from the plateau age.The similarity of all the ages for this sample indicates a minimal loss of radiogenic argon from low activation sites and the plateau age of 67.7$\pm$0.7 Ma corresponds to its formation age.

On the other hand, BHUJ-A has an isochron age of 62.1$\pm$1.0 Ma and an integrated age of 63.5$\pm$0.4 which are significantly lower than its plateau age of 66.6$\pm$0.9 Ma. This is due to loss of significant amount of radiogenic argon. The plateau age,although based on only 32% of ^{39}Ar,is regarded closest to its formation age.

Both these alkali basalts,KB83-13 and BHUJ-A also have

Table 3.11. Argon Isotopic Composition and Apparent Ages of KB85-54A

Sample No.	Step Temp. °C	36Ar 39Ar	37Ar 39Ar	40Ar 39Ar	40Ar* 39Ar	Fraction of 39Ar released	Apparent Age (Ma)	40Ar* %
KB85-54A	380	0.1740	1.1031	54.20	2.90	0.34	6.4	5.34
		0.0049	0.0065	1.93	2.41		5.3	
	470	0.0114	0.5259	33.12	30.17	8.24	66.8	92.06
		0.0004	0.0002	0.08	0.15		0.3	
	540	0.0034	0.4739	29.89	28.92	14.71	63.1	96.72
		0.0002	0.0002	0.05	0.08		0.2	
	605	0.0028	0.5889	30.17	29.40	14.78	64.1	97.42
		0.0002	0.0002	0.05	0.08		0.2	
	670	0.0036	0.6022	31.02	29.99	14.36	65.4	96.67
		0.0002	0.0002	0.05	0.09		0.2	
	740	0.0038	0.4723	32.05	30.96	10.30	67.1	96.57
		0.0004	0.0002	0.07	0.12		0.3	
	770	0.0061	0.4967	38.83	32.06	9.17	69.8	94.75
		0.0004	0.0005	0.08	0.14		0.3	
	820	0.0058	0.4460	32.94	31.24	6.03	68.1	94.84
		0.0006	0.0003	0.12	0.25		0.5	
	870	0.0110	0.4583	33.03	29.80	4.96	65.0	90.21
		0.0008	0.0007	0.15	0.28		0.6	

Table 3.11 contd.

900	0.0109 0.0010	0.5899 0.0013	31.63 0.18	28.46 0.34	4.21	62.1 0.7	89.95
1000	0.0101 0.0007	1.0448 0.0009	30.57 0.13	27.69 0.26	5.77	60.5 0.6	90.53
1060	0.0158 0.0012	5.5453 0.0008	31.27 0.21	27.29 0.40	4.09	59.6 0.9	86.99
1135	0.0476 0.0048	59.1737 0.0006	35.47 0.96	29.15 1.76	1.14	63.5 3.8	79.28
1310	0.1173 0.0099	7.2690 0.1137	79.53 1.67	56.17 3.55	1.78	120.6 7.4	67.54
1410	3.2477 0.4194	58.6280 0.1561	1074.70 115.73	125.91 175.54	0.12	259.9 337.5	11.32

$$J = 0.001231 \pm 0.000016$$

Table 3.12. The ^{40}Ar-^{39}Ar Plateau- Isochron- and Integrated- ages from samples from Kutch, Western India. The plateau ages are weighted mean of the individual fractions forming the plateau.

Sample No.	Plateau fractions		Isochron			Total
	Age(Ma)	%39Ar	Age(Ma)	Intercept	MSWD	Age(Ma)
BHUJ-F	65.3 ± 0.7	99	64.1 ± 1.1	299 ± 4	0.3	66.8 ± 1.0
KB85-58	66.8 ± 0.3	72	67.4 ± 1.7	286 ± 19	0.02	67.0 ± 0.6
KB83-13	64.4 ± 0.6	86	65.3 ± 1.8	263 ± 71	0.5	63.7 ± 0.5
KB83-11A	67.7 ± 0.7	32	65.7 ± 1.4[2]	330 ± 6	1.4	67.8 ± 1.2
BHUJ-A	66.6 ± 0.9	31	62.1 ± 1.0[2]	312 ± 6	1.7	63.5 ± 0.4
KB85-54A	65.1 ± 0.7[1]	62	64.3 ± 1.7	369 ± 96	0.2	66.0 ± 0.5

1. For low temp. phase only (upto 650°C).

2. Linear reg. of 600°C-1000°C fraction

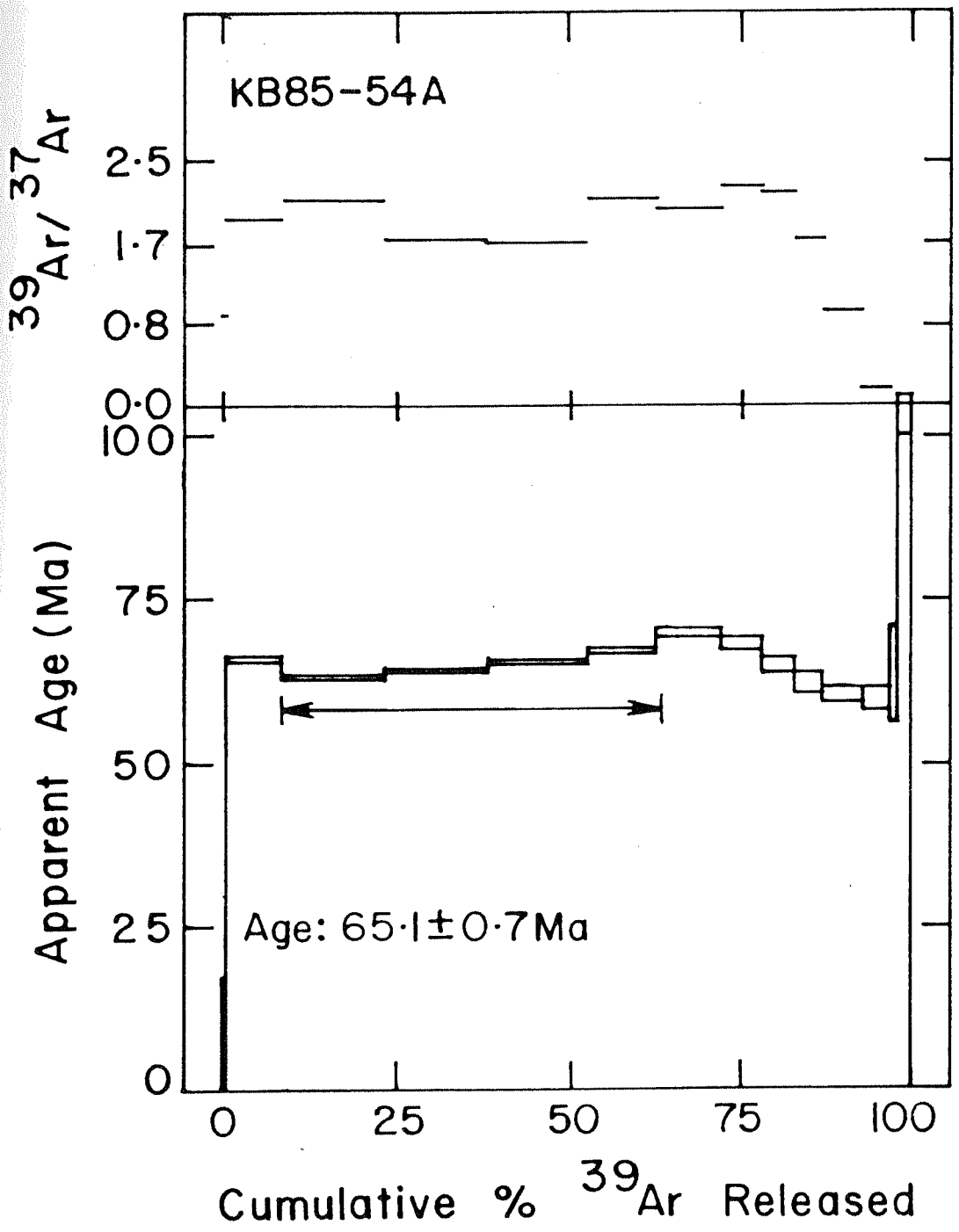


Fig. 3.20 Age spectrum for KB85-54A

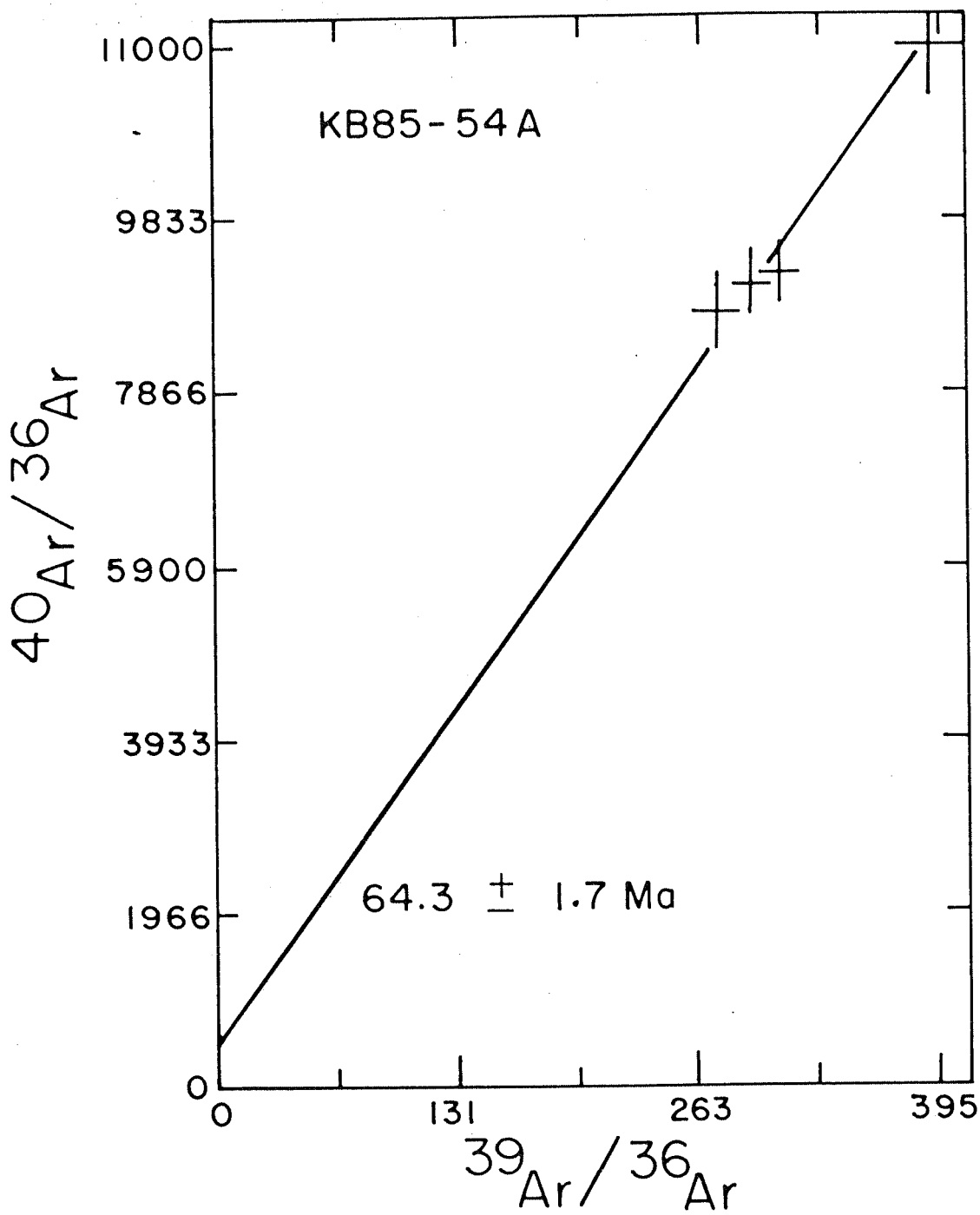


Fig. 3.21 Isochron plot for KB85-54A

formation ages around 66 Ma (at 2σ level) similar to those of the undisturbed alkali basalts and tholeiite from this region - once again indicating a close temporal relationship between the two types of magmatism in this region.

The fifth alkali basalt sample, KB85-54A, shows a bi-modal ^{39}Ar release pattern (fig. 3.20). The low temperature fractions, comprising 62% of ^{39}Ar released, form a plateau whereas the higher temperature steps display a staircase pattern with progressively decreasing apparent ages. This is also reflected in the K/Ca ratio diagram. The $^{39}Ar/^{37}Ar$ is relatively constant for the fractions which form the plateau whereas it decreases during the higher temperature fractions which form the staircase pattern. The plateau age corresponding to the low temperature plateau region is 65.1$\pm$0.7 Ma. The isochron age for the integrated age is 66.0$\pm$0.5 Ma. Within experimental errors, these ages are not significantly different from those given earlier.

The $^{40}Ar-^{39}Ar$ ages for the alkali and tholeiitic basalts from this region indicate that the two types formed at the same time about 66 Ma ago. The ages for the alkali basalts show a range between 64.4$\pm$0.6 Ma to 67.7$\pm$0.7 Ma indicating a span of 2 Ma (1σ level). The reality of this difference calls for more precise measurements. More important, however, is the fact that these ages fall within the range of ages for tholeiites from the 1200 m thick sequence at Mahabaleshwar of the main Deccan Province (see Chapter II). The basalts from Kutch therefore are coeval with the main Deccan volcanic phase.

3.8 SUMMARY

The ultramafic nodules can be classified as dunites and spinel peridotites. The dunites are probably of a cognate origin. The spinel peridotites resemble,both in texture and mineralogy, the mantle nodules described from other parts of the world and can be classified as Type 1 of Menzies (1983).

Among the constituent minerals of the spinel peridotites the Al_2O_3 rich chrome spinels show the maximum variation. The olivines, orthopyroxenes and clinopyroxenes show fairly uniform composition. Marginal interaction between the nodule and host rocks is minimal confined to only a thin 50-100 μm zone.These nodules are probably the residues of partial melting of upper mantle material.

The chemistry of host basalts reveals their undersatuated and alkaline nature.These are similar to the host alkali basalts found elsewhere in the world.In Bhujia two different basalt compositions are encountered which could represent either two different magma types or represent the compositional range of the magmas erupted at Bhujia.

The alkali and tholeiitic basalts from Kutch formed around 66 Ma and are coeval with the tholeiites from the Mahabaleshwar area of the main Deccan Province.

CHAPTER IV

RARE EARTH ELEMENT AND ISOTOPIC STUDIES

4.1. INTRODUCTION

Information about the inaccessible lithosphere can be obtained in a variety of ways but direct geochemical data are available only through the study of ultramafic xenoliths transported to the surface in alkali basalt and kimberlite magmas, or possibly study of alpine ultramafic massifs. The chemical and mineralogical compositions of ultramafic xenoliths have provided insights into the nature of upper mantle in a variety of tectonic settings, although most of the known major nodule localities in continental settings are associated with zones of crustal weakness, ranging from faults to major rifts.

Trace element and isotopic studies of mantle derived magmas and their included xenoliths have shown the earth's mantle to be extremely heterogeneous. While magmas that host the xenoliths appear to have a relatively homogeneous source, the xenoliths themselves represent fragments of many and varied heterogeneous reservoirs.

The chemical heterogeneity observed in lithsopheric mantle xenoliths is partly due to the fact that lithospheric mantle forms a structural barrier to the upward migration of asthenospheric melts.The lithosphere is thus transformed by invasion of fluids rich in large ion lithophile (LIL) elements and light rare earth elements (LREE) (Hawkesworth et. al., 1984; Menzies et. al.,1987). These metasomatic fluids generate chemical heterogeneity in otherwise depleted or possibly fertile peridotite.Mantle xenoliths represent fragments of the lithospheric mantle that evolve in response to differing trace element ratios for variable time periods producing chemically distinct reservoirs.

Spinel and garnet lherzolites, entrained in alkali basalts and alkaline magmas occasionally exhibit enriched trace element and isotopic characteristics, but majority have trace element and isotopic characteristics identical to those of MORB or OIB.These xenoliths exhibit a range in Sr and Nd isotopes compatible with a time-integrated depletion in Rb and LREE (Stosch et. al., 1980;Jagoutz et. al., 1980; Menzies and Murthy 1980;Roden et. al.,1984; Stosch and Lugmair 1986;Stosch et. al.,1986).Their isotopic data are similar to those in mid ocean ridge basalts (MORB) and ocean island basalt (OIB). In majority of enriched xenoliths, however, the isotopic composition does not represent a time-integrated response to the present trace element composition since most of them are enriched in LREE. This is because the Rb/Sr and Sm/Nd ratios have been

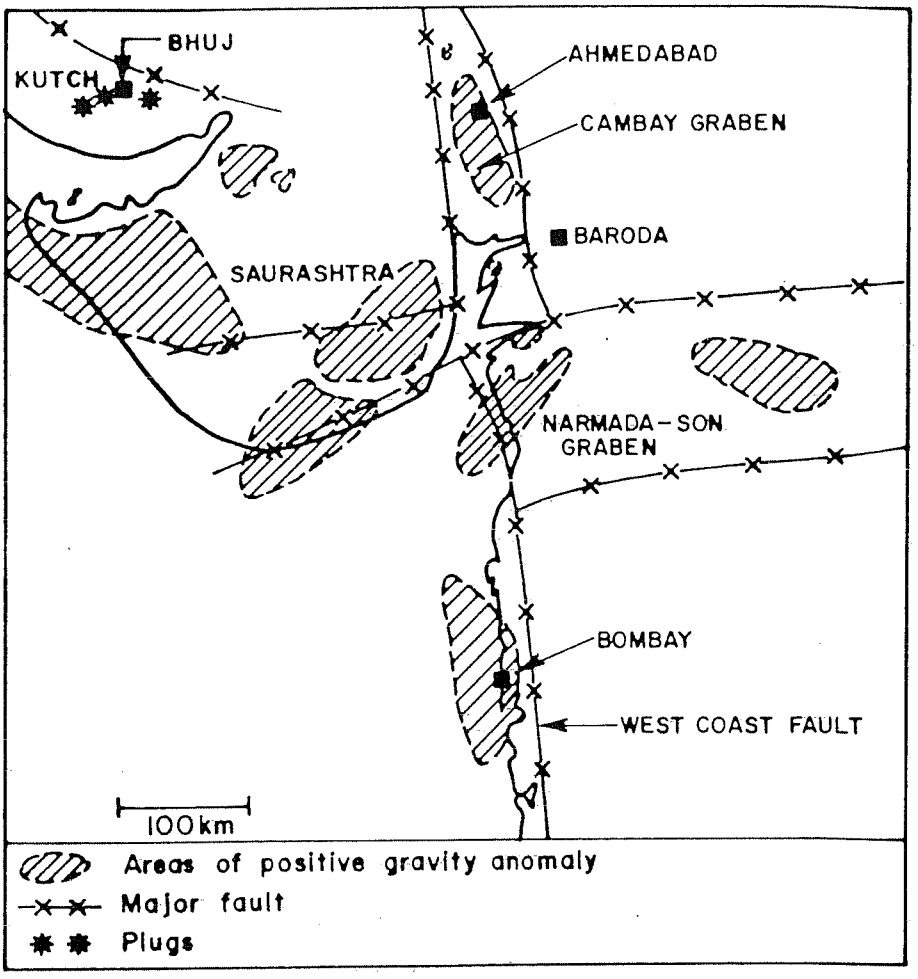


Fig. 4.1 MAP OF WESTERN INDIA SHOWING MAJOR RIFT ZONES, POSITIVE GRAVITY ANOMALIES AND THE PLUGS.

(MODIFIED AFTER BISWAS & DESHPANDE, 1973)

modified so recently (less than 100 Ma) that radiogenic growth did not result. In such cases the trace-element ratios are decoupled. This decoupling represents a relatively recent change effected by an enriched component into depleted lithosphere.

4.2. KUTCH ALKALI BASALTS AND SPINEL PERIODITITES

Alkali basalts are sometimes associated with continental flood basalt volcanism but reports of ultramafic xenoliths are rare, the only documented example being those from Patagonian Plateau basalts (Skewes and Stern, 1979) and Central Kutch, part of Deccan Trap province (De, 1964; Krishnamurthy et. al., 1988).

The alkali basalt plugs, in Kutch, some of which host mantle xenoliths are contemporaneous with the tholeiites of both Kutch and main Deccan activity (see Chapter 3). These basalts are associated with major fault zones as shown in the tectonic map of western India (Fig. 4.1). Rare earth element and isotopic characteristics of these basalts and spinel peridotites occurring in them are discussed in this chapter.

Rare earth elements were determined by instrumental neutron activation analysis at Johnson Space Centre by Dr. A.V. Murali. Mass-spectrometric determinations of Rb, Sr, Sm and Nd concentrations and isotopic compositions were made following the techniques described in Chapter III.

For isotopic and neutron activation studies of spinel peridotites clean, hand-pitched mineral separates were

Table 4.1. REE Data for Spinel Peridotites, Mineral Separates and Basalts

Sample No.	La	Ce	Nd	Sm	Eu	Tb	Tm	Yb	Lu	Sc	Co
BN-A CPX	1.90	6.6	2.31	0.56	0.26	-	-	0.86	0.13	82.0	22.0
BN-A OPX	0.25	1.4	0.07	0.01	0.03	-	-	0.15	0.03	18.0	54.0
BN-B CPX	6.81	16.7	9.30	2.61	0.90	0.60	-	1.23	0.16	76.0	18.0
BN-B OPX	0.10	-	0.07	0.02	0.02	-	-	0.12	0.02	16.0	52.0
BN-C CPX	2.07	8.3	-	0.70	0.28	0.32	-	1.10	0.14	80.0	24.0
BN-C OPX	0.17	-	-	-	0.05	-	-	0.16	0.03	17.0	52.0
DN-1 CPX	18.11	57.0	34.3	6.56	1.85	0.55	-	0.71	0.12	83.0	14.0
DN-1 OPX	0.11	1.0	0.1	0.03	0.02	-	-	0.08	0.02	13.0	49.0
85/13 CPX	3.10	10.6	3.9	0.96	0.33	0.17	-	0.87	0.15	72.0	17.0
BN-H CPX	-	-	1.5	0.56	-	-	-	-	-	-	-
BN-H OPX	-	-	0.1	0.01	-	-	-	-	-	-	-
BN-B Wr	2.29	4.9	2.2	0.41	0.13	0.06	-	0.15	0.02	7.7	106.0
BN-B WrL	1.13	3.0	-	0.21	0.08	-	-	0.09	0.01	6.1	112.0
BN-C Wr	2.65	5.5	2.4	0.44	0.13	0.06	-	0.13	0.02	4.2	117.0
BN-C WrL	1.10	3.3	2.5	0.17	0.06	-	-	0.09	0.01	4.1	128.0
BN-D Wr	6.90	13.5	6.0	0.95	0.28	0.11	-	0.24	0.02	6.7	113.0
BN-D WrL	3.17	7.5	3.5	0.64	0.20	0.08	-	0.17	0.02	7.0	130.0
DN-A Wr	2.27	5.0	-	0.44	0.12	0.04	-	0.08	0.01	6.9	102.0
DN-A WrL	1.65	4.2	2.7	0.44	0.13	0.05	-	0.13	0.02	7.4	109.0
DN-B Wr	1.70	3.7	-	0.28	0.08	-	-	0.09	0.01	4.7	109.0
DN-B WrL	0.97	2.6	-	0.24	0.07	-	-	0.07	0.01	5.0	113.0
BHUJ-A	62.40	120.0	45.0	10.10	2.84	1.14	-	1.70	0.21	23.7	83.8
BHUJ-B	65.10	127.0	40.0	10.60	2.97	1.30	-	1.80	0.20	18.9	70.9
DHRUB-A	30.30	63.0	30.0	6.70	2.07	0.90	-	1.50	0.18	20.7	69.8

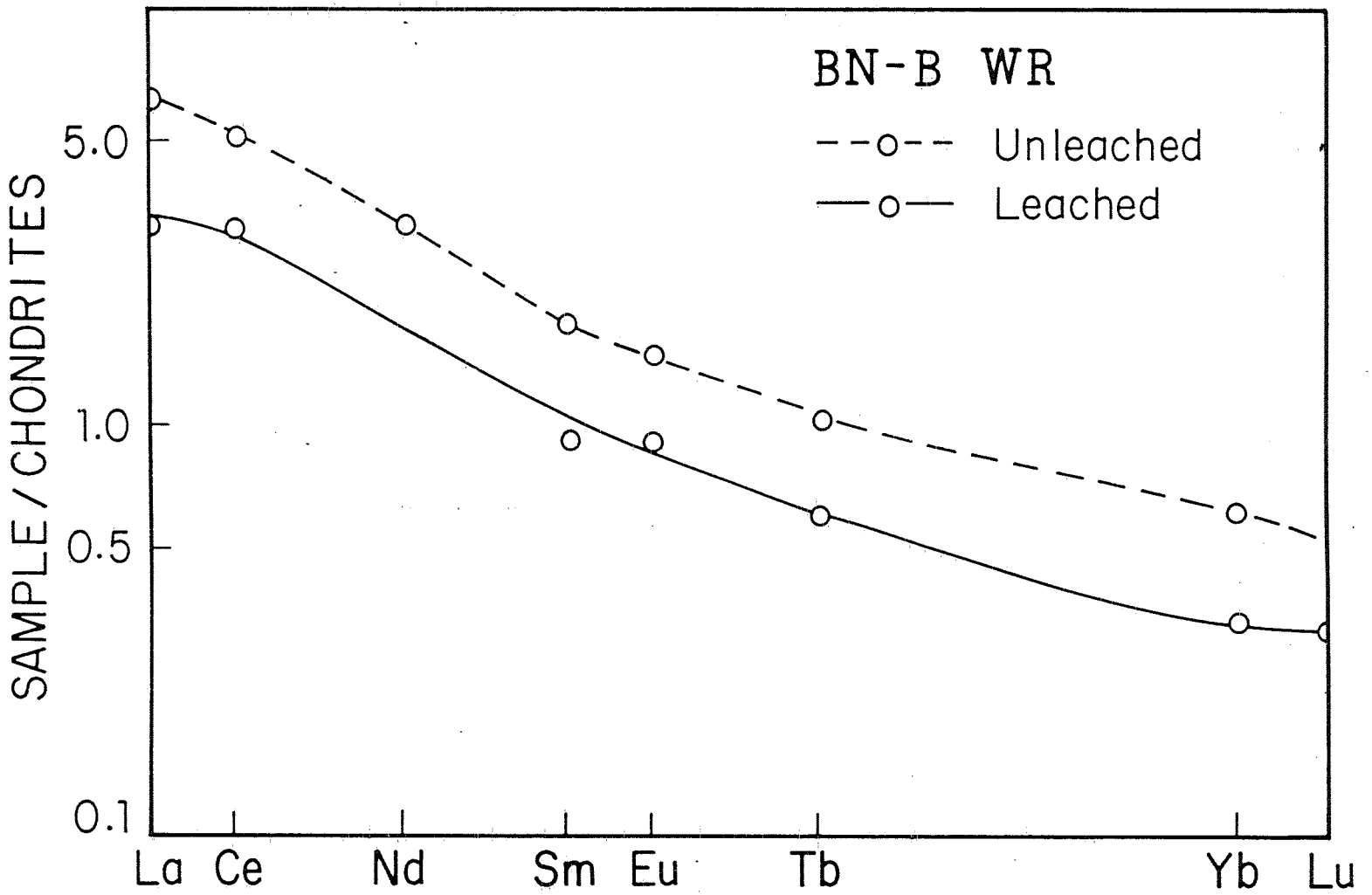


Fig. 4.2 Chondrite normalised REE pattern for BN-B.

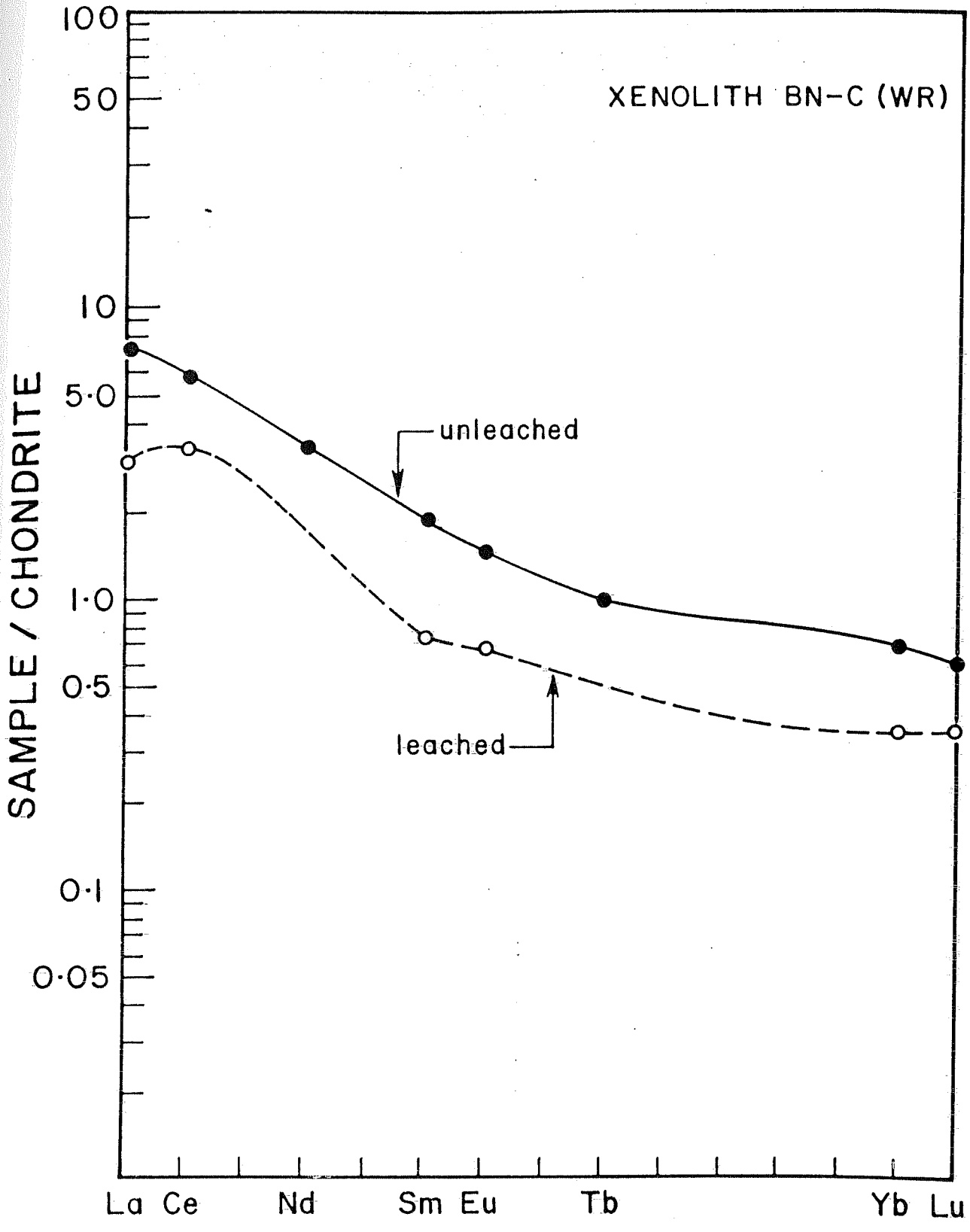


Fig. 4.3 Chondrite normalised REE pattern for BN-C.

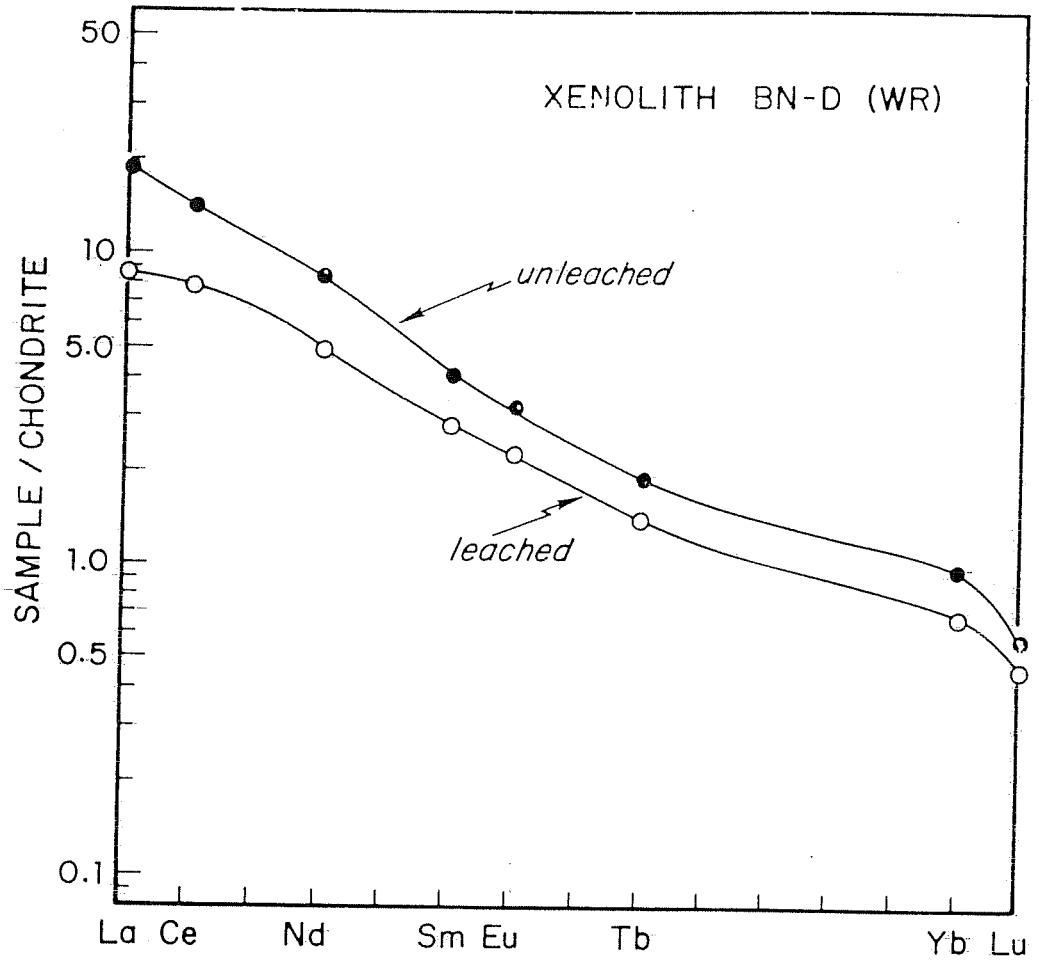


Fig. 4.4 Chondrite normalised REE pattern for BN-D.

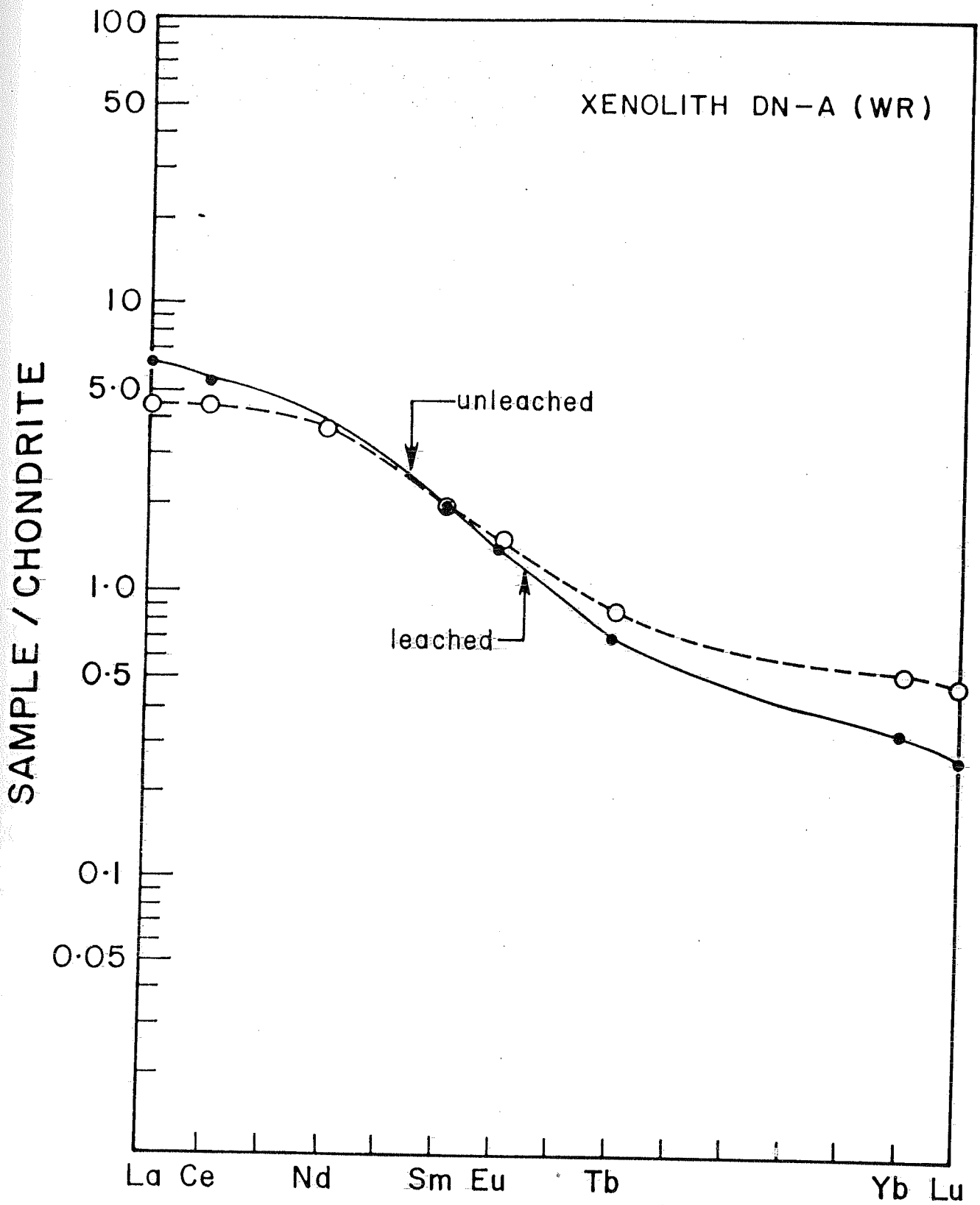


Fig. 4.5 Chondrite normalised REE pattern for DN-A.

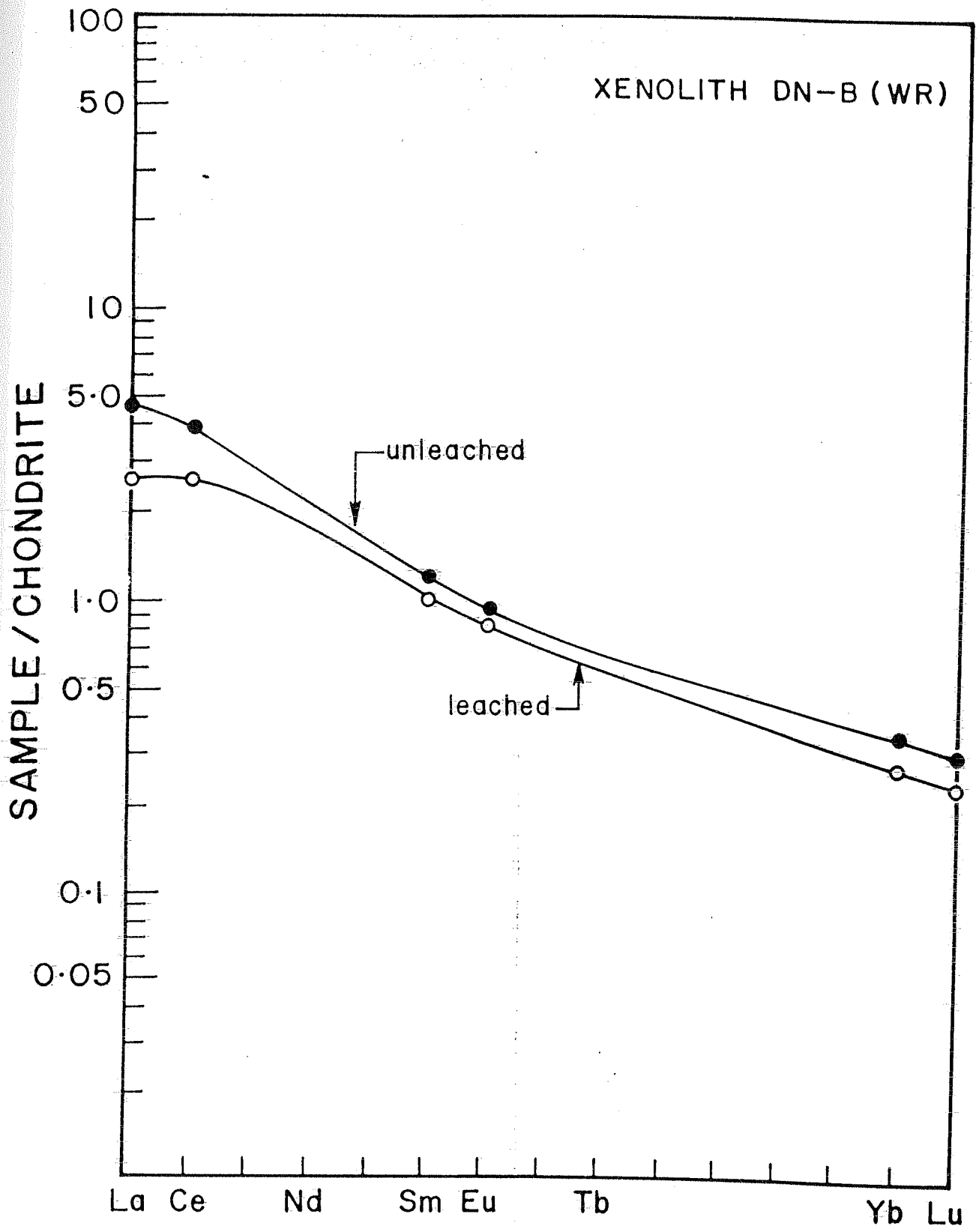


Fig. 4.6 Chondrite normalised REE pattern for DN-B.

analysed. In order to minimise contributions from grain surface components, all samples were acid leached prior to isotopic analysis. For a few samples the leaches were also analysed. For neutron activation analysis both leached and unleached aliquots were investigated.

4.3. RARE EARTH ELEMENTAL DATA

A.BULK XENOLITHS

The REE,Co and Sc concentrations of five bulk xenoliths are given in Table 4.1. Chondrite normalized REE concentrations are plotted in Fig. 4.2-4.6.Data are given for both acid-leached and unleached aliquots.The light REE enriched patterns for both unleached and leached aliquots are similar to those observed for spinel peridotites from other localities (review Frey,1984;Menzies,1983).

Although part of the difference between leached and unleached aliquots may be due to variable clinopyroxene contents, the differences are systematic and must primarily be due to the leaching process. Both concentrations and degree of LREE enrichment are less for leached compared to unleached samples (Table 4.1). La in the leached aliquots ranges from 42 to 73% of the concentrations in unleached samples. $(La/Yb)_n$ ranges from 8.3 to 12.5 in the leached samples, and 10.4 to 19.4 in the unleached, and is consistently lower for leached aliquots.Thus substantial fractions of the REE (and presumably other incompatible elements as well) must occur on grain surfaces and/or in soluble interstitial phases. Similar effects have been

analysed. In order to minimise contributions from grain surface components, all samples were acid leached prior to isotopic analysis. For a few samples the leaches were also analysed. For neutron activation analysis both leached and unleached aliquots were investigated.

4.3. RARE EARTH ELEMENTAL DATA

A.BULK XENOLITHS

The REE,Co and Sc concentrations of five bulk xenoliths are given in Table 4.1. Chondrite normalized REE concentrations are plotted in Fig. 4.2-4.6.Data are given for both acid-leached and unleached aliquots.The light REE enriched patterns for both unleached and leached aliquots are similar to those observed for spinel peridotites from other localities (review Frey,1984;Menzies,1983).

Although part of the difference between leached and unleached aliquots may be due to variable clinopyroxene contents, the differences are systematic and must primarily be due to the leaching process. Both concentrations and degree of LREE enrichment are less for leached compared to unleached samples (Table 4.1). La in the leached aliquots ranges from 42 to 73% of the concentrations in unleached samples. $(La/Yb)_n$ ranges from 8.3 to 12.5 in the leached samples, and 10.4 to 19.4 in the unleached, and is consistently lower for leached aliquots.Thus substantial fractions of the REE (and presumably other incompatible elements as well) must occur on grain surfaces and/or in soluble interstitial phases. Similar effects have been

reported by others (Jagoutz et. al.,1980;Kurat et. al.,1980; Stosch and Seck, 1980; Zindler and Jagoutz, 1986; Stosch et. al., 1986).These studies have demonstrated that isotopic and trace element characteristics of mantle derived ultramafic xenoliths can be easily altered and modified by components present on grain surfaces.The contaminants may be derived from a variety of sources such as (i) partial fusion of related or unrelated mantle material, (ii) groundwater percolating through these rocks after they have been brought to the surface,and (iii) melts from the host magma. The REE studies of leached and unleached aliquots of bulk xenoliths in the present study demonstrate the presence of such a phase on the grain boundaries.Isotopic data on the leach solutions suggest that the leachable component is derived primarily from the host rocks probably through ground water transport since there is no petrographic evidence for host-rock melt penetrating the xenoliths.

All of the leached bulk xenolith samples exhibit LREE enriched patterns (Fig. 4.2-4.6)."Dry" perioditites which have lost a partial melt fraction are expected to show LREE depleted patterns (Frey and Green,1974).Spinel peridotites with relative LREE enrichment are believed to be metasomatized either "modally" (Harte,1983) which is same as 'Patent metasomatism' (Dawson,1984b;Menzies 1983) if the presence of a hydrous phase such as phlogopite is detectable, or "cryptically" if hydrous phases are absent (Dawson, 1984b). In case of cryptic metasomatism there is a

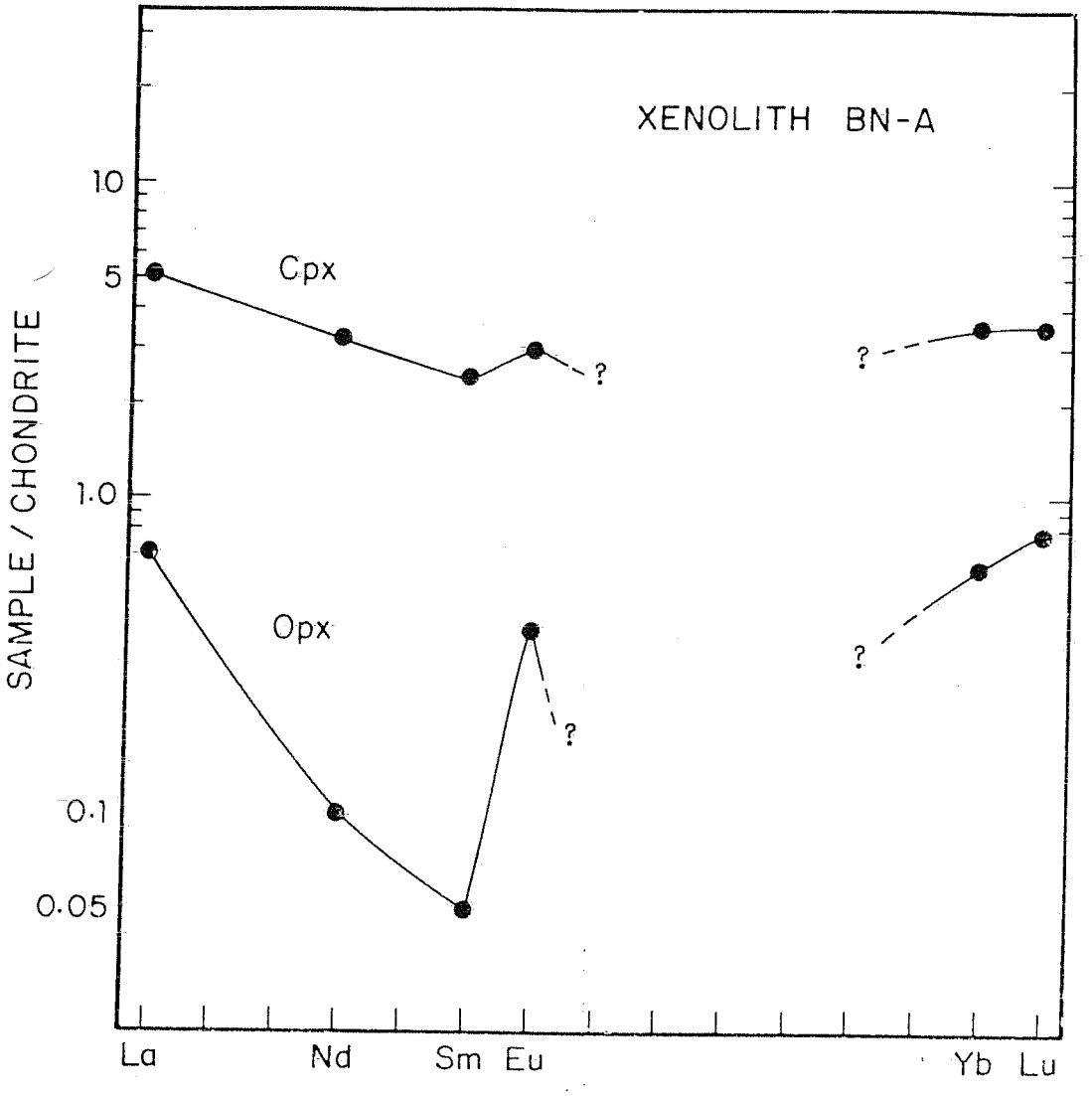


Fig. 4.7 Chondrite normalised REE pattern for Cpx and Opx BN-A.

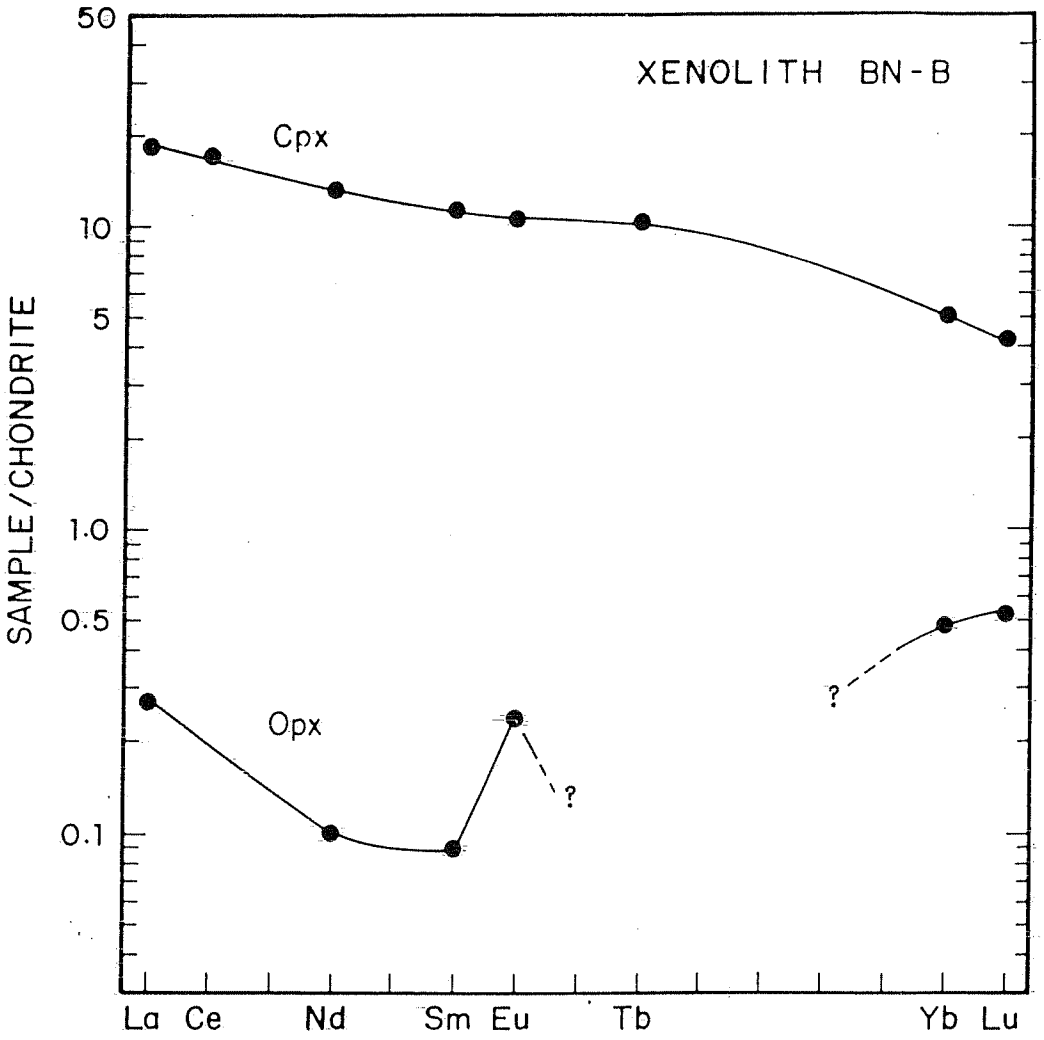


Fig. 4.8 Chondrite normalised REE pattern for Cpx and Opx BN-B.

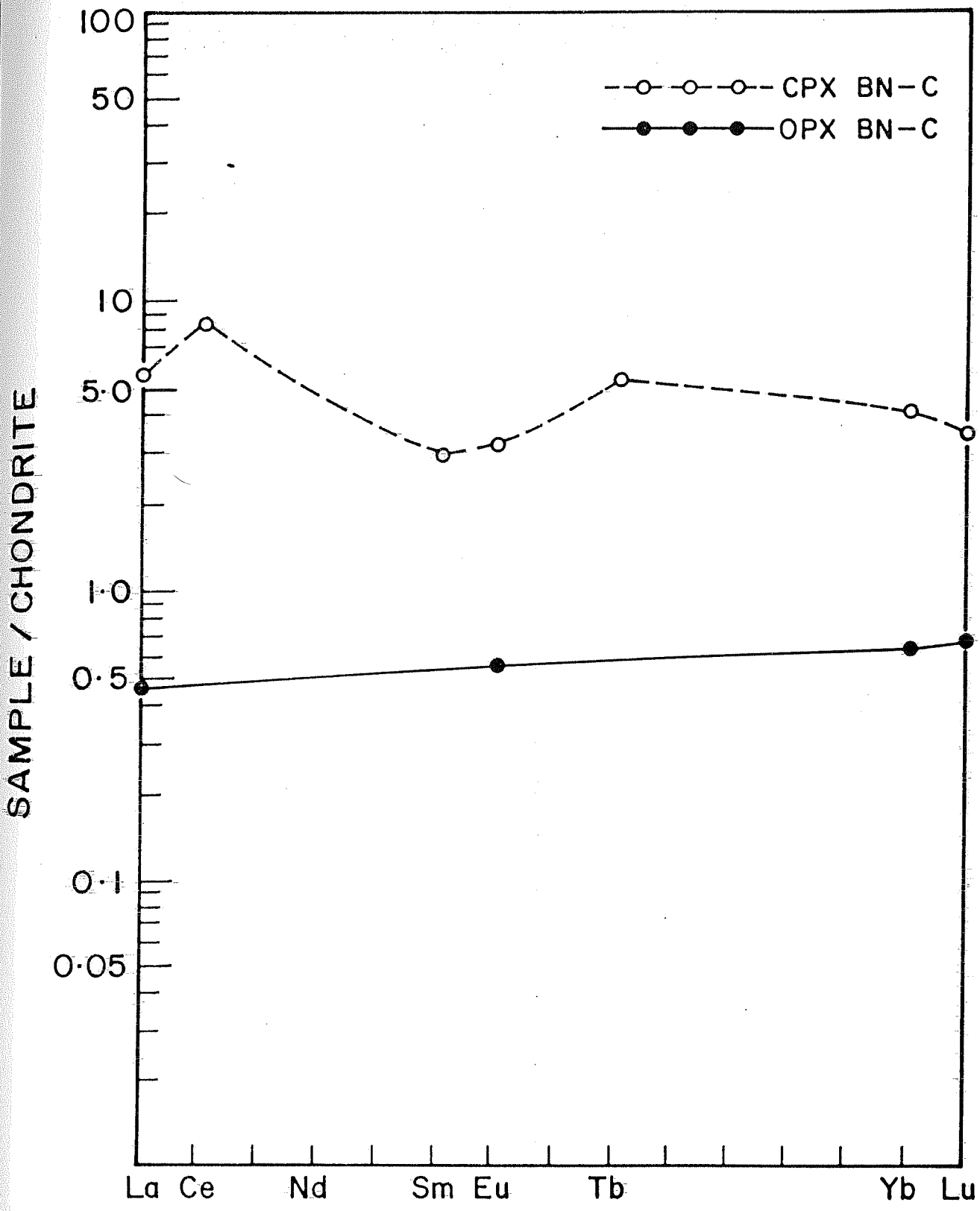


Fig. 4.9 Chondrite normalised REE pattern for Cpx and Opx BN-C.

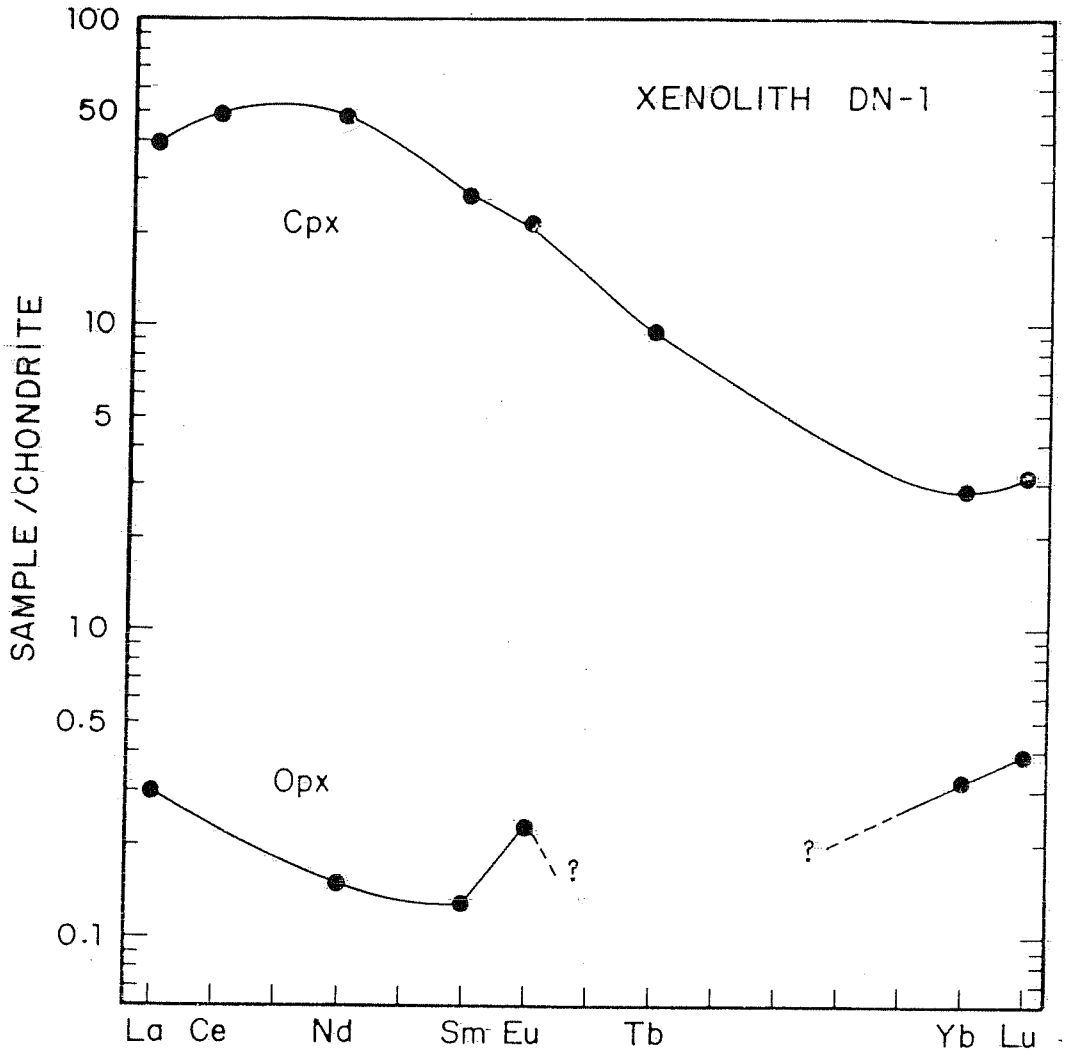


Fig. 4.10 Chondrite normalised REE pattern for Cpx and Opx DN-1.

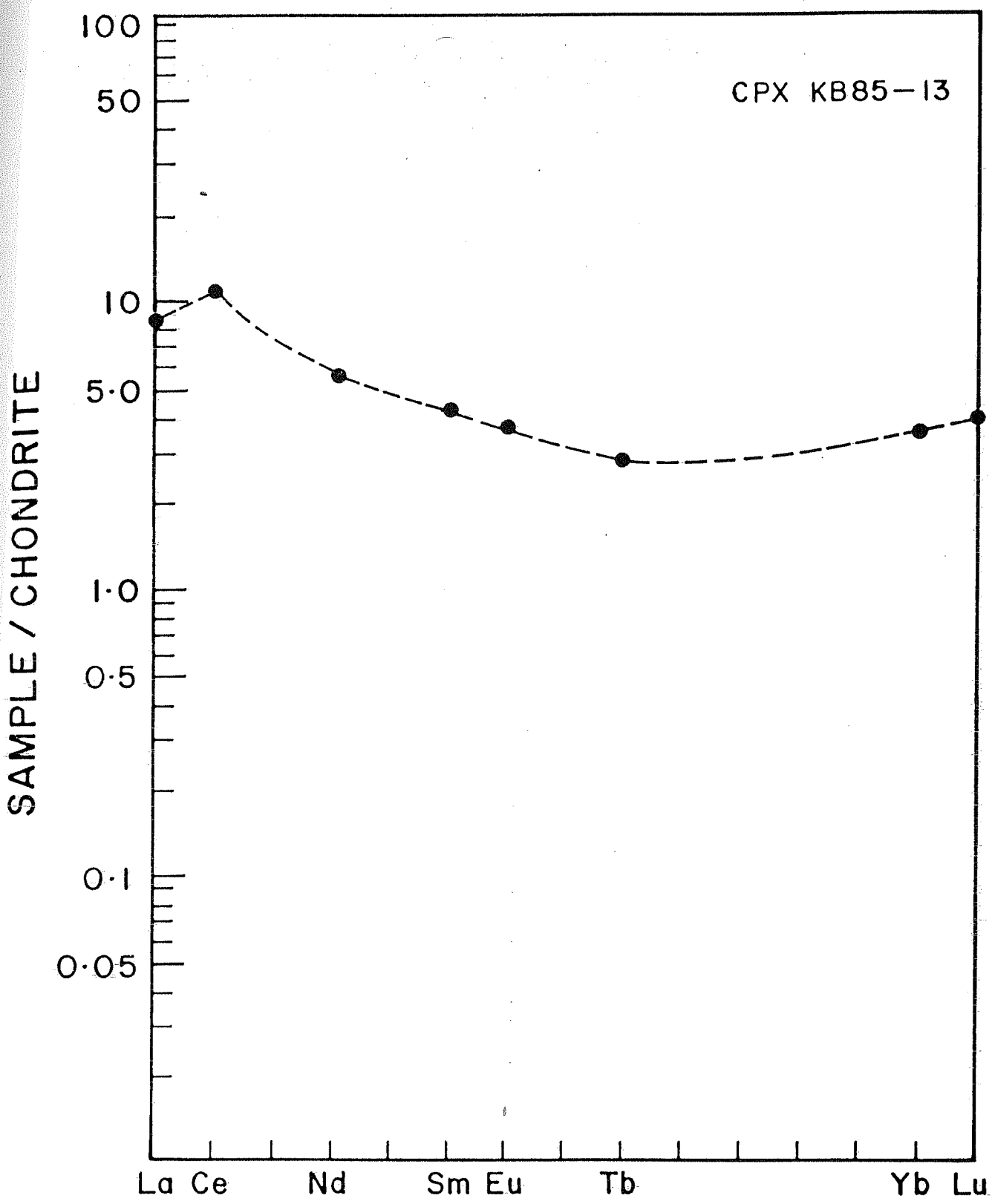


Fig. 4.11 Chondrite normalised REE pattern for Cpx KB85-13.

decoupling of trace element chemistry from major element chemistry. Metasomatized peridotites are generally believed to have undergone a multi-stage evolutionary history (Varne and Graham 1971;Frey and Green 1974;Menzies 1983;Frey 1984). An alternative view is that light REE enriched patterns in anhydrous spinel peridotites are due to contamination from the host rocks (e.g. Stosch et. al.,1986).In the case of the nodules from Kutch, leaching experiments and mineral separate data suggest that host rock contamination can be ruled out as a primary cause for the LREE enriched pattern. Thus the xenoliths can be placed in the cryptically metasomatised category.

B. CLINOPYROXENES AND ORTHOPYROXENES

The REE, Sc and Co concentration data are given in Table 4.1. Mineral separates were inclusion-free to the best of picking ability, and were leached prior to analysis,as discussed earlier (see Chapter II).Chondrite-normalized REE data are shown in Fig. 4.7-4.11.

All clinopyroxene separates are LREE enriched,although the concentrations and degree of enrichment vary widely.The REE patterns for the two separates for which whole xenolith data are also available parallel the bulk rock pattern.This type of pattern is characteristic of metasomatized spinel-peridotittes and dry spinel harzburgites from other localities (Frey 1984; Menzies 1983; Roden et. al.,1984). However, an interesting but puzzling feature is the small positive Eu anomaly shown by two samples,BN-A and BN-C.

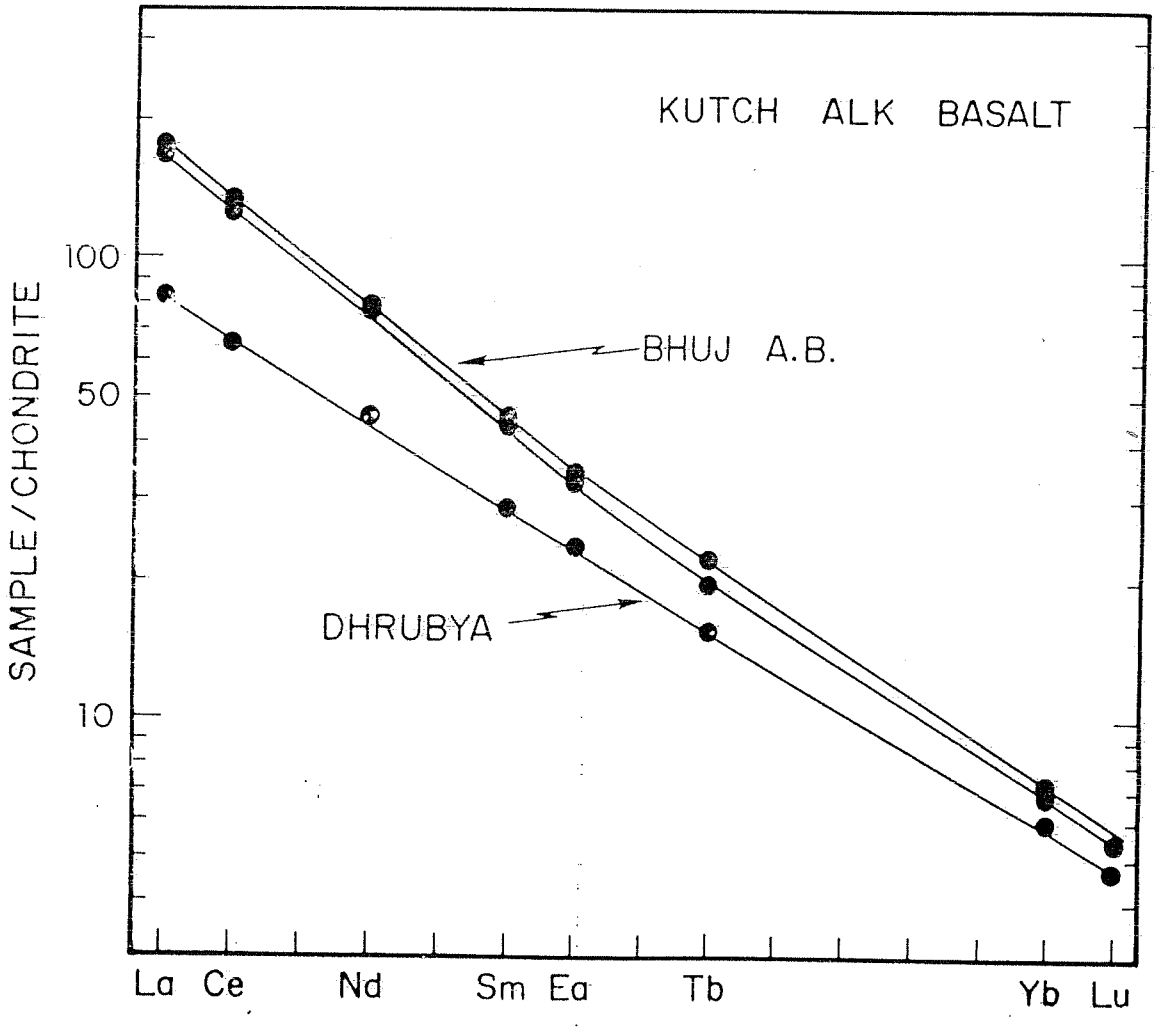


Fig. 4.12 Chondrite normalised REE pattern for basalts.

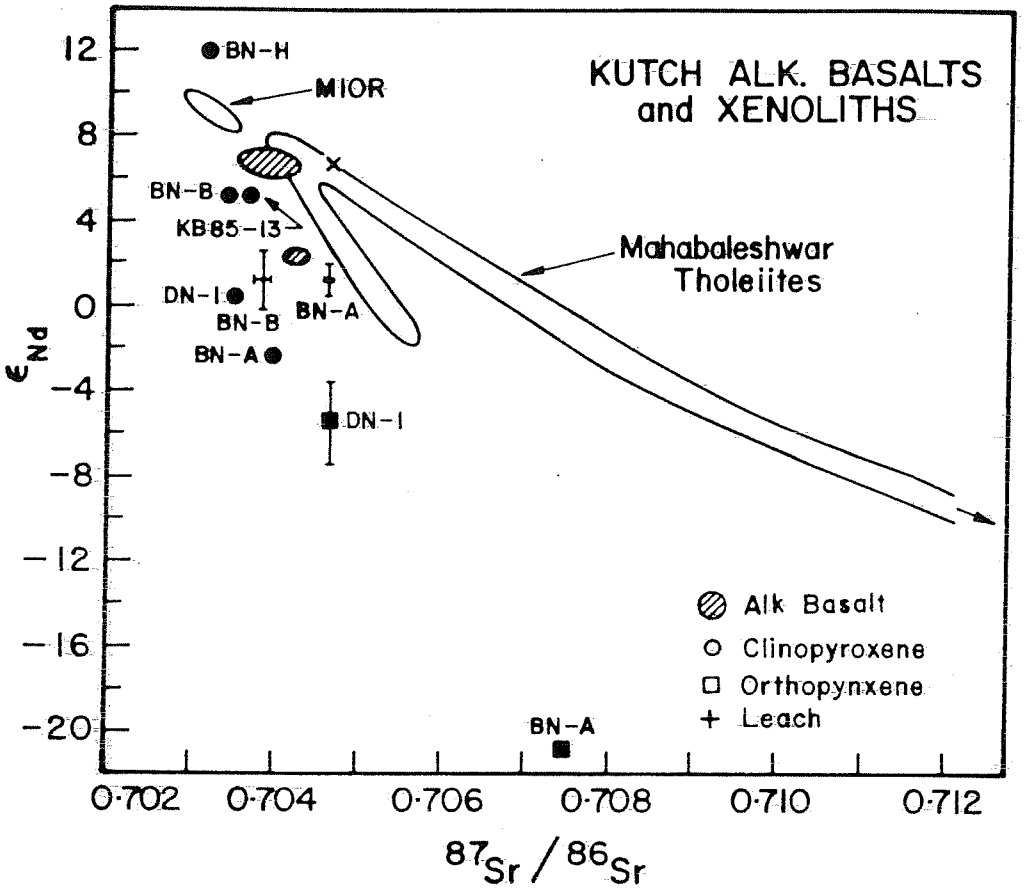


Fig. 4.13 Sr-Nd isotopic variation in nodules and basalts from Kutch.

Perhaps significantly,these two samples have the lowest REE concentrations.

The orthopyroxene separates, on the other hand,exhibit U-shaped to LREE depleted patterns. Those with U-shaped patterns also show significant positive Eu anomalies.While the Eu anomaly is present in both the clinopyroxene and orthopyroxene separates from sample BN-A, it is observed only in the orthopyroxene for samples DN-1 and BN-B.

The concave upward REE patterns of the orthopyroxene probably reflect their metasomatised nature resulting from the superimposition of a LREE enriched pattern over an originally LREE depleted trend. The significance of the positive Eu anomalies is not clear. It suggests the involvement of plagioclase in the REE history of this material,although when and how is very uncertain.

The three host rocks analyzed,two from Bhujia and one from Dhrubiya Hill,show strong LREE enrichment (Fig. 4.12, Table 4.1). Chondrite normalized La/Yb values are approximately 25 for Bhujia and 14 for Dhrubiya.

4.3.2. Nd AND Sr ISOTOPES

A. SPINEL PERIDOTITES

The isotopic composition of xenolith mineral separates along with acid leach from two of them are given in Table 4.2 and plotted in Fig. 4.13.The isotopic compositions of the xenolith clinopyroxenes are significantly different from those of the host alkali basalts.This is in contrast

Table 4.2. Nd and Sr Isotopic Composition of Mineral Separates

Sample	143/144	2 Sigma	ϵ Juv	87/86	2 Sigma	Rb(ppm)
BN-A cpx	0.512423	0.000012	-2.8	0.704006	0.000026	0.57
BN-A opx	0.511459	0.000030	-21.6	0.707509	0.000024	0.05
BN-B cpx	0.512824	0.000022	5.0	0.703452	0.000024	0.82
BN-B opx				0.704714	0.000026	0.12
BN-A cpx/opx Leach	0.512630	0.000036	1.2	0.704636	0.000042	-
BN-B cpx Leach	0.512629	0.000074	1.2	0.703842	0.000096	-
BN-B opx Leach				0.705165	0.000048	-
DN-1 cpx	0.512558	0.000006	-0.2	0.703511	0.000022	-
DN-1 opx	0.512278	0.000102	-5.5	0.704765	0.000030	0.06
BN-H cpx	0.513193	0.000030	12.3	0.703231	0.000028	0.61
BN-H opx				0.708071	0.000024	-
KB85-13 cpx	0.512813	0.000026	4.8	0.703747	0.000018	1.96

Table 4.2 contd.

Sample	Sr(ppm)	Sm(ppm)	Nd(ppm)	$^{147}Sm/^{144}Nd$	$^{87}Rb/^{86}Sr$
BN-A cpx	51.83	0.56	2.31	0.1462	0.0316
BN-A opx	3.39	0.01	0.07	0.0996	0.0419
BN-B cpx	114.56	2.61	9.30	0.1695	0.0207
BN-B opx	3.88	0.02	0.07	0.1782	0.0916
BN-A cpx/opx Leach	-	-	-	-	-
BN-B cpx Leach	-	-	-	-	-
BN-B opx Leach	-	-	-	-	-
DN-1 cpx	519.39	6.56	34.26	0.1157	-
DN-1 opx	1.31	0.03	0.11	0.1695	0.1236
BN-H cpx	40.24	0.56	1.50	0.2241	0.0439
BN-H opx	1.38	0.01	0.03	0.1435	-
KB85-13 cpx	65.90	0.96	3.92	0.1472	0.0862

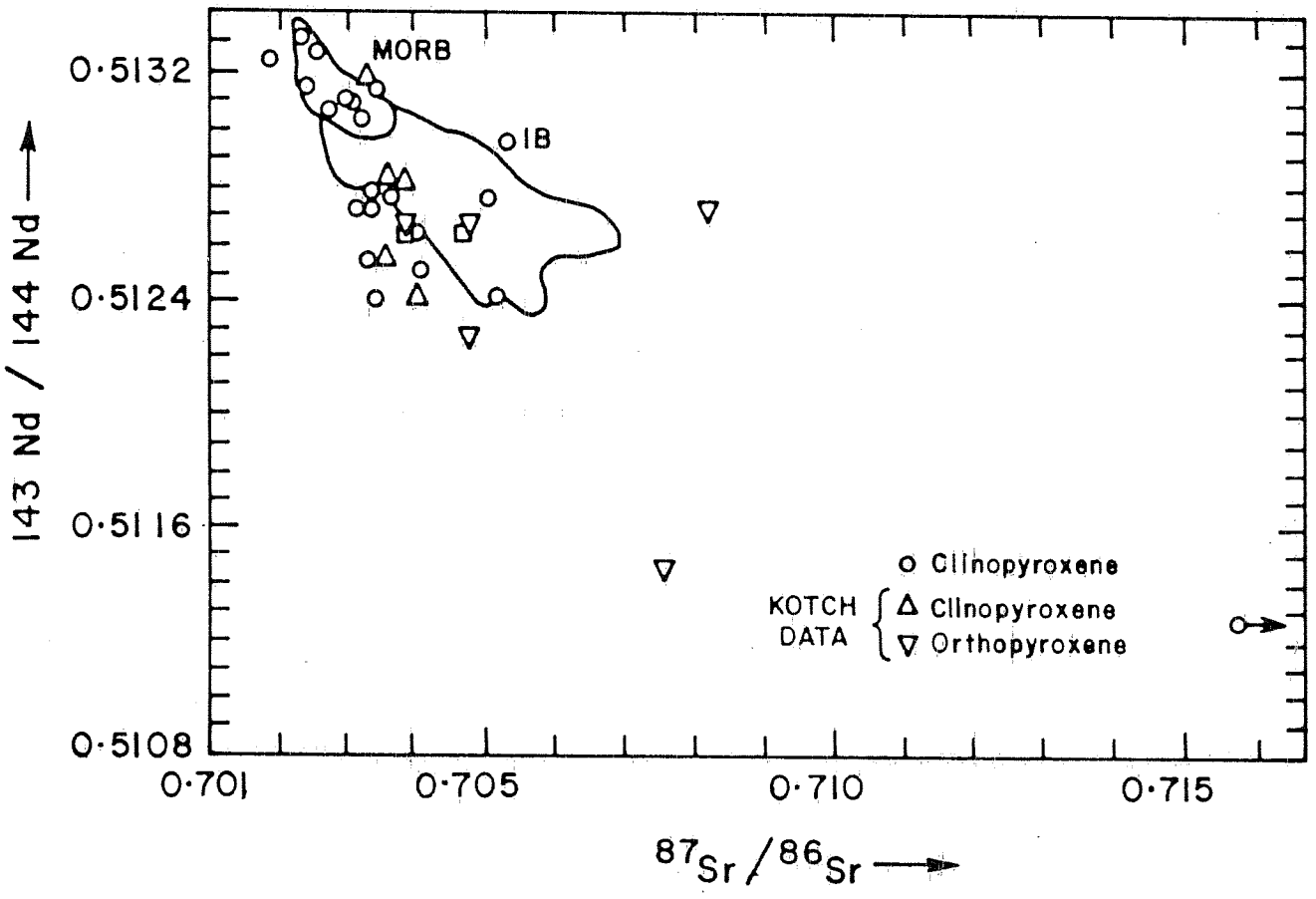


Fig. 4.14 ISOTOPIC COMPOSITIONS OF SPINEL PERIDOTITES FROM ALKAL, BASALTS (AFTER ZINDLER AND HART, 1986)

to the situation in some other areas, e.g.,South Yemen (Menzies and Murthy, 1980), Nunivak island (Zindler and Jagoutz, 1986) and San Carlos,Arizona (Zindler and Jagoutz, 1986, 1988) where the host basalts and included xenoliths have similar isotopic compositions. The data from Kutch suggest that the xenoliths are accidental inclusions in the basalt, unrelated to the source material of the host rocks. They are probably random samples of the upper part of the sub-Deccan continental lithosphere.

The isotopic compositions of the xenolith clinopyroxenes fall within the range observed for spinel peridotites worldwide (Fig. 4.14) (Zindler and Hart,1986; Stosch et. al., 1986; Stosch and Lugmair 1986).The large variation in $^{143}Nd/^{144}Nd$ and relatively smaller variation in $^{87}Sr/^{86}Sr$ are similar to the situation observed for hydrous xenoliths from Scotland (Menzies et. al.,1987).All clinopyroxene compositions fall to the left of the "mantle array", a common occurrence for metasomatized xenoliths (Menzies 1983;Stosch and Lugmair 1986;Menzies et. al.,1987).

Orthopyroxene isotopic compositions are distinct from those of coexisting clinopyroxene (Table 4.2,Fig. 4.13 and 4.14). Although combined Sr and Nd isotopic data are available for only two opx-cpx pairs, there is also a consistent Sr isotopic difference between two additional pairs (Table 4.2). In all cases,orthopyroxene shows more enriched compositions. These data are in contrast to most other recent studies of anhydrous mineral pairs from xenoliths, which, although often showing Sr isotopic

disequilibrium, usually exhibit constant Nd isotopic compositions (Jagoutz et. al., 1980; Stosch et. al.,1980; Menzies and Murthy 1980; Stosch et. al., 1986;Stosch and Lugmair 1986;Zindler and Jagoutz 1986).Significant isotopic disequilibrium is common,however,between clinopyroxene and hydrous phases (Menzies and Murthy,1980).

The isotopic compositions of the acid leachable fractions were determined for two samples (see Table 4.2). In one case (sample BN-B),clinopyroxene and orthopyroxene leach solutions were measured separately and in the second (sample BN-A) they were combined. The Nd isotopic composition for the two leachates is identical and similar to that of the host basalt.The Sr isotopic compositions show greater variation,with $^{87}Sr/^{86}Sr$ varying from .705165 to .703842.The orthopyroxene leach solution has the highest $^{87}Sr/^{86}Sr$ while the clinopyroxene leach has the lowest.It appears that this acid leachable phase has been derived primarily from the host alkali basalt.

B. BASALTS FROM KUTCH

The isotopic compositions of basalts are given in Table 4.3. Fig. 4.13 is a plot of $^{143}Nd/^{144}Nd$ vs. $^{87}Sr/^{86}Sr$ for these samples. For reference,the field of mid-Indian Ocean ridge basalts and the mixing trends defined by tholeiites at Mahabaleshwar, about 700 km to the southeast in the main Deccan Province,are shown (Mahoney et. al.,1982).

The alkali basalts measured for isotopic composition

Table 4.3. Nd and Sr Isotopic Compositions of Basalts from Kutch.

Sample ID	Sm ppm	Nd ppm	147Sm/ 144Nd	143Nd/ 144Nd	ε JUV	Rb ppm	Sr ppm	87Rb/ 86Sr	87Sr/ 86Sr
BHUJ-A	10.39	55.80	0.1126	0.512649 ±12	+1.6 ±0.2	52.57	973.80	0.156	0.704428 ±26
BHUJ-B	10.44	55.99	0.1127	0.512652 ±14	+1.7 ±0.3	51.77	858.80	0.1743	0.704373 ±24
BHUJ-E	6.69	32.21	0.1256	0.512880 ±10	+6.1 ±0.2	13.64	713.70	0.0553	0.704029 ±24
BHUJ-F	5.54	33.89	0.0974	0.512884 ±12	+6.2 ±0.2	16.03	713.44	0.0650	0.703931 ±28
DHRUB-A	6.75	32.50	0.1256	0.512896 ±12	+6.4 ±0.2	59.90	739.49	0.2342	0.703939 ±28
KB-1/83	7.26	35.19	0.1247	0.512883 ±14	+6.2 ±0.3	40.80	990.60	0.1191	0.704806 ±20
KB-4/83	7.44	35.46	0.1268	0.512893 ±10	+6.4 ±0.3	43.92	648.20	0.1856	0.704157 ±20
KB85-54(A)	6.61	30.77	0.1299	0.512887 ±18	+6.3 ±0.4	58.85	704.05	0.2056	0.703986 ±22
KB83-11(B)	5.49	20.53	0.1615	0.512884 ±10	+6.2 ±0.2	51.52	615.77	0.2419	0.704014 ±24
KB83-13	9.61	45.84	0.1276	0.512876 ±12	+6.0 ±0.2	44.97	801.89	0.1622	0.704210 ±32

Table 4.3 contd.

KB16/83	4.36	18.26	0.1443	0.511903 ±22	-12.9 ±0.4	22.05	218.80	0.0348	0.715350 ±24
KB85-58	6.67	25.11	0.1605	0.512701 ±14	+2.6 ±0.3	18.59	214.70	0.2504	0.705373 ±24
KB85-57	5.49	20.53	0.1615	0.512713 ±18	+2.9 ±0.4	13.23	224.80	0.1702	0.705124 ±20
KB85-56(B)	4.35	18.16	0.1448	0.511898 ±10	-13.0 ±0.2	25.11	206.02	0.3529	0.715607 ±24

represent various plugs from Kutch.Some are host rocks for the xenoliths analyzed in this study. Isotopically they define two discrete clusters on the $^{143}Nd/^{144}Nd$ vs $^{87}Sr/^{86}Sr$ diagram (Fig. 4.13). The majority fall within a very narrow field,with $^{143}Nd/^{144}Nd$ varying from 0.512876 to .512893 and $^{87}Sr/^{86}Sr$ varying from 0.70415 to 0.70421.Two samples from Bhujia hill, however, show a different composition, with $^{143}Nd/^{144}Nd$ = 0.512649 and $^{87}Sr/^{86}Sr$ = .704428. Samples from Bhujia plot in both groups,but no intermediate values occur. Significantly,these two samples can be distinguished from other alkali basalts on the basis of their major and trace element chemistry also as discussed in Chapter III.Without additional sampling it is not possible to say whether this represents the total range of variation for the alkali basalts.

Significantly, most of the alkali basalts from Kutch fall in the field defined by the least crustally contaminated Mahabaleshwar tholeiites.Moreoever,tholeiites from Kutch fall along the Mahabaleshwar mixing trend,but towards higher $^{87}Sr/^{86}Sr$ and lower $^{143}Nd/^{144}Nd$ than the alkali basalts (Fig. 4.13). These observations suggest a close association between the Kutch and Mahabaleshwar tholeiites, and between the mantle sources of the alkali and tholeiitic basalts. As is true for many alkali basalts,the depleted isotopic compositions contrast markedly with the strongly LREE enriched character of the rocks themselves. This indicates that the elemental enrichment is a relatively recent event superimposed on a source

Table 4.4. Initial Nd and Sr Isotopic Composition of Basalts and Minerals.

Sample ID	(143Nd/144Nd)I	$\epsilon_{JUV(T)}$	87Sr/86Sr)I
BHUJ-A	0.512600±12	+2.3±0.2	0.704282±26
BHUJ-B	0.512603±14	+2.3±0.3	0.704210±24
BHUJ-E	0.512826±10	+6.7±0.2	0.703977±24
BHUJ-F	0.512842±10	+7.0±0.2	0.703870±22
DHRUB-A	0.512842±12	+7.0±0.2	0.703719±28
KB-1/83	0.512829±14	+6.8±0.3	0.704694±20
KB-4/83	0.512838±10	+7.0±0.2	0.703983±20
KB85-54(A)	0.512831±18	+6.8±0.4	0.703793±22
KB83-11(B)	0.512814±10	+6.5±0.2	0.703787±24
KB83-13	0.512821±12	+6.6±0.2	0.704058±32
KB-16/83	0.511841±22	-12.5±0.4	0.715317±24
KB85-58	0.512632±14	+2.9±0.3	0.705138±24
KB85-57	0.512643±18	+3.1±0.4	0.704964±20
KB85-56(B)	0.511821±10	-12.7±0.2	0.715276±24

Table 4.4 contd.

Sample ID	(143Nd/144Nd)I	ϵJUV(T)	87Sr/86Sr)I
BN-A CPX	0.512360±12	-2.4±0.2	0.703976±26
BN-A OPX	0.511416±30	-20.8±0.6	0.707470±24
BN-B CPX	0.512751±22	+5.2±0.5	0.703433±24
BN-B OPX	0.512582±136	+2.0±2.6	0.704628±26
DN-1 CPX	0.512508±6	+0.5±0.1	0.703511±22
DN-1 OPX	0.512205±102	-5.4±1.9	0.704649±30
DN-1 OPX-2	0.512598±58	+2.3±1.1	0.703524±60
KB85-13 CPX	0.512749±26	+5.2±0.5	0.703666±18
BN-H CPX	0.513096±30	+12.0±0.5	0.703190±28
BN-H OPX	0.512671±810	+3.7±15.8	0.708040±24

composition that has been depleted over the long term.

4.3.3. DISCUSSION

The isotopic compositions of the alkali basalts define a very narrow field, with the exception of two rocks from Bhujia, samples BN-A and BN-B.Most of these basalts have Sr and Nd isotopic compositions which are strikingly similar to those of the most depleted tholeiites from the Mahabaleshwar region (Mahoney et. al., 1982) suggesting a genetic relationship or a source coincidentally similar in isotopic composition. The two more enriched rocks from Bhujia, BN-A and BN-B, must either represent a different although still depleted source,or be the result of mixing. No intermediate compositions were observed.The tholeiitic basalt from Kutch,on the other hand,show a much wider range and fall along the Mahabaleshwar mixing trend reinforcing the possibility of a genetic link between Mahabaleshwar tholeiites and Kutch alkali basalts.This relationship is also reflected in their similar ages as shown in Chapter III.

In contrast to the host basalts, the isotopic compositions of separated xenolith minerals exhibit a wide range from ϵNd+12 to -21 and $^{87}Sr/^{86}Sr$ from 0.7039 to 0.7075 (corrected for an age of 66 Ma) (Table 4.4).There is no overlap with the host basalts. Thus the peridotite nodules probably represent fragments of lithosphere unrelated to the source of either their host alkali basalts

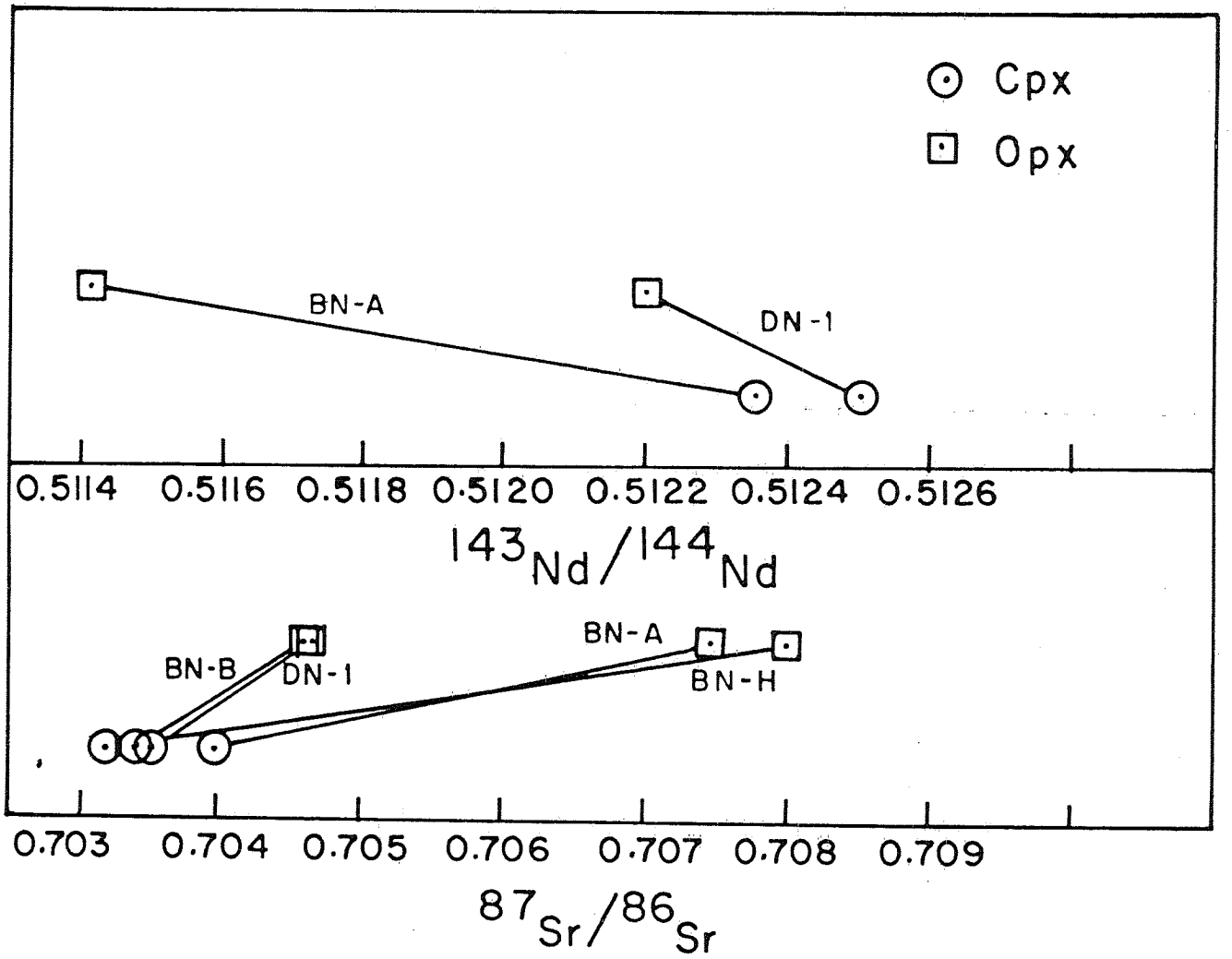


Fig. 4.15 Nd and Sr isotopic composition for co-existing Cpx and Opx.

or the tholeiites of the Deccan province.

The most striking feature of the mineral isotopic data is the extreme disequilibrium between clinopyroxene and orthopyroxene pairs from these nodules. The two cpx-opx pairs for which both Nd and Sr isotopic data are available show that the lower concentration orthopyroxenes have more enriched compositions, that is, lower $^{143}Nd/^{144}Nd$ and higher $^{87}Sr/^{86}Sr$ than the clinopyroxenes. For the three other pairs for which only Sr data is available the orthopyroxenes again show the more enriched compositions. The REE concentration data also reflect disequilibrium (Fig. 4.15) and together clearly demonstrate an enrichment event in the recent history of these xenoliths. As discussed earlier, the isotopic compositions of the leach solutions from two nodules are similar to the host rocks. Thus the acid leachable component does not appear to be related to the enrichment event.

Although the evident lack of isotopic equilibrium would seem to obviate any attempt to use a mineral geothermometer for these samples, the major element compositions may well still reflect equilibration conditions if the isotopic and trace element disequilibration results from action of a metasomatizing fluid. As pointed out in Chapter III, major element compositions are very homogeneous for both clinopyroxene and orthopyroxene. Based on the method of Wells (1977), equilibration temperatures in the range of 950 to 1000°C can be calculated for these samples. Such temperatures should be sufficient to attain isotopic

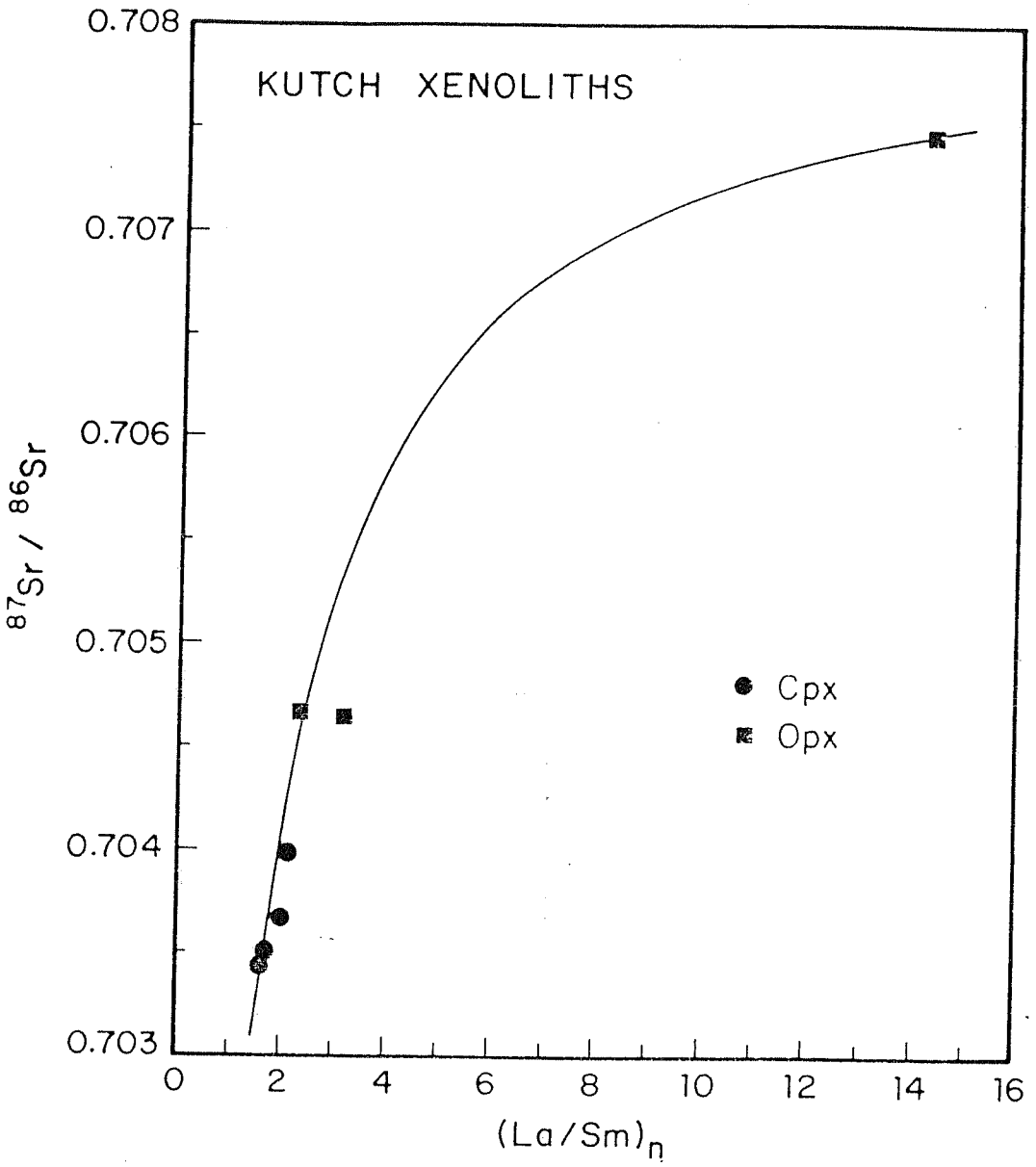


Fig. 4.16 $^{87}Sr/^{86}Sr$ versus $(La/Sm)_n$ in Cpx and Opx

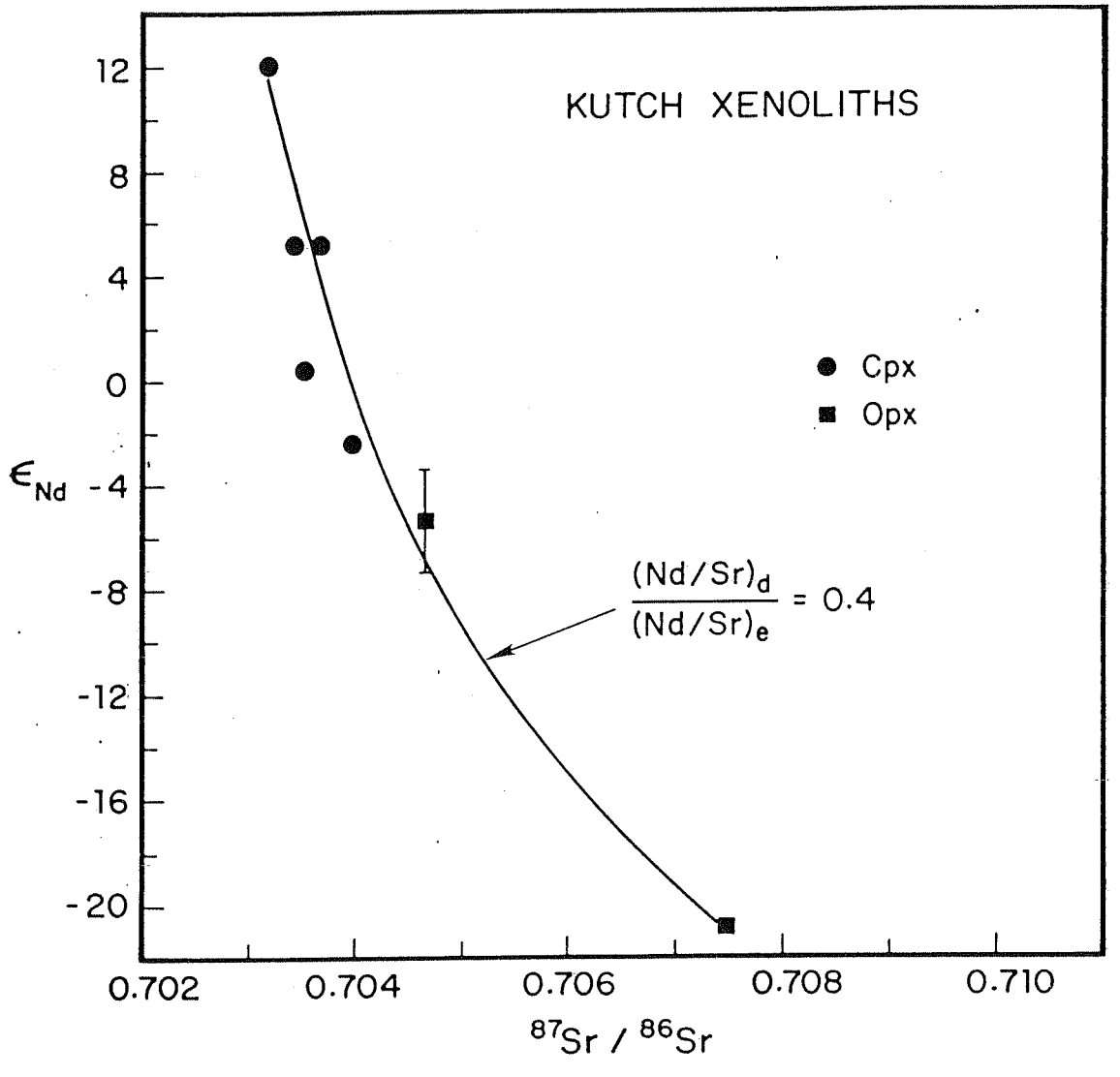


Fig. 4.17 ϵ_{Nd} versus $^{87}Sr/^{86}Sr$ in Cpx and Opx

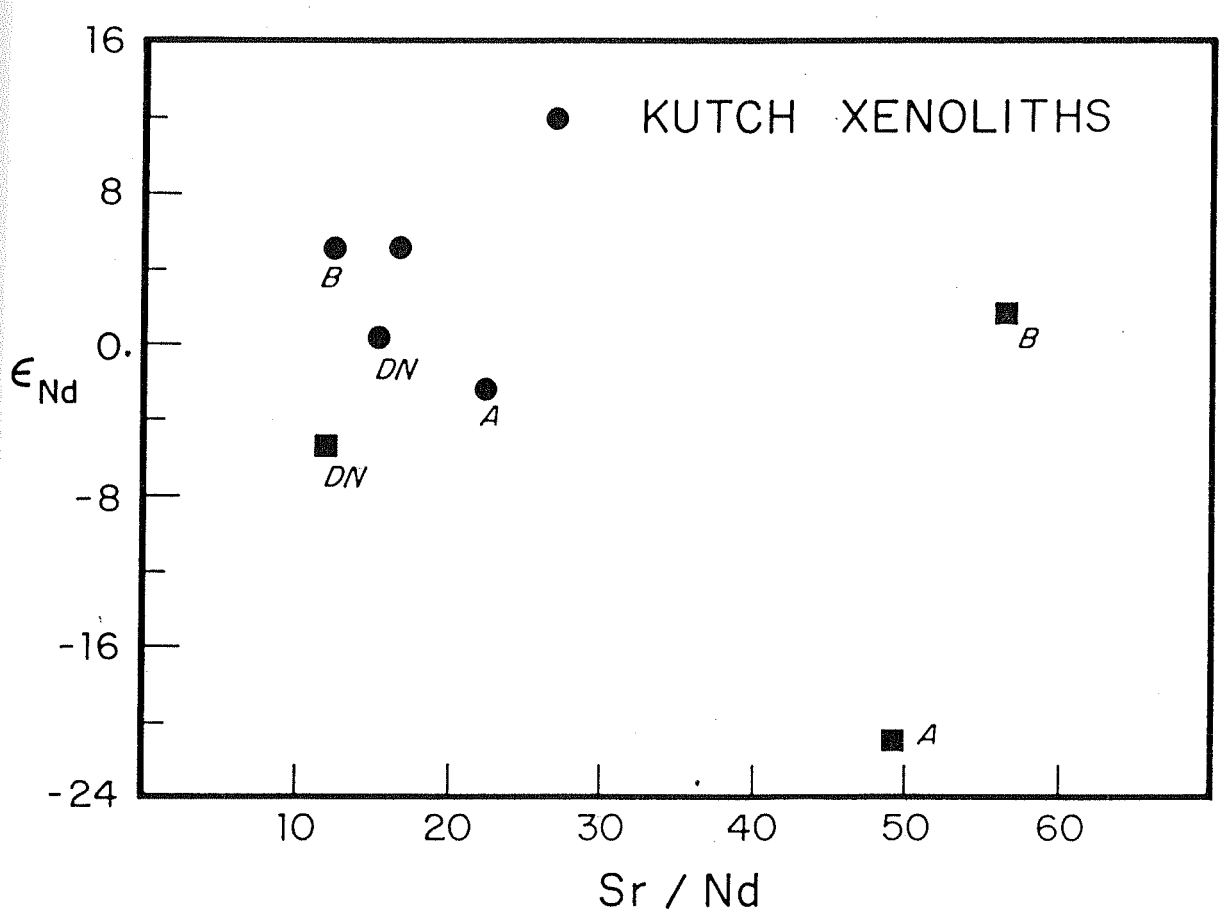


Fig. 4.18 ϵ_{Nd} versus Sr/Nd in Cpx and Opx.

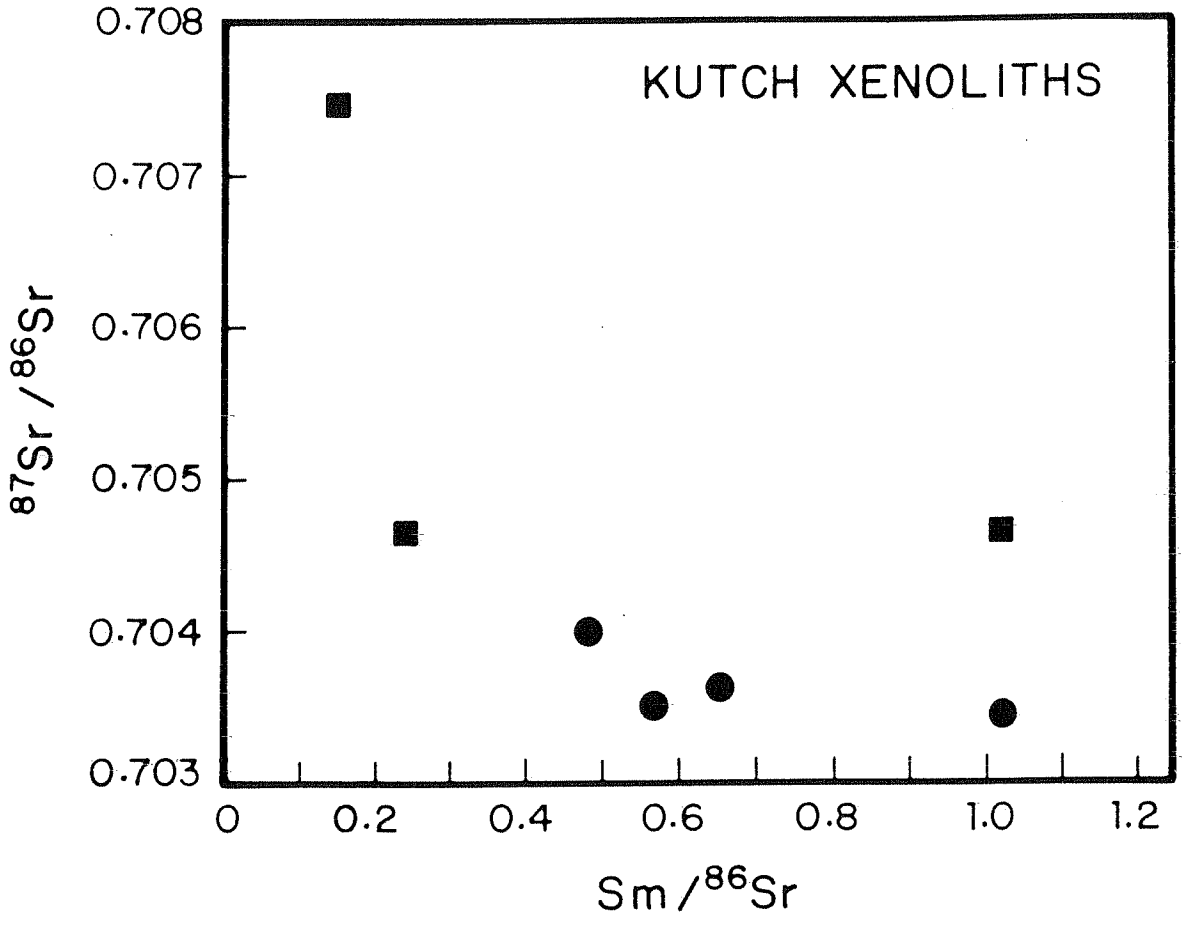


Fig. 4.19 $^{87}Sr/^{86}Sr$ versus $Sm/^{86}Sr$ in Cpx and Opx.

equilibrium on a centimeter scale over times of a few million years (Sneeringer et. al.,1984;Stosch et. al.,1986). Thus the metasomatic enrichment event is constrained to have occurred shortly before eruption of the alkali basalts.

At first glance,the mineral isotopic data appear to be a classic example of simple two component mixing. On ratio-ratio plots ($^{87}Sr/^{86}Sr$ vs.La/Sm and E_{Nd} vs $^{87}SR/^{86}Sr$) the fit to hyperbolic mixing curves is very good (Figs.4.16 and 4.17). However,the elemental ratios do not fit and even the sense of curvature is not what one might expect - Nd/Sr to be lower in enriched component than in the depleted one, whereas to fit the data requires it to be higher.This is apparent in the Langmuir-type comparison plots (Langmuir et. al., 1978) which are tests for two component mixing in that the data should plot on straight lines,which they do not, in ϵ_{Nd} vs Sr/Nd and $^{87}Sr/^{86}Sr$ vs $La/^{86}Sr$ plots (Figs 4.18 and 4.19).

As is the case at other xenolith localities,the Kutch peridotites have had a complex geochemical history, involving a minimum of two stages:an early partial melting event leading to the formation of a depleted spinel peridotite residue and a recent metasomatic enrichment event. Unlike most other cases (Jagoutz et. .,1980;McDonough and McCulloch 1987; Stosch et. .,1980;Stosch and Lugmair, 1986) where the timings of the initial depletion events have been obtained from concordant model ages calculated from both Sm-Nd and Rb-Sr systems,or from linear trends in the evolution curves for the two systems, no unique

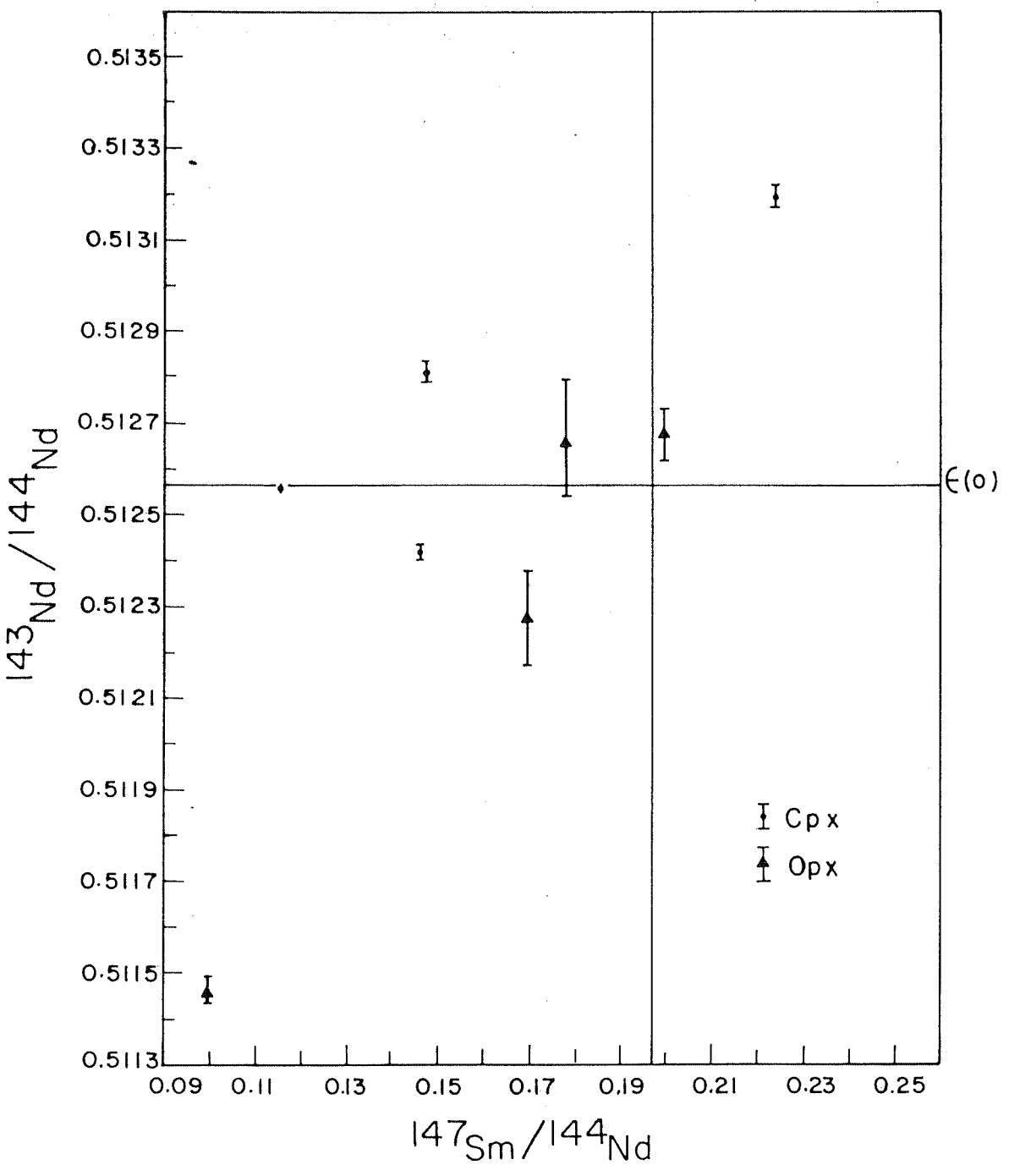


Fig. 4.20 $^{143}Nd/^{144}Nd$ versus $^{147}Sm/^{144}Nd$ for mineral separates.

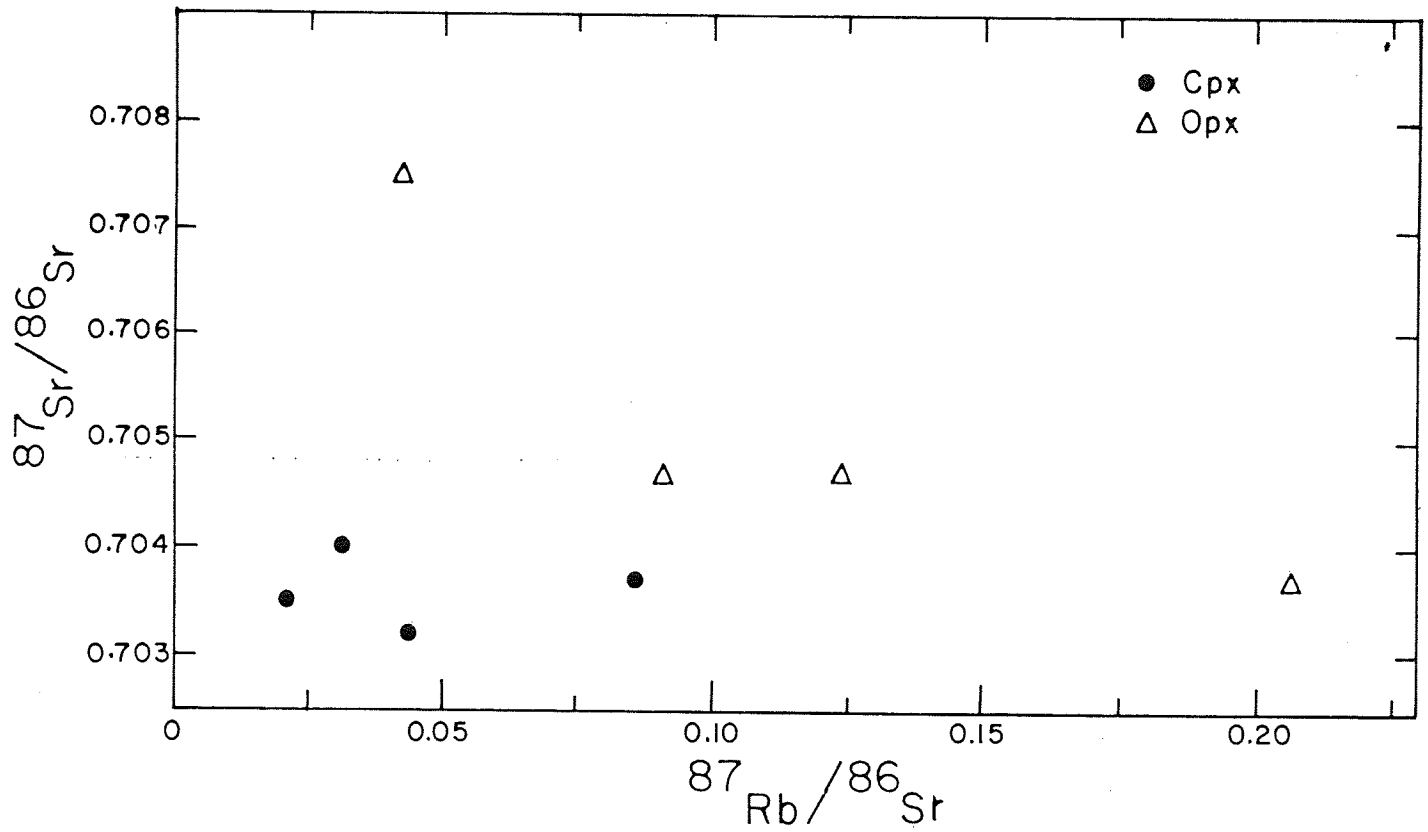


Fig. 4.21 $^{87}Sr/^{86}Sr$ versus $^{87}Rb/^{86}Sr$ for mineral separates.

depletion age can be estimated for these samples,apparently because of the masking effects of the metasomatic event(s). Evolution diagrams for the Sm-Nd and Rb-Sr systems show considerable scatter (Figs. 4.20 and 4.21).Considering only the pyroxenes,a rough linear trend can be discerned for the Sm-Nd system, but none is apparent in the Rb-Sr system (Figs. 4.20 and 4.21).

The enrichment of metasomatic event seems to have affected the isotopic compositions of the low concentration orthopyroxenes more severely than the higher concentration clinopyroxenes. The positive Eu anomaly is also most prominent in the lowest concentration orthopyroxene separate (sample BN-A) and among the pyroxenes is noticeable only in one low-concentration sample.Moreover, there is no mineralogical indication of the metasomatic event in the form of hydrous phases or significant chemical zoning of the pyroxenes. All these observattions suggest that the most depleted sample is probably least affected by recent metasomatism. The most depleted sample is clinopyroxene BN-H;it has the highest Nd isotopic ratio and, in contrast to the other clinopyroxene separates,has a chondrite-normalized Sm/Nd ratio > 1.The Sm-Nd model age for this sample,relative to a bulk earth with $^{147}Sm/^{144}Nd$ = .1967 and $^{143}Nd/^{144}Nd$ = 0.512624, is 3.1 Ba,and the Rb-Sr model age is 2.5 Ba, though with a relatively large uncertainty. These old ages suggest that there is an ancient stabilized lithosphere beneath this part of India.

4.4. SUMMARY

Considering together the data for alkali basalts and xenoliths, several important observations can be made:

1. The isotopic compositions of the alkali basalts are similar to the most depleted and least contaminated tholeiite from Mahabaleshwar suggesting that they were derived from a common, or at least similar, source.

2. The Deccan tholeiite source is postulated to be in the convecting upper mantle (Mahoney, 1984).

3. The alkali magmas are volumetrically very small compared to the tholeiites, and are confined to narrow, tectonically active regions.

4. For coexisting alkali and tholeiite basalts in the Narmada valley, it has been suggested (Mahoney et. al., 1985) that the two magma types were produced separately from isotopically similar but chemically distinct sources. Recent metasomatism produced source regions with higher abundances of elements such as K, Rb and Ba. It was these mantle regions which produced the alkali rocks while the more normal mantle acted as a source for tholeiites.

5. The xenoliths from Kutch bear evidence of a recent metasomatic event, although in this case the metasomatic component had a different isotopic signature than either that of the host alkali basalts

or the xenoliths themselves.

These observations lead to a possible scenario for basalt generation and lithospheric evolution. During the Archean, probably in the time range 2.5-3.1 Ba, partial melting of the mantle during crust formation led to formation of a depleted spinel peridotite residue. Although no Archean basement rocks are exposed in Kutch, the isotopic compositions of Kutch tholeiites suggest their presence. The stabilized lithospheric segment continued to evolve isotopically as an isolated entity until elevated temperatures about 65-68 Ma ago, perhaps due to a thermal plume, led to lithospheric thinning and large scale partial melting and volcanism, producing the voluminous tholeiites of the Deccan Traps. Away from the central plume region of large partial melt fractions, shallower thermal gradients permitted smaller degree melt fractions to be generated, possibly at greater depths, generating alkaline magmas. Such fluids would undoubtedly infiltrate the overlying lithosphere and could have been the source for alkaline enrichment of the source region for the Narmada Valley type alkaline basalts (Mahoney et. al., 1985). The generally elevated temperatures due to the Deccan episode also caused autometasomatism of the chemically complex lithosphere in Kutch and was responsible for the metasomatic enrichments seen in the Kutch xenoliths. In places where channels were available, for example, in the form of deep faults due to the tensional tectonic regime, the alkali magmas generated by

small degree partial melting reached the surface bringing with them the metasomatized xenoliths.

CHAPTER V

SUMMARY AND RECOMMENDATIONS

The data presented and discussed in the thesis represent the first effort at detailed investigation of spinel peridotites and their host alkali basalts from the Deccan volcanic province with a view to understand the sub-Deccan lithospheric evolution. Also reported are the first reliable Ar-Ar age data for the alkaline rocks of the Deccan province to unravel the temporal relationship between these two types of magmatism. This chapter brings out the main findings and discusses the aspects which need further study.

Spinel peridotite bearing alkali basalts occur as plug or sheet-like bodies in Kutch, Deccan volcanic province. These alkali basalt bodies intrude the flat-lying to gently dipping Jurassic sandstones but their relationship with the Deccan tholeiites cannot be deciphered in the field because these two types are nowhere seen in direct contact. Precise ^{40}Ar-^{39}Ar ages, ranging between 64-67Ma for the alkali and

tholeiitic basalts from Kutch indicate a close temporal relationship between these two types of basalts and their contemporaneity with the tholeiites of the Mahabaleshwar section. Though the present Ar-Ar data suggests a period of 3 Ma for the eruption of the alkali basalts,more samples need to be dated to confirm the extended duration or otherwise of the alkaline magmatism in Kutch.

The spinel peridotites so far found are rather small, averaging only 1-2 cm in diameter,although a few larger samples were recovered.Texturally these are medium to fine grained and are equigranular or porphyroclastic.Their small size precluded a meaningful evaluation of mineral modes. However, relative abundances are in the order olivine > orthopyroxene > clinopyroxene > spinel. Significantly,no trace of hydrous phases,like phlogopite,was observed in any of the xenoliths examined.Larger nodules should be looked for and need to be studied with a view to determine their modal mineral compositions and any hydrous phases.

The mineralogical composition of these xenoliths would place them in Cr-diopside group of Wilshire and Shervais (1975) Group I of Frey and Prinz (1978) and Type I of Menzies (1983). Olivines are quite homogeneous,averaging about Fo_{90}. Fluid inclusions are common in olivine crystals but are rare in pyroxenes.The orthopyroxenes are enstatites with a fairly uniform composition averaging $FO_{89.6}$ $FS_{9.7}$ $Wo_{0.7}$. Clinopyroxenes are chrome-diopsides with little variation, the observed range being $En_{48-49}Wo_{46-49}Fs_{4-5}$. Spinels exhibit the most chemical variability among the

nodule minerals; however, their average composition is quite similar to those found in spinel peridotites from other localities.

Rare earth element data for both leached and unleached whole rock xenoliths and leached mineral separates was obtained. The light REE enriched patterns for both leached and unleached aliquots are similar to those observed for spinel peridotites elsewhere. Both concentration and degree of enrichment are less for leached compared to unleached samples. Although part of the difference between these two fractions may be due to variable clinopyroxene contents, the differences are systematic and most probably be due to the leaching process. Thus substantial fraction of the REE (and presumably other incompatible elements as well) must occur on grain surfaces and/or as soluble interstial phases.

All clinopyroxenes are LREE enriched, although the concentrations and degree of enrichment vary widely. Their REE patterns are characteristic of metamomatised spinel peridotites. An interesting but puzzling feature is the small positive Eu anomaly shown by the two samples which, perhaps significantly, have the lowest REE concentrations. The orthopyroxene separates, on the other hand, exhibit, U-shaped to LREE depleted patterns. Those with U-shaped patterns also show significant positive Eu anomalies. The concave upward REE patterns of the orthopyroxenes probably reflect their metasomatised nature. The significance of the positive Eu anomalies is not clear. It suggests the involvement of plagioclase in the REE history of this

material, although when and how is very uncertain.This aspect needs further detailed study.

The host basalts show strong LREE enrichment, characteristic of alkali basalts world over.Their Sr and Nd isotopic compositions define two discrete clusters on $^{143}Nd/^{144}Nd$ versus $^{87}Sr/^{86}Sr$ diagram. The majority fall within a very narrow field,with $^{143}Nd/^{144}Nd$ varying from 0.512876 to 0.512893 and $^{87}Sr/^{86}Sr$ varying from 0.70415 to 0.70421. Two samples however show a different composition, with $^{143}Nd/^{144}Nd$ = 0.512649 and $^{87}Sr/^{86}Sr$ = 0.704428. Significantly these two samples can be distinguished from other alkali basalts on the basis of their major and trace element chemistry also.The composition of these two alkali basalt types may either represent the total range of variation for the alkali basalts or two different magma types. More samples need to be analysed to distinguish between the two possibilities.

Most of the alkali basalts fall in the field defined by the least crustally contaminated tholeiites from Mahabaleshwar, about 700 km southeast in the main Deccan province. Moreover, tholeiites from Kutch fall along the Mahabaleshwar mixing trend. These observations suggest a close association between the Kutch and Mahabaleshwar tholeiites and between the mantle sources of the alkali and tholeiitic basalts. This relationship is also reflected in their similar ages.

The isotopic composition of xenolith clinopyroxenes are distinctly different from those of the host alkali basalts.

There is no overlap with their composition. Thus the peridotites probably represent fragments of lithosphere unrelated to the source of either their host alkali basalts or the tholeiites of the Deccan province. The isotopic composition of Cpx falls within the range observed for spinel peridotites worldwide.They exhibit a large variation in $^{143}Nd/^{144}Nd$ and relatively smaller variation in $^{87}Sr/^{86}Sr$ and all compositions fall to the left of the 'mantle array'. These characteristics are typical of those observed for metasomatised xenoliths.Orthopyroxene isotopic compositions are distinct from those in co-existing clinopyroxenes. The most striking feature of the mineral isotopic data is the extreme disequilibrium between clinopyroxene (Cpx) and Orthopyroxene (Opx) pairs from the same nodules.The two Cpx-Opx pairs for which both Nd and Sr data are available show that lower concentration orthopyroxenes have more enriched compositions, that is, lower $^{143}Nd/^{144}Nd$ and higher $^{87}Sr/^{86}Sr$ than the clinopyroxenes. For the three other pairs for which only Sr data are available the orthopyroxenes again show more enriched compositions.The isotopic disequilibrium on a very small scale within individual nodules,i.e. between Cpx and Opx needs more detailed investigations. There are indications that the disequilibrium is not phase specific;a second Opx separate from two of the nodules yielded different Sr isotopic during preliminary study.The isotopic composition of acid leachable phases/components from two nodules are similar to the host rock and do not seem to be

related to the enrichment events.

The Kutch peridotites have had a complex geochemical history, involving a minimum of two stages:an early partial melting event leading to the formation of a depleted spinel peridotite residue and a very recent metasomatic enrichment event. Unlike most other cases no unique depletion age can be determined for these samples,apparently because of the masking effects of the metasomatic event(s). Evolution diagrams for the Sm-Nd and Rb-Sr systems show considerable scatter. Considering only the pyroxenes,a rough linear trend can be discerned for the Sm-Nd system,but none is apparent in the Rb-Sr systematics.

The enrichment or metasomatic event seems to have affected the isotopic compositions of the low concentration orthopyroxenes more severely than the higher concentration clinopyroxenes. The positive Eu anomaly is also most prominent in the lowest concentration orthopyroxene separate (sample BN-A) and among the clinopyroxenes is noticeable only in one low-concentration sample.Moreover, there is no mineralogical indication of the metasomatic event in the form of hydrous phases or significant chemical zoning of the pyroxenes.All these observations suggest that the most depleted samples is probably least affected by recent metasomatism. The most depleted sample is clinopyroxene BN-H;it has the highest Nd isotopic ratio and, in contrast to the other clinopyroxene separates,has a chondrite-normalized Sm/Nd ratio >1.The Sm-Nd model age for this sample, relative to the bulk earth with $^{147}Sm/^{144}Nd$ =

0.1967 and $^{143}Nd/^{144}Nd$ = 0.512624, is 3.1 Ba, and the Rb-Sr model age is 2.5 Ba, with a relatively large uncertainty. These old ages suggest hat there is an ancient stabilized lithosphere beneath this part of India. More samples need to be analysed to evaluate this.

The present data lead to a possible scenario for basalt generation and lithospheric evolution. During the Archean, probably in the time range 2.5-3.1 Ba, partial melting of the mantle during crust formation led to formation of a depleted spinel peridotite residue. Although no Archean basement rocks are exposed in Kutch, the isotopic compositions of Kutch and Mahabaleshwar tholeiites suggest its presence. The stabilized lithospheric segment continued to evolve isotopically as an isolated entity until elevated temperatures about 65-68 Ma ago, perhaps due to a thermal plume, led to lithospheric thinning and large scale partial melting and volcanism, producing the voluminous tholeiites of the Deccan Traps. Away from the central plume region of large partial melt fractions, shallower thermal gradients permitted smaller degree melt fractions to be generated, possibly at greater depths, generating alkaline magmas. Such fluids would undoubtedly infiltrate the overlying lithosphere and could have been the source for the enrichment of the source region for the Narmada Valley type alkaline basalts. The generally elevated temperatures due to the Deccan episode also caused autometasomatism of the chemically complex lithosphere in Kutch and was responsible for the metasomatic enrichments seen in the Kutch xenoliths.

In places where channels were available, for example, in the form of deep faults due to the tensional tectonic regime, the alkali magmas generated by small degree partial melting reached the surface, bringing with them the metasomatized xenoliths.

REFERENCES

1. Allegre, C.J. (1982) Chemical Geodynamics Tectono Physics,81 109-132.

2. Allegre, C.J. (1987) Isotope Geodynamics,Earth Planet. Sci. Lett. 86 175-203.

3. Allegre, C.J., Hart, S.R. and Minster, J.F. (1983) Chemical Structure and evolution of the mantle and continents determined by inversion of Nd and Sr isotopic data,II. Numerical Experiments and discussion, Earth and Planet. Sci. Lett. 66 191-213.

4. Anderson, D.L. (1982) Isotopic evolution of the mantle: a model,Earth Planet. Sci. Lett. 57 13-24.

5. Bailey, D.K. (1970) Volatile flux,heat focussing and the generation of magma, Geol. J. Spec. Issue 2 177-186.

6. Bailey, D.K. (1972) Uplift, rifting and magmatism and continental plates,J. Earth Sci. (Leeds) 8 225-239.

7. Bailey, D.K. (1982) Mantle metasomatism - continuing chemical change within the earth,Nature 296 525-530.

8. Bailey, D.K. (1984) 'The mantle sample' formed by ultrametasomatism, In Kornprobst, ed. Kimberlites I: 323-333.

9. Basaltic Volcanism Study Project (1981) Basaltic volcanism on the terrestrial planets,Pergamon Press Inc.,N.Y.,pp.1286.

10. Basu, A.R. and Murthy,V.R. (1977) Ancient lithospheric lherzolite xenolith in alkali basalt from Baja, California,Earth Planet. Sci. Lett. 35 239-246.

11. Basu, A.R. and Macgregor, I.D. (1975) Chomite spinels from ultramafic xenoliths,Geochim. Cosmochim. Acta 39 937-945.

12. Basu, A.R. (1975) Hot-spots,mantle plumes and a model for the origin of ultramafic xenoliths in alkali Basalts,Earth Planet. Sci. Lett. 28 261-274.

13. Bevington, P.R. (1969) Data reduction and error analysis for the physical sciences,McGraw-Hill Book Co.,New York.

14. Boettcher, A.L. (1984) The Source Regions of Alkaline Volcanoes in Explosive Volcanism Inception,Evolution and Hazards, National Academy Press,Waghington,D.C., 13-22.

15. Boettcher, A.L., O'Neil, J.R.,Windom,K.E.,Stewart,D.C., and Wilshire, H.G. (1979) Metasomatism of the upper mantle and the genesis of Kimberlites and alkali basalts. In: The Mantle Sample Inclusions in Kimberlites and other Volcanics (Ed. F.R. Boyd and H.O.A. Meyer),pp. 173-182 AGU,Washington.

16. Biswas, S.K. and Deshpande, S.V. (1973) A note on the mode of eruption of the Deccan Trap lavas with special reference to Kutch,Jour. Geol. Soc. India 14 134-141.

17. Biswas, S.K. (1970) A note on the geology of Kutch, Quart. Jour. Geol. Min. & Melt. Soc. India 43 223-235.

18. Bose, M.K. (1980) Alkaline magmatism in the Deccan Volcanic Province,Jour. Geol. Soc. India 21 317-329.

19. Brooks, C., James, D.E., Hart, S.R. (1976) Ancient lithosphere its role in young continental volcanism, Science 193 1086-1094.

20. Bowen, N.L. (1927) An analcite-rich rock from the Deccan Traps of India,Jour. Wash. Acad. Sci. 17 57-60.

21. Boyd, F.R. and Meyer, H.O.A. (Eds.) (1979),The mantle sample inclusions in Kimberlites and other volcanics (Proc. Int. Kimberlite Conf., No.2, Vol.2) pp.424, American Geophysical Union,Washington,D.C.

22. Brereton, N.R. (1970) Corrections for interfering isotopes in the $^{40}Ar/^{39}Ar$ dating method,Earth Planet. Sci. Lett. 8 No.6,427-433.

23. Carlson, R.W. (1980) Crust-Mantle differentiation on the Earth and Moon Evidence from isotopic studies for contrasting mechanism and Duration.,Unpublished Ph.D. Thesis,University of California,San Diego,pp.219.

24. Carlson, R.W., Lugmair, G.W. and Macdougall,J.D. (1981) Columbia River Volcanism the question of mantle heterogeneity or crustal contamination, Geochim. Cosmochim. Acta 45 2483-2499.

25. Chatterjee, S.C. (1961) Some problems of the Deccan Traps,Mahadevan Volume,Osmania University,pp.102-106.

26. Chen, C-Y. and Frey,F.A. (1981) Multi stage geochemical events in the upper mantle evidences from geochemical studies of spinel lherzolites from Mount Leura, Australia,EOS 62,415.

27. Dalrymple, G.B., Alexander Jr., E.C.,Lanphere,M.A. and Kraker, G.P. (1981) Irradiation of sample for $^{40}Ar/^{39}Ar$ dating using the geological survey TRIGA reactor, U.S.G.S. Professional Paper,1176.

28. Dasch, E.J. and Green, D.H. (1975) Strontium isotope geochemistry of lherzolite inclusions and host basaltic rocks, Victoria, Australia, Amer. J. Sci. 275 461-469

29. Dawson, J.B. (1980) Kimberlites and their xenoliths, Berlin Springer Verlag,pp.252.

30. Dawson, J.B. (1984) Xenoliths in Kimberlites Clues to the earth's upper mantle,Sci. Prog. Oxf. 69 65-81.

31. Dawson, J.B. (1984b) Contrasting types of upper mantle

metasomatism? In Kimberlites II The mantle and crust relationships (ed. J. Kornprobst),Elsevier,Amsterdam, pp.289-294.

32. De, A. (1964) Iron-Titanium oxides and silicate minerals of alkaline olivine basalts,tholeeites and acidic rocks of the Deccan trap series and their significance, Int. Geol. Cong. Rept., 22nd Sess. New Delhi Pt. III,126-138.

33. De, A., (1981) Late Mesozoic-Lower Tertiary magma types of Kutch and Saurashtra. In Deccan Volcanism and Related basalt provinces in other parts of the World, Geological Society of India Memoir No. 3,327-339.

34. DePaolo, D.J. (1980) Crustal growth and mantle evolution inferences from the models of element transfer and Nd and Sr isotopes,Geochim. Cosmochim. Acta 44 1185-1196.

35. DePaolo, D.J. (1981) Trace element and isotopic effects of combined wallrock assimilation and fractional crystallization,Earth Planet. Sci. Lett. 53 189-202.

36. Erlank, A.J.,Allsopp,H.J.,Hawkesworth,C.J.,Menzies,M.A. (1982) Chemical and isotopic characterization of upper mantle metasomatism in peridotite nodules from the Bulfontein Kimberlite,Terra Cognita 2 216-263.

37. Forbes, R.B., Kuno, H. (1967) Peridotite inclusions and basaltic host rocks, In:Ultramafic and related rocks,

Wyllie P.J. (ed.),Wiley,New York,328-337.

38. Forbes R.B. (1963) Utrabasic inclusions from the basalts of the Hut point area,Ross Island,Bull. Volc. 26 13-21.

39. Forbes, R.B. and Kuno,H. (1965) The regional petrology of peridotite inclusions and basaltic host rocks,Proc. 22nd Intern. Geol. Cong. Upper Mantle Symp. (New Delhi),161-179.

40. Francis, D.M. (1976) The original of amphibole in lherzolite Xenoliths from Nunivak Island, Alaska,J. Petrol. 17 357-378.

41. Frey, F.A. (1984) Rare earth element abundances in upper mantle rocks,In:Rare Earth Element Geochemistry, (ed. P. Henderson),Elsevier,Amsterdam,pp.153-203.

42. Frey, F.A. and Prinz, M. (1978) Ultramafic inclusions from San Carlos, Arizona Petrologic and geochemical data bearing on their petrogenesis,Earth Planet. Sci. Lett. 38 129-176.

43. Frey, F.A. and Green, D.H. (1974) The mineralogy, geochemistry and origins of lherzolite inclusions in the Victorian basanites, Geochim. Cosmochim. Acta 38 1023-1059.

44. Ganpathy, R. and Anders,E. (1974) Bulk composition of the Moon and Earth,estimated from meteorites,Proc. 5th

Lunar Sci. conf., Geochim, Cosmochim. Acta Suppl. 5 1181-1206.

45. Gast, P.W. (1968) Trace element fractionation and origin of tholeiitic and alkaline magma types,Geochim. Cosmochim. Acta 32 1057-1086.

46. Griffin,W.L. and Murthy,V.R. (1968) Abundances of K,Rb, Sr and Ba in some ultramafic rocks and minerals,Earth Planet. Sci. Lett. 4 497-501.

47. Haggerty, S.E. (1979) Spinels in high pressure regimes, In the Mantle Samples Inclusions in Kimberlites and other volcanices, Proc. 2nd Int. Kimberlite Conf.,Vol. 2,183-196,Am. Geophys. Unions,Washington,D.C.

48. Hart, S.R. and Zindler, A. (1986) In search of a bulk Earth composition,Chem. Geol. 57,247-269.

49. Harte, B. (1983) Mantle peridotites and processes - the Kimberlite sample. In: Continental basalts and mantle xenoliths, ed. C.J. Hawkesworth, M.J. Norry,pp.46-91, Cheshire Eng. Shiva,pp 272.

50. Harte, B. (1977) Rock Nomenclature with particular relation to deformation and recrystallization textures in olivine bearing xenoliths,J. Geol. 85 279-288.

51. Hawkesworth, C.J., Rogers, N.W., Van Calsteren, P. and Menzies, M.A. (1984) Mantle Enrichment Processes,Nature 311 331-335.

52. Hawkesworth, C.J., Erlank, A.J.,Marsh,J.S.,Menzies,M.A. and Van Calsteren, P. (1983) Evolution of the continental lithosphere evidence from volcanices and xenoliths in southern Africa. In:Continental Basalts and Mantle Xenoliths,ed. C.J. Hawkesworth,M.J. Norry, pp. 111-138,Cheshire,Engl. Shiva,pp.272.

53. Hutchinson, R., Paul, D.K. and Harris, P.G. (1970) Chemical composition of the Upper mantle,Mineral. Mag. 37 726-729.

54. Irving, A.J. (1980) Petrology and Geochemistry of composite ultramafic xenoliths in alkalic basalts and implications for magmatic processes within the mantle, Am. J. Sci. 280-A 389-426.

55. Irving, A.J. and Dungan,M.A. (Eds.) (1980) The Jackson Volume,Am. J. Sci. 280-A.

56. Jacobson, S.B. and Wasserburg,G.J. (1979) The mean age of mantle and crustal reservoirs,J. Geophys. Res. 84 7411-7427.

57. Jagoutz, E., Palme,H.,Baddenhausen,H.,Blum,K.,Cendales, M., Dribus,G.,Spettel,B.,Lorentz,V. and Wanke,H. (1979) The abundances of major, minor and trace elements in Earth's mantle as derived from primitive ultramafic nodules, Proc. Lunar Planet. Sci. Conf. 10th,Geochim. Cosmochim. Acta,Suppl. II,2031-2050.

58. Jagoutz, E., Carlson, R.W., Lugmair, G.W. (1980) Equilibrated Nd- unequilibrated Sr isotopes in mantle xenoliths,Nature 296 708-710.

59. Kaneoka, L. (1980) $^{40}Ar/^{39}Ar$ dating on volcanic rocks of Deccan Traps, India, Earth Planet. Sci. Lett. 46 233-243.

60. Kempton, P.D., Menzies, M.A. and Dungan, M.A. (1984) Petrography, petrology and geochemistry of xenoliths and megacrysts from the Geromino volcanic field, Southeastern Arizona. In Kornprobst (eds.) Kimberlites II, the mantle and the crust mantle relationships,Devs. Petrology,11B pp. 71-84,Elsevier,Amsterdam.

61. Krishnamurthy, P., Pande, K.,Gopalan,K. and Macdougall, J.D. (1988) Upper mantle xenoliths in alkali basalts related to Deccan Trap Volcanism, Jour. Geol. Soc. India (in press).

62. Kurat, G., Spettel, B., Baddenhausen, H.,Hofmeister H., Palme C. and Wanke, H. (1980) Geochemistry of ultramafic xenoliths from Kapfenstein,Austria evidence for variety of upper mantle processes, Geochim. Cosmochim. Acta 44 45-60.

63. Kushiro, I., Kuno, H. (1963) Origin of primary basalt magmas and classification of basaltic rocks, Jour. Petrol 4 75-89.

64. Langmuir, C.J.,Vocke,Jr.,R.D.,Hanson,G.N. and Hart,S.R. (1978) A general mixing equation with application to Icelandic basalt,Earth Planet. Sci. Lett. 37 380-392.

65. Lloyd, F.E. and Bailey, D.K. (1975) Light element metasomatism of the continental mantle the evidence and the consequences,Phys. Chem. Earth. 9 389-416.

66. Loubet, M., Shimizu, N. and Allegre, C.J. (1975) Rare earth elements in Alpine Peridotites,Contrib. Mineral. Petrol. 53 1-12.

68. Mahoney, J., Macdougall, J.D., Langmuir,G.W.,Gopalan,K. and Krishnamurthy, P. (1985) Origin of contemporaneous tholeiitic and K-rich alkali lavas A case study from the northern Deccan Plateau,India,Earth Planet. Sci. Lett. 72 39-53.

69. Mahoney, J., Macdougall, J.D.,Lugmair,G.W.,Murali,A.V., Shanker Das, M.,Gopalan,K. (1982) Origin of the Deccan Trap flows at Mahabaleshwar inferred from Nd and Sr isotopic and chemical evidence, Earth Planet. Sci. Lett. 60 47-60.

70. Mahoney, J. (1984) Isotopic and chemical studies of Deccan and Rajmahal traps, India Mantle sources and petrogenesis, Unpublished Ph.D. Thesis, University of California,San Diego,189.

71. Mcdonough, W.F., McCulloch, M.T. and Sun, S.S. (1985) Isotopic and geochemical systematics in tertiary - Recent basalts from Southeastern Australia and implications for the evolution of the sub-continental lithosphere,Geochim. Cosmochim. Acta 49 2051-2067.

72. Mcdonough, W.F. and McCulloch,M.T. (1987) The Southeast Australian lithospheric mantle : isotopic and geochemical constraints on its growth and evolution, Earth Planet. Sci. Lett. 86 327-340.

73. Menzies,M.A.,Halliday,A.N.,Palacz,Z.,Hunter,R.H.,Upton, B.G.J., Aspen, P. and Hawkesworth,C.J. (1987) Evidence from mantle xenoliths for an enriched lithospheric keel under the outer Hebrides,Nature 325 44-50.

74. Menzies, M.A. and Hawkesworth,C.J. (Eds.) (1987) Mantle metasomatism,Academic Press,London.,pp.472.

75. Menzies, M.A. (1983) Mantle ultramafic xenoliths in alkaline magmas evidence for mantle heterogeneity modified by magmatic activity,in:Continental Basalts and Mantle Xenoliths, eds. C.J. Hawkesworth and M.J. Norry,pp.92-110,Shiva Publishing Nantwich,U.K.,

76. Menzies, M.A. and Murthy,V.R. (1980) Nd and Sr isotope geochemistry of hydrous mantle nodules and their host alkali basalts implications for local heterogeneities in metasomatically veined mantle, Earth Planet. Sci.

Lett. 46 323-334.

77. Menzies, M.A., Kempton, P. and Dungan, M.A. (1985) Interaction of continental lithosphere and asthenospheric melts below the Geronimo volcanic field, Arizona,U.S.A.,J. Petrol. 26 663-693.

78. Menzies, M.A., Leeman, W.P., Hawkesworth, C.J. (1983) Isotope Geochemistry of Cenozoic volcanic rocks reveals mantle heterogeneity below western U.S.A., Nature 303 205-209.

79. Menzies, M.A., Leeman, W.P. and Hawkesworth,C.J. (1984) Geochemical and isotopic evidence for the origin of continental flood basalt with particular reference to the Snake River Plain,Idaho,U.S.A.,Philos. Trans. R. Soc. Lond. A. 310 643-660.

80. Mercier, J.-C.C. and Nicolas, A. (1975) Textures and fabrics of upper mantle peridotites as illustrated by basalt xenoliths,J. Petrol. 16 454-487,

81. Mitchell, J.G. (1968) The ^{40}Ar-^{39}Ar method for potassium-argon age determinations,Geochim. Cosmochim. Acta 32 No.7,pp.781-790.

82. O'Hara, M.J. and Mercy, E.L.P. (1963) Petrology and petrogenesis of some garnetiferous peridotites,Trans. R. Soc. Edinb. 65 251-314.

83. O'Nions, R.K., Hamilton, P.J. (1981) Isotope and trace

element models of crustal evolution,Philos. Trans. R. Soc. London,Ser. A 301,473-487.

84. O'Nions, R.K., Evenson, N.M. and Hamilton,P.J. (1979) Geochemical modeling of mantle differentiation and crustal growth,J. Geophys. Res. 84 No.6,6091-6101.

85. Richardson, S.H., Erlank, A.J. and Hart, S.R. (1985) Kimberlite-borne garnet peridotite xenoliths from old enriched subcontinental lithosphere,Earth Planet. Sci. Lett. 75 116-128.

86. Ringwood, A.E. (1975) Composition and petrology of the earth's mantle,McGraw-Hill.,pp.618.

87. Roden, M.F., Frey, F.A. and Francis, D.M. (1984) An example of consequent mantle metasomatism in peridotite inclusions from Nunivak Island,Alaska,J. Petrol. 25 546-577.

88. Roden, M.F. and Murthy,V.R. (1985) Mantle Metasomatism, Ann. Rev. Earth. Planet. Sci. 13 269-296.

89. Roddick, J.C., Cliff, R.A.. and Rex, D.C. (1980) The evolution of excess argon in alpine biotites - A ^{40}Ar-^{39}Ar analysis, Earth Planet. Sci. Lett. 48 185-208.

90. Ross, C.S. Foster,M.D. and Myers,A.T. (1954) Origin of dunites and olivine-rich inclusions in baslatic rocks, Amer. Min. 39 693-737.

91. Samson, S.D. and Alexander, Jr., B.C. (1986) Interlaboratory calibration of the ^{40}Ar-^{39}Ar dating standard MnHb-1,Terra-Cognita 6 No.2,171.

92. Schwarzer, R.R. and Rogers, J.J. (1974) A world-wide comparison of alkali olivine basalts and their differentiation trends, Earth Planet. Sci. Lett. 23 286-296.

93. Simkin, A. and Smith, J.V. (1970) Minor element distribution in olivine,J. Geol. 78 304-325.

94. Skewes, M.A and Stern, C.R. (1979) Petrology and geochemistry of alkali basalts and ultramafic inclusions from the Palei-Aike volcanic field in southern Chile and the origin of the Patagonian Plateau lavas,J. Volc. Geotherm. Res. 6 3-25.

95. Sneeringer, M.,Hart,S.R. and Shimizu,N. (1984) Strotium and Samarium diffusion in diopside,Geochim. Cosmochim. Acta 48 1589-1608.

96. Stosch, H.G. and Lugmair,G.W. (1986) Trace element and Sr and Nd isotope geochemistry of peridotite and xenoliths from the Eifel (West Germany) and their bearing on the evolution of the subcontinental lithosphere,Earth Planet. Sci. Lett. 80 281-298.

97. Stosch, H.G., Lugmair, G.W. and Kovalenko,V.I. (1986)

Spinel peridotite xenoliths from the Tariat Depression, Mangolia II Geochemistry and Nd and Sr isotopic composition and their implications for the evolution of the sub-continental lithosphere,Geochim. Cosmochim. Acta 50 2601-2614.

98. Stosch, H.G., Carlson, R.W. and Lugmair, G.W. (1980) Episodic mantle differentiation Nd and Sr isotopic evidence,Earth Planet. Sci. Lett. 47 263-271.

99. Stosch, H.G. and Seck, H.A. (1980) Geochemistry and mineraology of two spinel peridotite suites from Drieser Weiher, West Germany,Geochim. Cosmochim. Acta 44 457-470.

100. Stueber, A.M. and Ikramuddin, M. (1974) Rb, Sr and isotopic composition of strontium and ultramafic nodule minerals and host basalts,Geochim. Cosmochim. Acta 38 207-216.

101. Sun, S.S. (1982) Chemical composition and origin of the earth's primitive mantle, Geochim. Cosmochim. Acta 46 179-192.

102. Tetley, N., Mcdougall, I. and Heydegger, H.R. (1980) Thermal nuetron interferences in the $^{40}Ar/^{39}Ar$ dating technique, Jour. Geophy. Res. 85 7201-7205.

103. Turcotte, D.L. and Kellogg, L.H. (1986) Isotopic modeling of the evolution of mantle and crust,Reviews of Geophysics,24 No.2,311-328.

104. Turner, G. (1971) ^{40}Ar-^{39}Ar dating the optimization of irradiation parameters, Earth Planet. Sci. Lett. 10 No.2,227-234.

105. Turner, G. (1972) ^{40}Ar-^{39}Ar age and cosmic ray irradiation history of Apollo-15 anorthosite 15415, Earth. Planet. Sci. Lett. 14 169-175.

106. Varne, R. and Grahem,A.L. (1971) Rare earth abundances in hornblende and clinopyroxene of a hornblende lherzolite xenolith implications for upper mantle fractionation processes, Earth Planet. Sci. Lett. 13 11-18.

107. Walker, G.P.L. (1969) Some observations and interpretations of the Deccan Traps,Unpublished report submitted to the University of Sagar.

108. Wanke, H. (1981) Constitution of terrestrial planets, Philos. Trans. R. Soc. Lond. A303 287-302.

109. Wanke, H., Dribus, G. and Jagoutz, E. (1984) Mantle chemistry and accretion history of the earth,Archean Geochemistry,1-24.

110. Wass, S.Y. and Rogers,N.W. (1980) Mantle metasomatism - Precursor to continental alkaline volcanism,Geochim. Cosmochim. Acta 44 1811-1824.

111. Well, P.R.A. (1977) Pyroxene thermometry in simple and

complex systems,Contrib. Mineral. Petrol. 62 129-139.

112. Williamson, J.H. (1968) Least square fitting of a straight line,Can. Jour. Phys. 46 1845-1847.

113. White, W.M. (1966) Ultramafic inclusions in basaltic rocks from Hawaii, Contrib. Mineral. Petrol. 12 245-314.

114. Wilshire,H.G. (1984) Mantle metasomatism the REE story, Geology 12 395-398.

115. Wilshire, H.G. and Shervais,J.W. (1975) Al augite and Cr diopside ultramafic xenoliths in basaltic rocks from the western United States, Phys. Cham. Earth 9 257-272.

116. Zindler, A. and Hart,S.R. (1986) Chemical Geodynamics, Ann. Rev. Earth Planet. Sci. 14 493-571.

117. Zindler, A. and Jagoutz,E. (1986) Trace element and Nd and Sr isotope systematics of peridotite nodules from Peridot Mesa, San Carlos, Arizona,Geochim. Cosmochim. Acta (submitted).

118. Zindler, A. and Jagoutz, E. (1988) Mantle Cryptology, Geochim. Cosmochim. Acta 52 319-333.